EVALUATION OF WEATHER RESEARCH FORCASTING (WRF) MICROPHYSICS IN CAPTURING SHORT RAIN OVER ETHIOPIA

A Thesis Submited in Partial Fulfillment of the
Requirments for the Degree of
Master of Science in Physics

Addis Ababa University
College of Natural and Computational Sciences
Department of Physics

AMARECH ALEBIE
Addis Ababa, Ethiopia
July 2016

Addis Ababa University
College of Natural and Computational Sciences
Department of Physics

The undersigned here by certify that they have read and recommend to the School of Graduate Studies for acceptance a thesis entitled "**EVALUATION OF WEATHER RESEARCH FORCASTING (WRF) MICROPHYSICS IN CAPTURING SHORT RAIN OVER ETHIOPIA**" by **AMARECH ALEBIE** in partial fulfillment of the requirements for the degree of **Master of Science in Physics**.

Dated: July 2016

Supervisor: _____ _____

Prof. Gizaw Mengistu,
Professor, Department of Physics,
AAU, AA, Ethiopia

Examiner: _____ _____

Dr. Belayneh Mesfin,
Assistant Professor, Department of Physics,
AAU, AA, Ethiopia

Examiner: _____ _____

Prof. A. V. Gholap,
Professor, Department of Physics,
AAU, AA, Ethiopia

ADDIS ABABA UNIVERSITY

Date: **July 2016**

Author: **AMARECH ALEBIE**

Title: **EVALUATION OF WEATHER RESEARCH FORCASTING (WRF) MICROPHYSICS IN CAPTURING SHORT RAIN OVER ETHIOPIA**

Department: **Department of Physics**

Degree: **M.Sc.** Convocation: **JUNE** Year: **2016**

Permission is herewith granted to Addis Ababa University to circulate and to have copied for non-commercial purposes, at its discretion, the above title upon the request of individuals or institutions.

Signature of Author

Contents

List of Tables

List of Figures

Abstract

The Weather Research and Forecasting (WRF) model has been used to simulate clouds and their effects on precipitation over Ethiopia. The results have been compared with the Global Precipitation Climatology Center (GPCC) observations. This study identifies the precipitation capturing skill of the ten microphysics in weather research and forecasting (WRF) model during three years namely; El Niño, La Niña, and Normal years. The study domain covers Ethiopia with 10 km by 10 km horizontal grid resolution. The statistical tools used are correlation coefficient (R), bias, mean absolute error (MAE), and root mean square error (RMSE).

The analysis has shown that precipitation capturing skill of most microphysics are almost the same for all years. The result has pointed out that Morrison 2-moment, Thompson, and WSM6 are the best three microphysics for El Niño year; Thompson, Goddard, and Morrison 2-moment are the first 3 microphysics for La Niña year; and Thompson, Goddard, and Morrison 2-moment become the best 3 microphysics for Normal year.

Acknowledgments

Above all, I would like to thank the almighty; God, for letting me accomplish this thesis.

I would like to express my sincere gratitude to my supervisor, Prof. Gizaw Mengistu, for his support, guidance and suggestions throughout the research period. His vast knowledge and experience shared will remain as base for my future research career.

I am also thankful to Mr. Beyene Alemu for his patient financial support and for being with my side throughout my study time.

I am deeply indebted to Mr. Abera Debebe, for his suggestions and support during this research. I would like to thank him very much for his support on computational programs which has indispensable role to do my thesis. His mentoring and inspirational advice were the source of my strength. Moreover, I would like to thank Mr. Gezahegn Sufa for his timeless help throughout the year. Without his effort this thesis would have not been completed. I am also thankful to all Space and Atmospheric Physics graduate students in general.

I am highly indebted to the staff of the Department of Physics specially Mr. Semehegn Abayneh, for arranging me to utilize computational resources.

The last but not the least thanks goes to my family, who strongly supported me during the research.

Acronyms

HWC	**H**adley **W**alker **C**irculation
WSM3	**W**RF **S**ingle-**M**oment **3**-class scheme
WSM5	**W**RF **S**ingle-**M**oment **5**-class scheme
EGCP01	**E**ta **G**rid-scale **C**loud and **P**recipitation **(2001)** scheme
BMP	**B**ulk **M**icrophysical **P**arameterization
GCE	**G**oddard **C**umulus **E**nsemble
CRM	**C**loud **R**esolving **M**odel
NASA	**N**ational **A**eronautics and **S**pace **A**dmenstration
WDM5	**W**RF **D**ouble-**M**oment **5**-class scheme
PBL	**P**lanetary **B**oundary **L**ayer
YSU	**Y**on**s**ei **U**niversity
MRFM	**M**edium **R**ange **F**orecast **M**odel
LSMs	**L**and-**S**urface **M**odels
OSU	**O**hio **S**tate **U**niversity
RRTM	**R**apid **R**adiative **T**ransfer **M**odel
MSLP	**M**ean **S**ea **L**evel **P**ressure
UPC	**P**olytechnical **U**niversity of **C**atalonia
MP	**M**icro**p**hysics
NCEP	**N**ational **C**enter for **E**nvironmental **P**rediction
SOND	**S**eptember **O**ctover **N**ovember **D**ecember
GPCC	**G**lobal **P**recipitation **C**limatology **C**enter

Chapter 1

Introduction

The weather research and forecasting (WRF) model is a numerical weather predication (NWP) and atmosphere simulation system designed for both research and operational application. Therefore this study we have used WRF as a dynamical downscaling numerical model to simulate precipitation. The precipitation can be captured by using cumulus parametrization scheme for coarser grid resolution (grid separation > 10 km) and cloud physics called microphysics (MP) scheme suitable for fine grid resolution (grid separation ≤ 10 km).

In this study, our objective is to identify the microphysics skill in capturing precipitation for El Niño, La Niña, and Normal years. For this study, ten selected microphysics scheme are taken and the simulation is performed for each case keeping the other schemes identical. The domain of the study covers Ethiopia as whole with 10 km by 10 km grid resolution.

To evaluate the skill of each microphysics, statistical tools like correlation coefficient (R), bias, mean absolute error (MAE), and root mean square error (RMSE) are used. The selected season is September-December (SOND) which is east Africa's short rain season. The simulation period selected for the study are 1997 for El Niño, 1999 for La Niña, and 2004 for Normal year. The data used as observation is taken from Global precipitation

Climatology Center (GPCC) which is assimilated data from satellite observation.

This thesis consists of seven chapters in which the second chapter deals with the fundamental dynamical equations that govern the atmospheric circulation system mainly the basic governing equations interms of conservation of mass, energy, and momentum. The third chapter explains different physics scheme and especially ten microphysics schemes selected for the study. The fourth chapter describes short rain distribution, characteristics of climate, and rainfall regions over Ethiopia as documented in literature from previous studies.

Chapter five deals with methodology of the study and the employed statistical tools such as correlation coefficient, mean absolute error, root mean square error, and bias. The sixth chapter consists of result and discussion. Finally chapter seven deals with conclusion and summary.

Chapter 2

Dynamics of the Atmosphere

This chapter describes the fundamental dynamical equations that govern the atmospheric circulation system mainly the basic governing equations and atmospheric oscillation such as, El Niño and La Niña events.

2.1 Basic Conservation Laws

Atmospheric motions are governed by three fundamental physical principles:

- conservation of mass,
- conservation of momentum, and
- conservation of energy.

The mathematical relations that express these laws may be derived by considering the budgets of mass, momentum, and energy for an infinitesimal control volume in the fluid. Two types of control volume are commonly used in fluid dynamics: the Eulerian and Lagrangian [1].

In the Lagrangian frame, the control volume consists of an infinitesimal mass of "tagged" fluid particles; thus, the control volume moves about following the motion of the fluid, always containing the same fluid particle, and it is necessary to follow the time evolution

of the fields for various individual fluid parcels.

The Eulerian system is however, more convenient for solving most problems because in that system the field variables are related by a set of partial differential equations in which the independent variables are the coordinates x, y, z, and t. In this frame of reference the control volume consists of a parallelepiped of sides $\delta x, \delta y, \delta z$, whose position is fixed relative to the coordinate axes. Mass, momentum, and energy budgets will depend on fluxes caused by the flow of fluid through the boundaries of the control volume and hence Eulerian refinance frame is selected for the derivation of conservation equations.

2.1.1 Conservation of Mass

One of the three fundamental conservation principles, used to derive equation for the atmospheric motion, is the conservation of mass. The equation developed based on this principle is continuity equation.

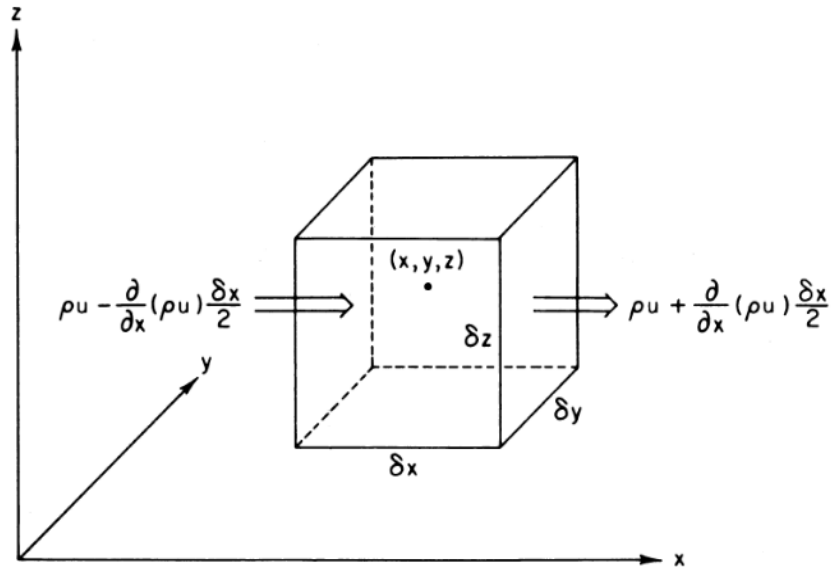

Figure 2.1: Mass inflow and mass outflow of a fixed volume element due to motion parallel to the x axis.

According to the law of conservation of mass, the net rate of mass inflow through the side must equal the rate of accumulation of mass within the volume. The rate of mass inflow per unit area through the left side is (see Fig. 2.1)

$$\rho\mathbf{U} - \frac{\partial(\rho u)}{\partial x}\frac{\delta x}{2}, \tag{2.1.1}$$

where u is velocity in the x-direction and ρ is density of air mass. And the rate of mass outflow per unit area through the right side is

$$\rho\mathbf{U} + \frac{\partial(\rho u)}{\partial x}\frac{\delta x}{2}. \tag{2.1.2}$$

Since the area of each of these faces is $\delta y\delta z$, the net rate of flow into the volume due to the x velocity component is

$$\{[\rho\mathbf{U} - \frac{\partial(\rho u)}{\partial x}\frac{\delta x}{2}] - [\rho\mathbf{U} + \frac{\partial(\rho u)}{\partial x}\frac{\delta x}{2}]\}\delta y\delta z = -\frac{\partial(\rho u)}{\partial x}\delta x\delta y\delta z. \tag{2.1.3}$$

Including y and z components and dividing by the volume $[\delta x\delta y\delta z]$ gives the rate of change of density

$$\frac{\partial\rho}{\partial t} = -[\frac{\partial(\rho u)}{\partial x} + \frac{\partial(\rho v)}{\partial y} + \frac{\partial(\rho w)}{\partial z}] \tag{2.1.4}$$

$$\frac{\partial\rho}{\partial t} = -\bigtriangledown.(\rho\mathbf{U}) \tag{2.1.5}$$

where, $\mathbf{U} = u_i + v_j + w_k$

This equation is the mass derivative form of the continuity equation, and states that the local rate of change of density is equal to minus the mass divergence [2].

2.1.2 Conservation of Momentum

Atmospheric motions are governed by Newtons second law of motion which is stated as the rate of change of momentum of an object equals the sum of all the forces acting on it. Even if Newton's laws of motion are applicable in all inertial reference frame, they

need some modification to make them applicable in non-inertial reference frame. This modification evolves the addition of some fictious forces, Newton's second law of motion (in an inertial reference frame) may be symbolically written as

$$\frac{d_\alpha \mathbf{U}_\alpha}{dt} = \Sigma \mathbf{F}. \tag{2.1.6}$$

The left-hand side represents the rate of change of the absolute velocity $\mathbf{U}_\alpha$, following the motion as viewed in an inertial system. The right-hand side represents the sum of all forces (real and apparent) acting per unit mass. When the motion is viewed in a rotating coordinate system certain additional apparent forces must be included if Newton's second law is to be valid. The same result may be obtained by a formal transformation of coordinates in Eq. (2.1.6).

In order to transform Eq. (2.1.6) to rotating coordinates (e.g on the earth). The relationship between $\mathbf{U}_\alpha$ and the velocity relative to the rotating system $\mathbf{U}$ (earth) is obtained by applying the total derivative to the position vector r for an air parcel on the rotating earth:

$$\frac{D_\alpha r}{Dt} = \frac{Dr}{Dt} + \Omega \times r \tag{2.1.7}$$

but $\frac{D_\alpha r}{Dt} \equiv \mathbf{U}_\alpha$ and $\frac{Dr}{Dt} \equiv \mathbf{U}$; therefore Eq (2.1.7) may be written as

$$\mathbf{U}_\alpha = \mathbf{U} + \Omega \times r \tag{2.1.8}$$

which states simply that the absolute velocity of an object on the rotating earth is equal to its velocity relative to the earth plus the velocity due to the rotation of the earth. Now we apply Eq. (2.1.7) to the velocity vector $\mathbf{U}_\alpha$ and obtain

$$\frac{D_\alpha \mathbf{U}_\alpha}{Dt} = \frac{D\mathbf{U}_\alpha}{Dt} + \Omega \times \mathbf{U}_\alpha \tag{2.1.9}$$

Substituting from Eq. (2.1.8) into the right-hand side of Eq. (2.1.9) gives

$$\frac{D_\alpha \mathbf{U}_\alpha}{Dt} = \frac{D(\mathbf{U} + \Omega \times r)}{Dt} + \Omega \times (\mathbf{U} + \Omega \times r) = \frac{D\mathbf{U}}{Dt} + 2\Omega \times \mathbf{U} - \Omega^2 \times R \tag{2.1.10}$$

where Ω is assumed to be constant. Here R is a vector perpendicular to the axis of rotation, with magnitude equal to the distance to the axis of rotation, so that with the aid of a vector identity.

$$\Omega \times (\Omega \times r) = \Omega \times (\Omega \times R) = -\Omega^2 \times R \tag{2.1.11}$$

Eq. (2.1.10) states that the acceleration following the motion in an inertial system equals the rate of change of relative velocity following the relative motion in the rotating frame plus the Coriolis acceleration due to relative motion in the rotating frame plus the centripetal acceleration caused by the rotation of the coordinates. The real and apparent forces acting on the atmosphere are the pressure gradient force, gravitation, and friction and Newton's second law Eq. (2.1.6) with the aid of Eq. (2.1.10) becomes

$$\frac{D\mathbf{U}}{Dt} = -\frac{1}{\rho} \bigtriangledown P + g + F_r \tag{2.1.12}$$

where F_r designates the frictional force per unit mass, and the centrifugal force has been combined with gravitation in the gravity term g. The vectorial form of momentum equation, is the statement of Newton's second law for motion relative to a rotating coordinate frame becomes

$$\frac{D\mathbf{U}}{Dt} = -2\Omega\mathbf{U} - \frac{1}{\rho} \bigtriangledown P + g + F_r \tag{2.1.13}$$

It states that the acceleration following the relative motion in the rotating frame equals the sum of the Coriolis force, the pressure gradient force, effective gravity, and friction force per unit mass. This form of the momentum equation is basic to most work in dynamic meteorology.

2.1.3 Conservation of Energy

The third fundamental principle of atmospheric dynamics is the conservation of energy which can be described in terms of the first law of thermodynamics. The first law of

thermodynamics states that the change in internal energy of the system is equal to the difference between the heat added to the system and the work done by the system. i.e,

$$d\mathbf{U} = dQ - dW \tag{2.1.14}$$

where, d**U**=C_vdT, dW =PdV

where, C_v=specific heat capacity at a constant volume, dT=change of temperature, P=pressure, and dV change of volume.

The above equation relates the change in temperature of a parcel of air to energy transfer between the parcel of air and the environment and work done by or on a parcel. If energy is added to the system, then some of it is used to change the internal energy (and temperature) and the rest is used by the parcel of air to do work. Energy is released to the air during condensation of water vapor, deposition of water vapor, freezing of liquid water. Energy is removed from the air during melting of ice, sublimation of ice, and evaporation of liquid water [3].

The thermodynamic state of the atmosphere at any point is determined by the values of pressure, temperature, and density (or specific volume) at that point. These field variables are related to each other by the equation of state for an ideal gas. A real gas is ideal only to the extent that intermolecular forces are small, which occurs when pressures are low enough or temperatures are high enough for the gas to be sufficiently dilute.

The equation of state for dry air is expressed as

$$P\alpha = RT, \tag{2.1.15}$$

where R is the gas constant for dry air and $\alpha \equiv \frac{1}{\rho}$ is specific volume. The energy exchange equations in the atmosphere can be derived by combining the first law of thermodynamics (Eq. 2.1.14) with equation of state (Eq. 2.1.15) for an air parcel as

$$dQ = C_v dT + Pd\alpha. \tag{2.1.16}$$

Since $d(P\alpha) = Pd\alpha + \alpha dP$, we can rewrite the above equation as

$$dQ = C_v dT + d(P\alpha) - \alpha dP \tag{2.1.17}$$

From equation of state, $d(P\alpha)$= RdT and using $C_p = C_v$ + R, we obtain

$$dQ = (C_v + R)dT - \alpha dP = C_p dT - \alpha dP \tag{2.1.18}$$

and by substituting $\alpha = \frac{1}{\rho}$ and rearranging gives the thermodynamic energy equation;

$$dT = \frac{1}{C_p} dQ + \frac{1}{\rho C_p} dP. \tag{2.1.19}$$

2.2 El Niño Events

El Niño is a warm, nutrient poor, ocean current that flows southward along the coast of northern Peru [4] and creates sometimes catastrophic effects on local and sometimes global fishing and biogeochemical systems. This event, named El Niño (the Christ Child) because it occurs around Christmas time, was once thought of as happening only abnormally. It is known now, however, that El Niño is actually the result of a Pacific Ocean oriented cycle that lasts from three to five years. The event itself lasts about 12 to 18 months.

The El Niño or, more precisely, the El Niño Southern Oscillation (ENSO), for which it and its related phenomena are called, is produced primarily by the interaction between the winds in the atmosphere and the sea surface in the Pacific Ocean. This interaction is tracked by observing, through remote satellites, the changing patterns of sea surface temperatures in the Pacific, sea level changes, and pressure oscillations. Two types of waves are especially important for El Niño: internal Kelvin waves and Rossby waves. Both waves can have modes that are conned to a narrow, north-south region centered on the equator. These are equatorial trapped waves. Both exist in slightly different forms at higher latitudes.

Ethiopia is facing a massive drought and food insecurity crisis. The impact of failed rains and droughts have been worsened by the 2015 El Niño, which itself has been supercharged by climate change. **U**rgent humanitarian action is needed to support millions of people who have lost food, water, and livelihoods. And long-term investment is needed so that communities can become more resilient and reduce their vulnerability to weather events in the future [5].

2.3 La Niña Events

La Niña is described as cooler-than-normal sea surface temperatures in the central and eastern Pacific Ocean, near the equator off the west coast of South America. La Niña the trade winds (winds that flow toward the equator) blow from east to west across the coastal waters of the eastern Pacific. In doing so, they drag the warm surface waters of the equatorial Pacific with them. This causes an upwelling of cooler, nutrient-rich waters on which the fish population in the region depends on. This 'air/sea interaction' is accompanied by the circulation of large internal waves (waves that have their peaks under the ocean surface) across the Pacific ocean mainly in the equatorial region. These internal waves are referred to as Kelvin and Rossby waves [6].

Kelvin waves travel eastward along the equator and are not subjected to the Coriolis force. Rossby waves, unlike Kelvin waves, travel westward and are a result of the changes that the Kelvin waves introduced to the area. Rossby waves, since they move away, but parallel, to the equator are not relieved of the Coriolis force; thus they travel up to about three times slower.

La Niña is the name given to the cooling of the surface of the central and eastern Pacific Ocean that occurs every two to five years. It keeps East Africa drier than usual and sparks food-security concerns in areas lacking irrigation, including parts of Somalia, Kenya, Ethiopia and Tanzania.

Chapter 3

Physics Package

3.1 Introduction

Cloud physics is the study of the physical processes that lead to the formation, growth and precipitation of atmospheric clouds. Clouds consist of microscopic droplets of liquid water (warm clouds), tiny crystals of ice (cold clouds), or both (mixed phase clouds). Cloud droplets initially form by the condensation of water vapor onto condensation nuclei when the supersaturation of air exceeds a critical value according to Kõhler theory [7, 8, 9]. Cloud condensation nuclei are necessary for cloud droplets formation because of the Kelvin effect, which describes the change in saturation vapor pressure due to a curved surface. At small radii, the amount of supersaturation needed for condensation to occur is so large, that it does not happen naturally. Raoult's Law describes how the vapor pressure is dependent on the amount of solute in a solution. At high concentrations, when the cloud droplets are small, the supersaturation required is smaller than without the presence of a nucleus.

In 1847 Agustus Waller used spider web to examine droplets under the microscope [10]. In this chapter all are going to explain selected physics package such as microphysics, cumulus parameterization, planetary boundary layer, Land Surface model, Atmospheric Radiation physics, and Surface Layer physics.

3.2 Microphysics Schemes

Microphysics includes explicitly resolved water vapor, cloud, and precipitation processes. The model is general enough to accommodate any number of mass mixing-ratio variables, and other quantities such as number of concentrations. For this study we have used ten cloud microphysics namely Kessler, Lin et al (purdue), WRF Single-Moment 3-class, WRF Single-Moment 5-class, Eta (Ferrier), WRF Single-Moment 6-class, Goddard microphysics, New Thompson et al., Morrison double-moment, and WRF Double-Moment 5-class scheme.

3.2.1 Kessler Scheme

Kessler scheme is a simple warm cloud scheme that includes water vapor, cloud water, and rain. The microphysical processes included are: the production, fall, and evaporation of rain.

Kessler [11] pioneered the introduction of the effect of varying updraughts into cloud models. In his approach, all water is first condensed as cloud water, with small drop size (roughly $5-30\mu m$) and negligible terminal velocity. Then a process called autoconversion begins. This involves the formation of precipitation particles either by the aggregation of several cloud particles or by the action of giant salt nuclei, or similar processes [12].

.

3.2.2 Purdue Lin Scheme

In Purdue Lin microphysics scheme, six classes of hydrometers are included: water vapor, cloud water, rain, cloud ice, snow, and grapple. All parameterization production terms are based on with some modifications, including saturation adjustment following and ice sedimentation [13, 14, 15]. The cloud water and cloud ice particles are assumed to be small enough so that their terminal velocity is very insignificant. Rain, snow and hail

possess appreciable terminal velocities. This is a relatively sophisticated microphysics scheme in WRF, and it is most suitable for use in research studies. The scheme is taken from the Purdue cloud model.

3.2.3 WRF Single-Moment 3-class (WSM3) Scheme

WRF Single-Moment 3-class (WSM3) scheme predicting mixing ratio of three species (water vapor, and cloud water/ice and rain/snow) based on Hong et al [16]. It follows Dudhia in assuming cloud water and rain for temperatures above freezing, and cloud ice and snow for temperatures below freezing. This scheme is computationally efficient for the inclusion of ice processes, but lacks supercooled water and gradual melting rates. This scheme is computationally efficient for the inclusion of ice processes, but lacks supercooled water and gradual melting rates [17].

3.2.4 WRF Single-Moment 5-class (WSM5) Scheme

WSM5 is similar to the WSM3 simple ice scheme. It includes, vapor, rain, snow, cloud ice, and cloud water are held in five different arrays. WSM5 allows supercooled water to exist and gradual making of snow falling below the melting layer. The scheme is efficient in intermediate grids between the mesoscale and cloud resolving grids [17].

3.2.5 WRF Single-Moment 6-class (WSM6) Scheme

WSM6 scheme has been developed by adding additional processes related to graupel to WSM5 scheme. It includes six variables namely: water vapor, cloud water, cloud ice, snow, rain and graupel.

A new method for representing mixed-phase particle fall speeds for the snow and graupel particles by assigning a single fallspeed to both that is weighted by the mixing ratios, and applying that fallspeed to both sedimentation and accretion processes is introduced in Dudhia et al [17]. The behavior of the WSM3, WSM5, and WSM6 schemes differ little

for coarser mesoscale grids, but they work much differently on cloud-resolving grids. Of the three WSM schemes, the WSM6 scheme is the most suitable for cloud-resolving grids, considering the efficiency and theoretical backgrounds [18].

3.2.6 Eta Grid-scale Cloud and Precipitation (2001) Scheme

This is also known as the Eta Ferrier scheme. The scheme predicts changes in water vapor and condensate in the forms of cloud water, rain, cloud ice, and precipitation ice (snow/graupel/sleet). The individual hydrometer fields are combined into total condensate, and it is the water vapor and total condensate that are advocated in the model. Local storage arrays retain first-guess information that extract contributions of cloud water, rain, cloud ice, and precipitation ice of variable density in the form of snow, graupel, or sleet. The density of precipitation ice is estimated from a local array that stores information on the total growth of ice by vapor deposition and accretion of liquid water. Sedimentation is treated by partitioning the time averaged flux of precipitation in to a grid box between local storage in the box and fall out through the bottom of the box. This approach, together with modifications in the treatment of rapid microphysical processes, permits large time steps to be used with stable results. The mean size of precipitation ice is assumed to be a function of temperature [19].

3.2.7 New Thompson et al. Scheme

A new scheme with ice, snow and graupel processes suitable for high-resolution simulations. A new bulk microphysical parameterization (BMP) has been developed for use with WRF or other mesoscale models. Compared to earlier single-moment BMPs, the new scheme incorporates a large number of improvements to both physical processes and computer coding plus employs many techniques found in far more sophisticated spectral/bin schemes using look-up tables. Unlike any other BMP, the assumed snow size distribution depends on both ice water content and temperature and is represented as a sum of exponential and gamma distributions. Furthermore, snow assumes a nonspherical shape with a bulk

density that varies inversely with diameter as found in observations and in contrast to nearly all other BMPs that assume spherical snow with constant density. New features specific to this version of the bulk scheme details are discribed by the Thompson et al. [20].

- generalized gamma distribution shape for each hydrometeor species,
- non-spherical, variable density snow, and size distribution matching observations,
- y-intercept of rain depends on rain mixing ratio and whether apparent source is melted,
- y-intercept of graupel depends on graupel mixing ratio,
- a more accurate saturation adjustment scheme,
- variable gamma distribution shape parameter for cloud water droplets based on observations,
- look-up table for freezing of water drops,
- look-up table for transferring cloud ice into snow category,
- improved vapor deposition/sublimation and evaporation,
- variable collection efficiency for rain, snow, and graupel collecting cloud droplets, and
- improved rain collecting snow and graupel.

3.2.8 Goddard Cumulus Ensemble Model Scheme

GCE model, a cloud resolving model (CRM), has been developed and improved at National Aeronautics and Space Administration (NASA) Goddard Space Flight Center over the past two decades. The development and main features of the GCE model were

published in Tao and Simpson [21].

The Goddard microphysics schemes have several modifications, such as an option to choose insure super saturation (sub-saturation) give a guarantee that all sink process associated one species will not exceed its mass for water budget.

3.2.9 Morrison et al. 2-Moment Scheme

The Morrison scheme is based on the two-moment bulk microphysics scheme of Morrison and Pinto [22]. Six species of water are included: vapor, cloud droplets, cloud ice, rain, snow, and graupel/hail. Prognostic variables include number concentrations and mixing ratios of cloud ice, rain, snow, and graupel/hail, and mixing ratios of cloud droplets and water vapor (total of 10 variables).

3.2.10 WRF Double-Moment 5-class (WDM5) Scheme

WDM5 scheme is a mixed ice bulk microphysics scheme. It predicts not only the mixing ratio of hydrometer but also their number concentrations for warm rain species including clouds and rain. In this scheme cloud condensation nuclear (CCN), and number concentrations of cloud and rain are predicts.

3.3 Cumulus Parameterization

Cumulus parameterizations are theoretically only valid for coarser grid sizes, (e.g., greater than 10 km), where they are necessary to properly release latent heat on a realistic time scale in the convective columns. While the assumptions about the convective eddies being entirely sub-grid-scale break down for finer grid sizes, sometimes these schemes have been found to be helpful in triggering convection in 5-10 km grid applications. Generally, they should not be used when the model can resolve the convective eddies itself ($e.g., \leq 5km$

grid). In these study we use only Kain-Fritsch scheme.

The Kain-Fritsch [23] cumulus parameterization will be used for this study. This scheme uses a sophisticated cloud mixing scheme to determine entrainment/detrainment and removing all available buoyant energy in the relaxation time. This scheme also predicts both updraft and downdraft properties.

3.4 Planetary Boundary Layer Scheme

The planetary boundary layer (PBL) is responsible for vertical sub-grid-scale fluxes due to eddy transports in the whole atmospheric column, not just the boundary layer. Thus, when a PBL scheme is activated, explicit vertical diffusion is de-activated with the assumption that the PBL scheme will handle this process. In this study, we use only Yonsei University (YSU) PBL.

The Yonsei University PBL is the next generation of the Medium Range Forecast Model (MRF) PBL, also using the counter gradient terms to represent fluxes due to non-local gradients. This adds to the MRF PBL an explicit treatment of the entrainment layer at the PBL top. The entrainment is made proportional to the surface buoyancy flux in line with results from studies with large-eddy models [24].

3.5 Land Surface Model

The land-surface models (LSMs) use atmospheric information from the surface layer scheme, radiative forcing from the radiation scheme, and precipitation forcing from the microphysics and convective schemes, together with internal information on the lands state variables and land-surface properties, to provide heat and moisture fluxes over land points and sea-ice points. In these study we have used Noah Land Surface Model (LSM) scheme.

Noah-MP is a land surface model (LSM) using multiple options for key land-hydrology processes. Noah-MP contains a separate vegetation canopy defined by a canopy top and bottom; crown radius; and leaves with prescribed dimensions, orientation, density, and radiometric properties. The canopy employs a two-stream radiation transfer approach along with shading effects necessary to achieve proper surface energy and water transfer processes including under-canopy snow processes. Noah-MP contains a multi-layer snow pack with liquid water storage and melt/refreeze capability and a snow-interception model describing loading/unloading, melt/refreeze capability, and sublimation of canopy-intercepted snow [25].

3.6 Atmospheric Radiation Physics

The radiation schemes provide atmospheric heating due to radiative flux divergence and surface downward long wave and shortwave radiation for the ground heat budget. Long wave radiation includes infrared or thermal radiation absorbed and emitted by gases and surfaces. Shortwave radiation includes visible and surrounding wavelengths that make up the solar spectrum.

In this study long wave radiation physics used to Rapid radiative transfer Model(RRTM) scheme is specially used. RRTM scheme is the rapid and accurate radiative transfer model (RRTM) aims to calculate fluxes and cooling rates comparable with the line-by-line radiative transfer model (LBLRTM), while performing a smaller number of radiative transfer operations. Short wave radiation physics used Dudhia scheme which is Simple downward integration allowing for efficient cloud and clear-sky absorption and scattering [17].

3.7 Surface Layer Physics

The lowest layer of the atmosphere, the surface layer, directly influences the daily activities of nearly all life on planet Earth. Extending up to an altitude of order 50-100 meters, it possesses physical and chemical properties long recognized as having a controlling influence over a wide range of human and societal interests. In this study we have used only Mesoscale Meteorological version 5 (MM5) scheme [26].

Chapter 4

Short Rain over Ethiopia

4.1 Introduction

Interannual fluctuation of short rains affects agriculture, drinking water, health, power, and the very livelihood of millions over equatorial East Africa. The climate of equatorial Eastern Africa is dominated by September to November (short rains) [27].
This chapter deals with Characteristics of climate, and rainfall regions over Ethiopia.

4.2 Characteristics of Climate in Ethiopia

Ethiopia is in the tropical zone lying between the Equator and the Tropic of Cancer. Ethiopia has three different climate zones according to elevation.

- **Kolla** (Tropical zone) - is below 1830 meters in elevation and has an average annual temperature of about 27 degree Celsius with annual rainfall about 510 millimeters.

- **Woina dega** (Subtropical zone) - includes the highlands areas of 1830 - 2440 meters in elevation has an average annual temperature of about 22 degree Celsius with annual rainfall between 510 and 1530 millimeters.

- **Dega** (Cool zone) - is above 2440 meters in elevation with an average annual temperature of about 16 degree Celsius with annual rainfall between 1270 and 1280 millimeters [28].

In most parts of Ethiopia, precipitation increases with elevation. However, there are also regions where the annual amount of precipitation decreases with height, most importantly in the northern and southern mountainous regions [29]. Precipitation increases up to about 2000 m.a.s.l., then decrases with elevation. It is suggested that the main cause of decreasing precipitation with height is moisture depletion, as most of the moisture is released as rain before reaching the top of the mountains [30].

Ethiopia has three climatological seasons: The main rainy season of June-September (Kiremt), and the dry season of October-January (Bega), the Belg rainy season of February/March-May. It should be noted that this is seen from a highland perspective [31].

4.3 Rainfall Regions in Ethiopia

The rainfall region in Ethiopia is characterised as uni-modal and bi-modal systems influenced by topographical variation in the country, seasonal cycles and opposing responses to regional and global weather systems. Accordingly, the rainfall over Ethiopia is commonly grouped into three; regions **A**, regions **B**, and regions **C**, as shown in Fig 4.1 [32].

The region **A** includes the central and the eastern part of Ethiopia. This region has a bi-modal rain. The long rainy season (June-September) and short rain season (March-May). The rest of the months (October to February) are dry period.

The region **B** includes the western part of the country (from southwest through to northwest) has uni-modal rainfall pattern (June-September), and the rainy period ranges from February through November mainly in the western and south-western part of the country, and decreases northwards.

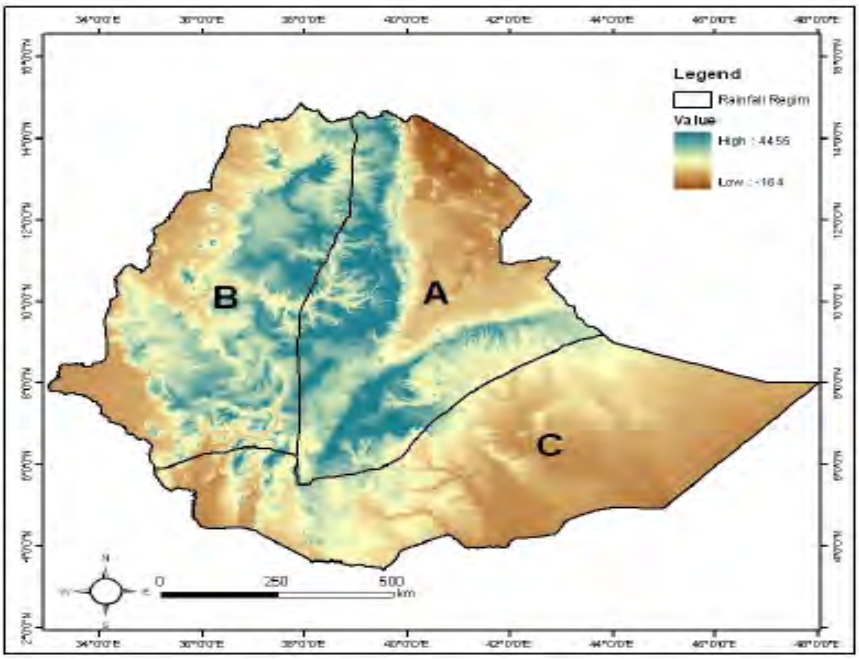

Figure 4.1: Topographic map of Ethiopia showing rainfall regimes (Modified from NMSA, 1996)

The region **C** includes the south and south-eastern part of Ethiopia has two distinct wet and dry seasons. The main rain season is from February through May, and short rains from October to November, and the dry periods are June to September and December to February.

Chapter 5

Data and Methodologies

This chapter gives overview of data sets used for validation, data analysis methods, model description and domain of study. After describing bias, root mean square error, mean absolute error and correlation coefficient, weather research forecasting (WRF) technique used in this study is briefly discussed. We have used 10 types of cloud microphysics, running once for each microphysics scheme keeping the other scheme the same. The simulated results have been compared with observation.

5.1 Model Description

To test how we can model precipitation during the three extrem years El Niño (1997), La Niña (1999), and Normal year (2004) over Ethiopia, we have used the weather research and forecasting (WRF) model. The simulation domains is delimited using one domain with horizontal grid separation 10 km by 10 km which covers Ethiopia and surroundings. For this study, the physics schemes used are summarized in Table 5.1.

NO	Physics Scheme	Scheme type
1	Kessler (MP1)	Microphysics
2	Lin (Purdue) (MP2)	Microphysics
3	WSM3 (MP3)	Microphysics
4	WSM5 (MP4)	Microphysics
5	Eta (Ferrier) (MP5)	Microphysics
6	WSM6 (MP6)	Microphysics
7	Goddard (MP7)	Microphysics
8	Thompson (MP8)	Microphysics
9	Merrison 2-momunt (MP10)	Microphysics
10	WRF Double-Moment 5-class scheme (MP14)	Microphysics
11	Yonsei University Scheme (YUS)	Planetary BL
12	Mesoscale Model Version 5 Similarity Scheme (MMS)	Surface layer
13	Noah Land Surface Model	Land Surface layer
14	Kain Fritsch Scheme	Cumulos Parametrization
15	Rapid radiative transfer model (RRTM)	Long wave radiation
16	Dodiha	Short wave radiation

Table 5.1: Physics schemes used in this study.

During the simulation the radiation physics rapid radiative transfer model (RRTM) for long wave radiation, Dodiha for short wave radiation Yonsei University Scheme (YUS) for planetary boundary layer, Mesoscale Model Version 5 Similarity Scheme (MMS) for surface layer physics, Noah land surface model for land surface layer physics, Kain Fritsch Scheme for cumulus physics are common for a domain. The experiment (simulation) is done for each cloud microphysics namely; Kessler, Purdue Lin, WRF single moment 3-class, WRF single moment 5-class, WRF single moment 6-class, Eta (Ferrie), Goddard, New Thompson, Merrison 2-momunt, WRF Double-Moment 5-class scheme.

5.2 Area of Study

The region taken for the experiment (simulation) covers from 32^o - 48^{o}E longitude and 2^o - 16^o N latitude which covers Ethiopia as a whole and some part of Kenya, Somalia, Djibouti as a whole, Eritrea and Sudan. The analysis using statistical tools are considered over Ethiopia (Fig. 5.1).

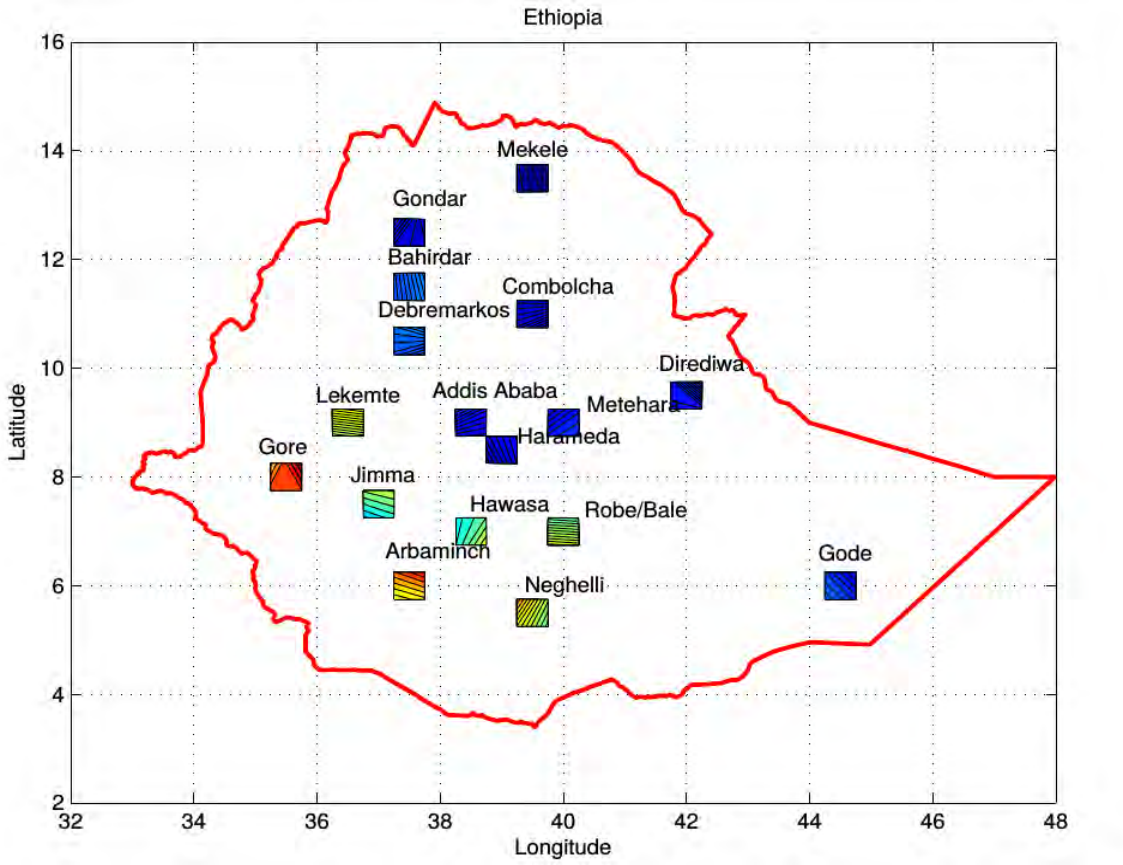

Figure 5.1: Study area Latitude vs Longitude, for the domain

5.3 Validation Data

In most cases, gridded data sets of observations are used for the validation of the simulated precipitation. In this study validation data used Global Climatology Precipitation Center (GPCC) data with a horizontal grid separation 50 km by 50 km [33].

The Global Precipitation Climatology Center (GPCC) provides the international research community with monthly precipitation analyses based on in-situ observed data from rain gauge networks. In particular, the Center delivers the in-situ basis (its so called Monitoring Product) for the satellite-gauge combinations of GPCP and NCEP, but in general, it contributes to analysis of monitoring and research activities related to climate and water. The technical functions comprise data collection, quality control, spatial analysis, and error quantification.

The aim of the GPCC is to serve user requirements spatially with regard to accuracy of the gridded precipitation analyses and timeliness of the product availability.

5.4 Statistical Tools

The performance of the ten options of microphysics schemes in WRF is evaluated quantitatively by analyzing the bias, root mean square error, mean absolute error, and correlation coefficient of the simulations relative to the observation data.

Bias

The primary measure of simulation skill is the model bias (a time average of the error), defined as the average of the difference between the observed and simulated precipitation. Mathematically it is given by the equation

$$Bias = \frac{1}{n}\Sigma(y_p - y_o) \tag{5.4.1}$$

where y_p is predicated (model values), y_o is observed values, and n is number of observations.

For the difference between simulated and observed (measured) values (precipitation in this case) are not squared, it can be either positive or negative. Negative bias indicate underestimation and positive shows overestimation. A small bias indicates that the

model has good skill in capturing precipitation [34].

Root Mean Square Error

The root mean square error (RMSE) represents the sample standard deviation of the difference between predicted and model values. A small value indicates better model performance and vice versa. In equation form RMSE is given by the equation

$$RMSE = \sqrt{\frac{\Sigma(y_p - y_o)^2}{n}}. \tag{5.4.2}$$

The RMSE is a quadratic scoring rule which measures the average magnitude of the error. The equation for the RMSE is given in both of the references. Expressing the formula in words, the difference between forecast and corresponding observed values are each squared and then averaged over the sample. Finally, the square root of the average is taken. Since the errors are squared before they are averaged, the RMSE gives a relatively high weight to large errors. This means the RMSE is most useful when large errors are particularly undesirable.

Correlation Coefficient

A correlation coefficient measures the strength and direction of a linear association between two variables. The correlation coefficient between simulated and observed quantity is defined as

$$R = \frac{\Sigma(y_{pi} - \bar{y_p})(y_{oi} - \bar{y_o})}{\sqrt{(\Sigma(y_{pi} - \bar{y_p})^2)(\Sigma(y_{oi-\bar{y_o}})^2)}} \tag{5.4.3}$$

The value of correlation coefficient is between zero and one. When the value is near to one the simulated value is highly related with the observed or measured value. On the

other hand when the value is very small or near to zero, the simulated value is unrelated with the measured or observed value and said to be uncorrelated. If the value is negative, the two values correlated inversely that means as one increase the other decreases [34].

Mean Absolute Error (MAE)

Mean absolute error (MAE) measures the average magnitude of the errors in a set of forecasts, without considering their direction. It measures accuracy for continuous variables. The MAE is a linear score which means that all the individual differences are weighted equally in the average. Mathematically it is defined as

$$MAE = \frac{\Sigma|y_p - y_o|}{n} = \frac{\Sigma e_i}{n} \tag{5.4.4}$$

As the name suggests, the mean absolute error is an average of the absolute errors $e_i = |y_p - y_o|$, where y_p is the prediction and y_o the true value.

Chapter 6

Results and Discusions

6.1 Introduction

This chapter examines the precipitation that are obtained from the WRFV3 simulation for ten different microphysics using global climate model (GCM) data as a lateral boundary forcing and initial conditions for the El Niño, La Niña, and Normal year. The results of model Precipitation from all microphysics are compared with observed precipitation [33]. The statistical tools used to determine the best microphysics are bias, root mean square error, mean absolute error, and correletion coefficient.

6.2 Grid Scale Precipitation Compared to Observed Precipitation for El Niño Year (1997)

6.2.1 Accumulated Total Grid Scale Precipitation over Ethiopia

Accumulated total grid scale precipitation captured by all the selected microphysics and accumulated observation precipitation (GPCC) using contour plot is given in Fig. 6.1. The figure roughly shows that the maximum GPCC precipitation is observed along the western and southern territory of the country whereas the model precipitation maximum values are shifted to the center except MP1. Concerning the maximum value, the observed (GPCC) precipitation is same as MP2, MP3, MP4, MP6, MP7, MP8, MP10, and MP14

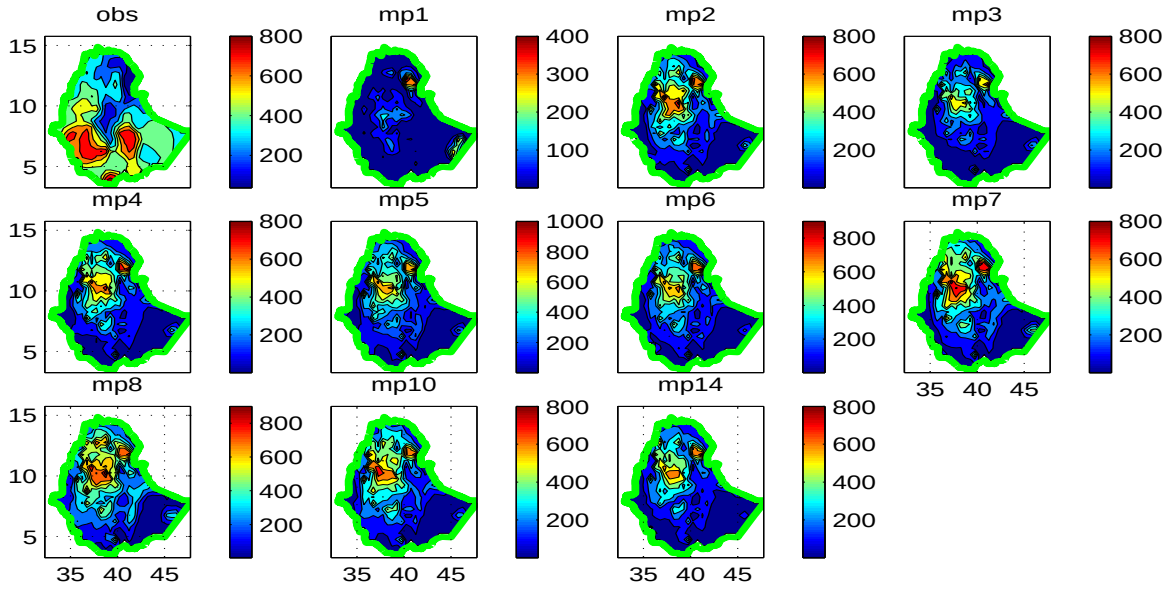

Figure 6.1: Precipitation over Ethiopia: Accumulated total grid scale precipitation and GPCC accumulated precipitation.

precipitation which is 800 mm. The rest two micro physics, MP1, and MP5 have captured a maximum of 400 mm and 1000 mm, respectively.

6.2.2 Grid Scale Accumulated Precipitation for Selected Places

To identify the best MP accumulated precipitation, line plots are considered for the selected places. The plot for the country and each selected places are given hereunder. Fig 6.2 shows that eventhough all MP underestimate the GPCC precipitation, the order of precipitation capturing skill is MP8, MP7, MP5, MP10, MP2, MP6, MP4, MP14, MP3, and MP1.

The accumulated total grid scale precipitation and the accumulated GPCC precipitation line plot for the selected sample region also given in Fig. 6.3.

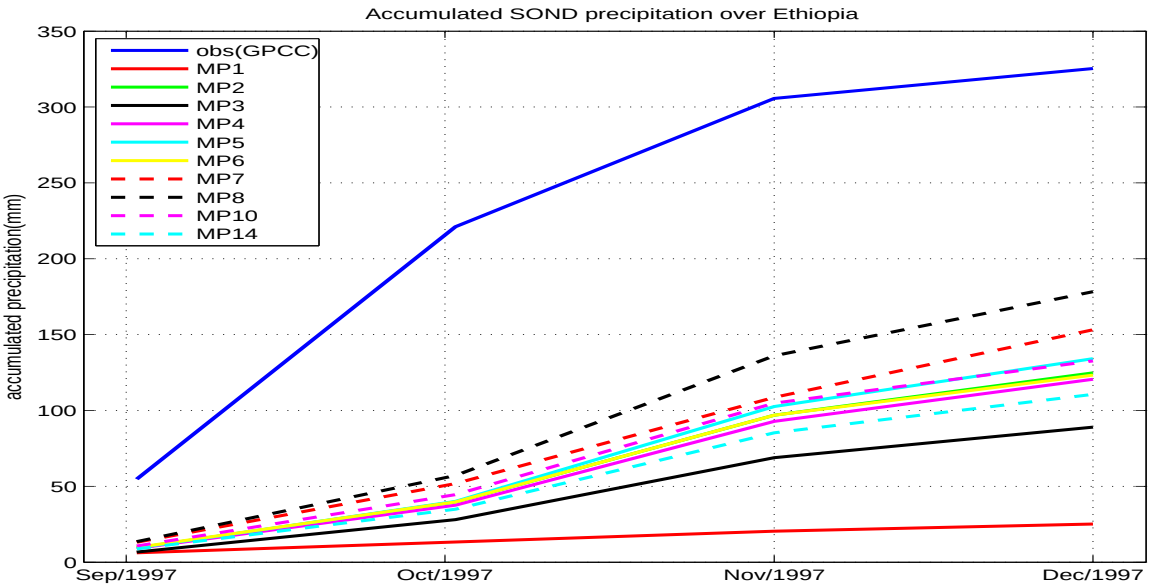

Figure 6.2: Accumulated total grid precipitation and GPCC accumulated precipitation line plot using spatial mean for Ethiopia.

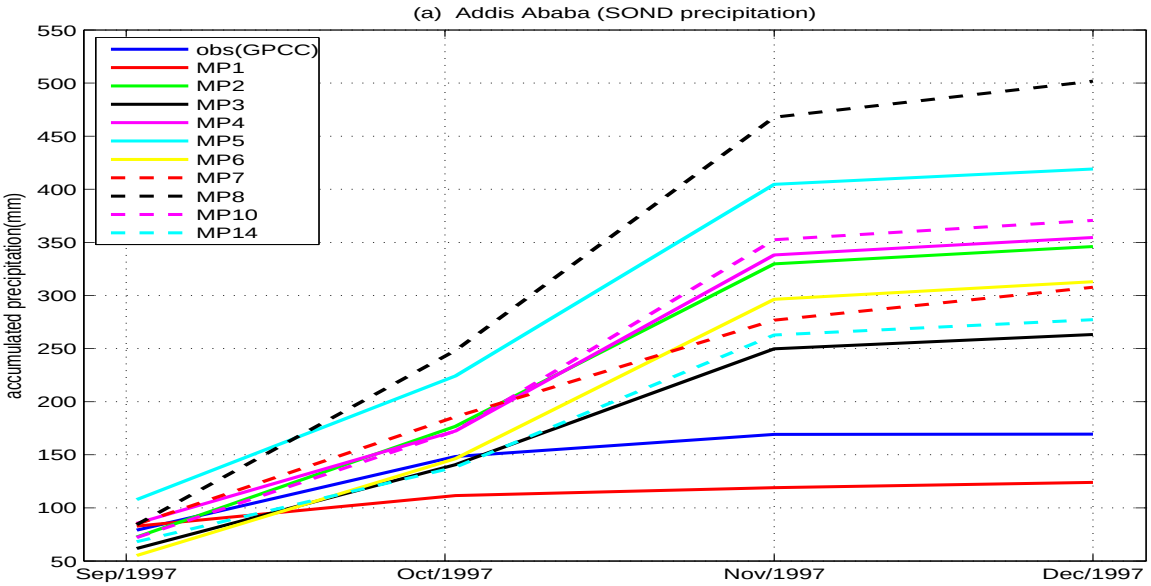

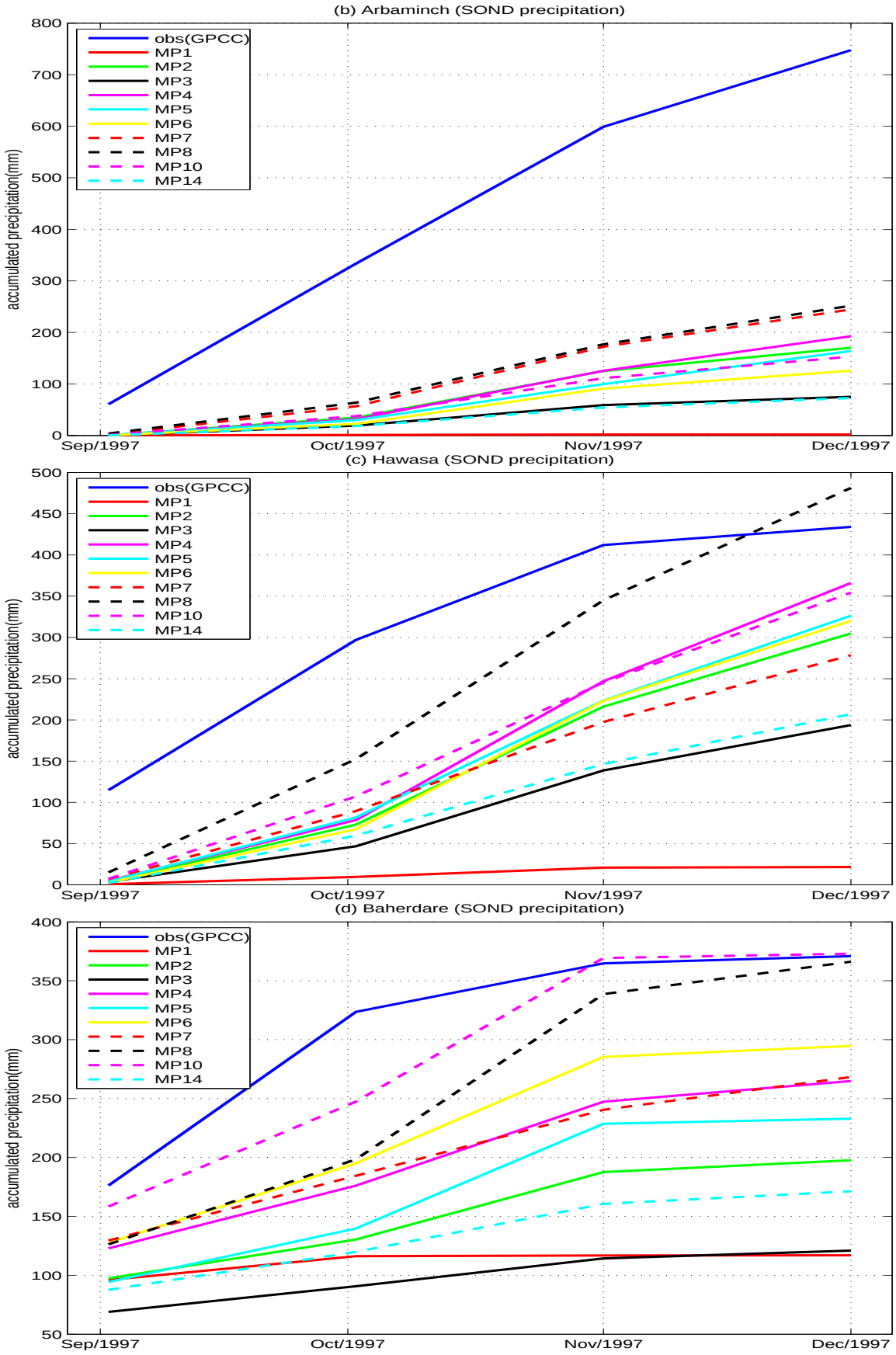
(b) Arbaminch (SOND precipitation)
accumulated precipitation(mm)
obs(GPCC)
MP1
MP2
MP3
MP4
MP5
MP6
MP7
MP8
MP10
MP14
Sep/1997
Oct/1997
Nov/1997
Dec/1997
(c) Hawasa (SOND precipitation)
accumulated precipitation(mm)
(d) Baherdare (SOND precipitation)
accumulated precipitation(mm)

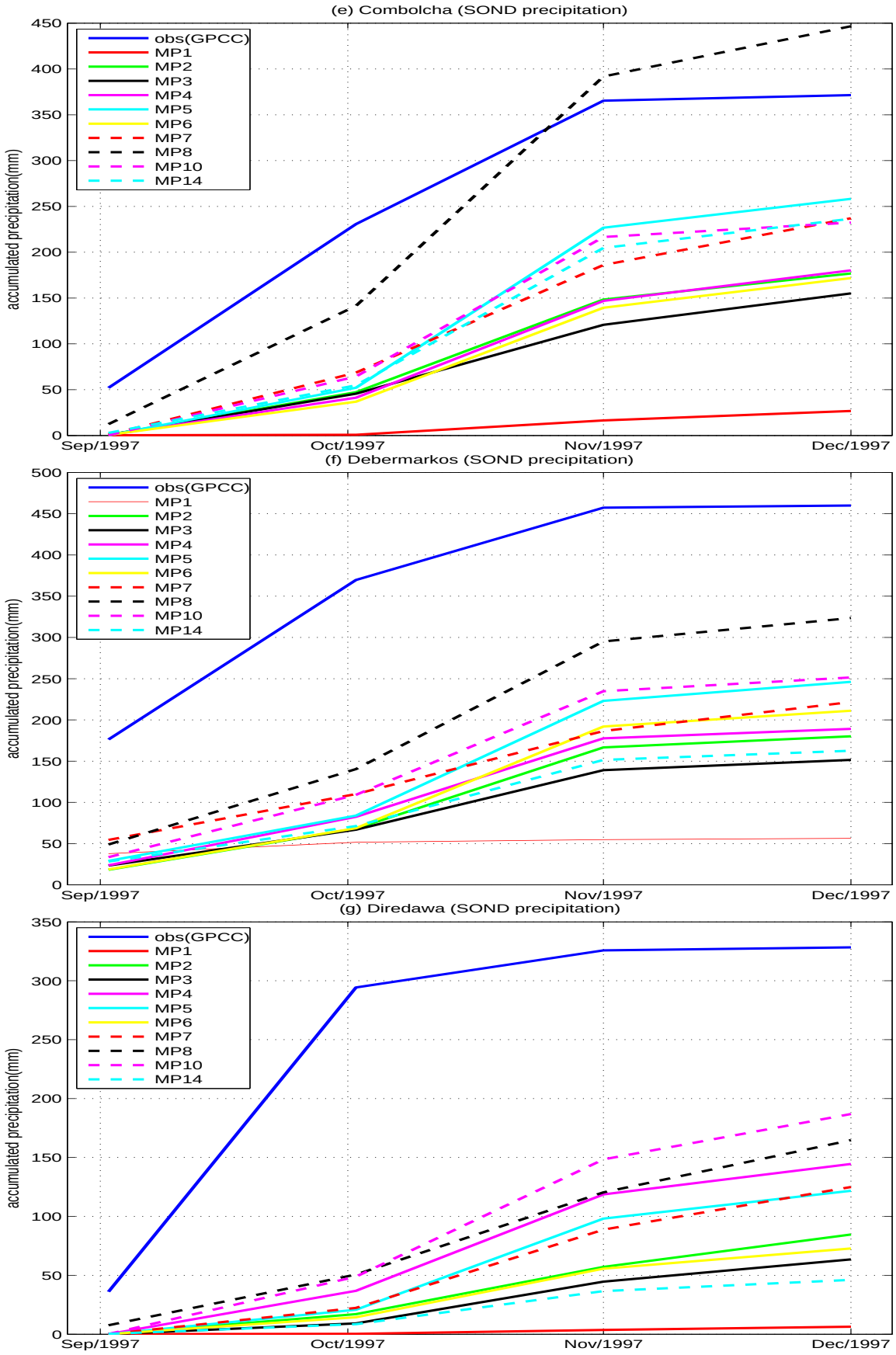
(e) Combolcha (SOND precipitation)
accumulated precipitation(mm)
obs(GPCC)
MP1
MP2
MP3
MP4
MP5
MP6
MP7
MP8
MP10
MP14
Sep/1997
Oct/1997
Nov/1997
Dec/1997
(f) Debermarkos (SOND precipitation)
accumulated precipitation(mm)
obs(GPCC)
MP1
MP2
MP3
MP4
MP5
MP6
MP7
MP8
MP10
MP14
Sep/1997
Oct/1997
Nov/1997
Dec/1997
(g) Diredawa (SOND precipitation)
accumulated precipitation(mm)
obs(GPCC)
MP1
MP2
MP3
MP4
MP5
MP6
MP7
MP8
MP10
MP14
Sep/1997
Oct/1997
Nov/1997
Dec/1997

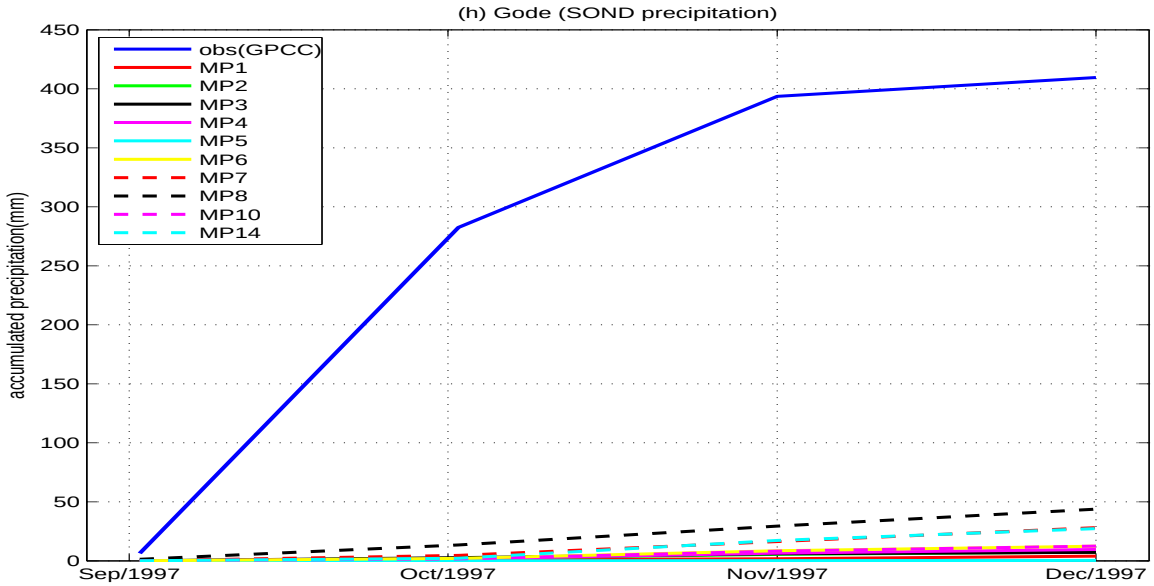
(h) Gode (SOND precipitation)
accumulated precipitation(mm)
obs(GPCC)
MP1
MP2
MP3
MP4
MP5
MP6
MP7
MP8
MP10
MP14
0
50
100
150
200
250
300
350
400
450
Sep/1997
Oct/1997
Nov/1997
Dec/1997

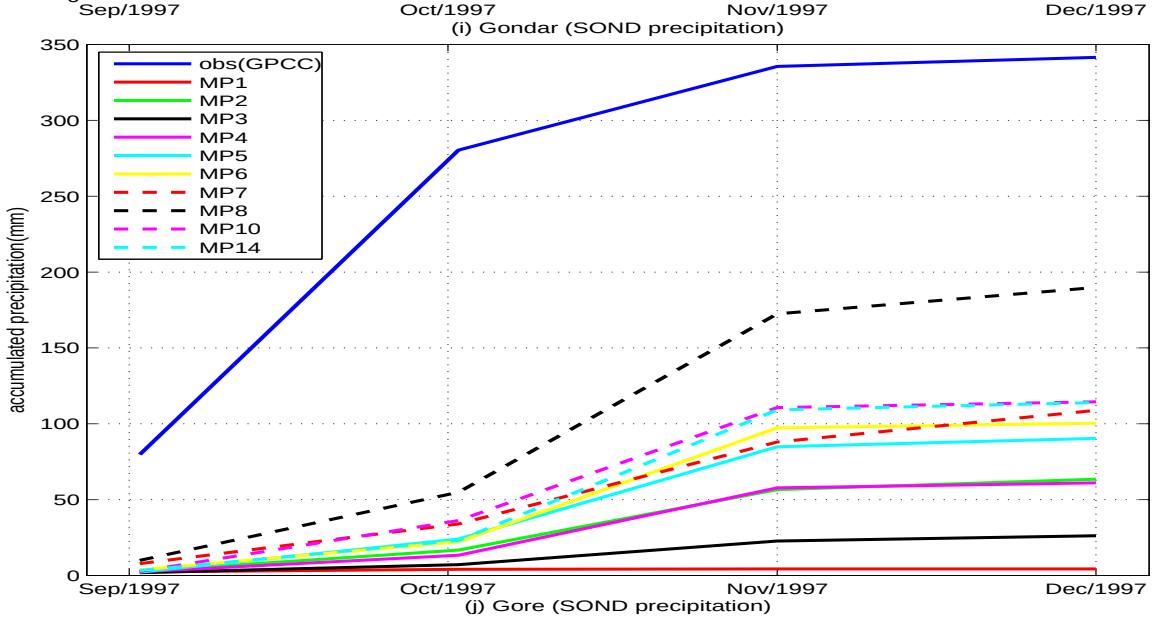
(i) Gondar (SOND precipitation)
accumulated precipitation(mm)
obs(GPCC)
MP1
MP2
MP3
MP4
MP5
MP6
MP7
MP8
MP10
MP14
0
50
100
150
200
250
300
350
Sep/1997
Oct/1997
Nov/1997
Dec/1997

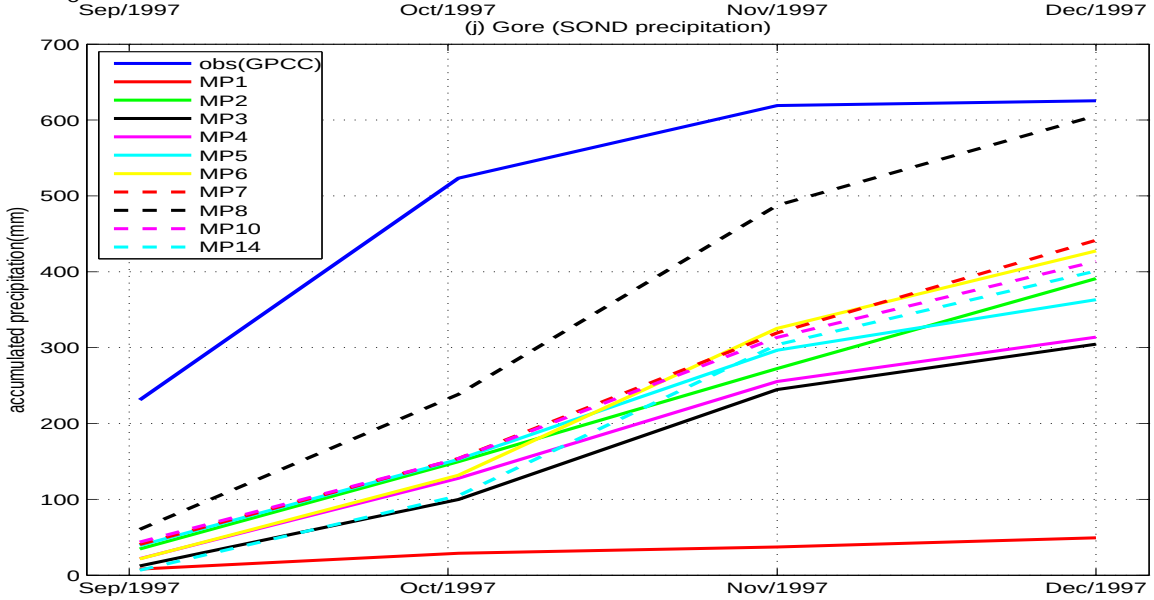
(j) Gore (SOND precipitation)
accumulated precipitation(mm)
obs(GPCC)
MP1
MP2
MP3
MP4
MP5
MP6
MP7
MP8
MP10
MP14
0
100
200
300
400
500
600
700
Sep/1997
Oct/1997
Nov/1997
Dec/1997

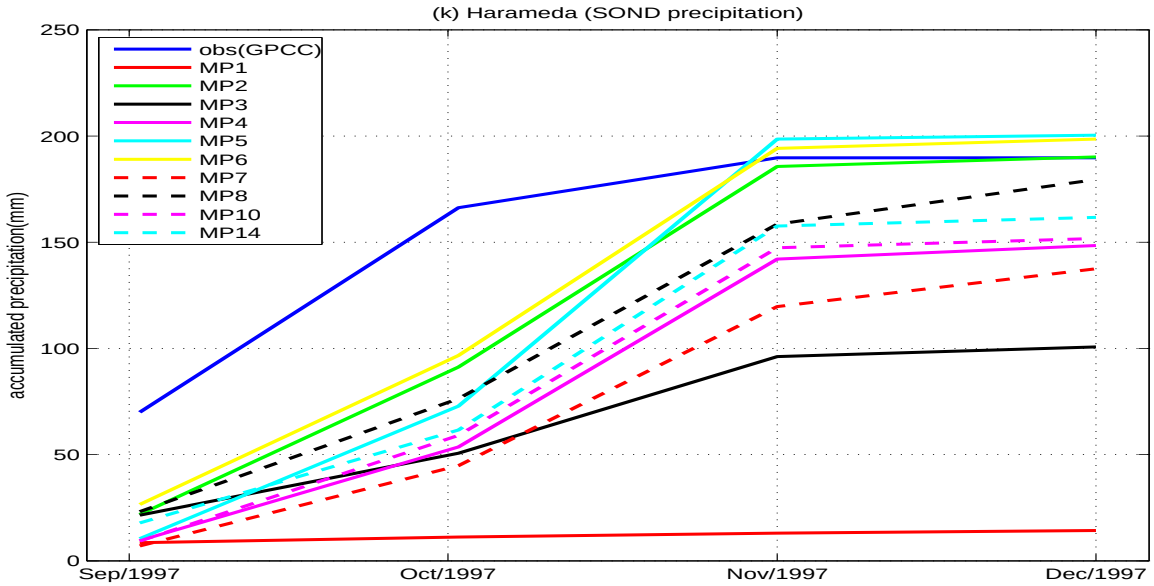
(k) Harameda (SOND precipitation)
accumulated precipitation(mm)
obs(GPCC)
MP1
MP2
MP3
MP4
MP5
MP6
MP7
MP8
MP10
MP14
0
50
100
150
200
250
Sep/1997
Oct/1997
Nov/1997
Dec/1997

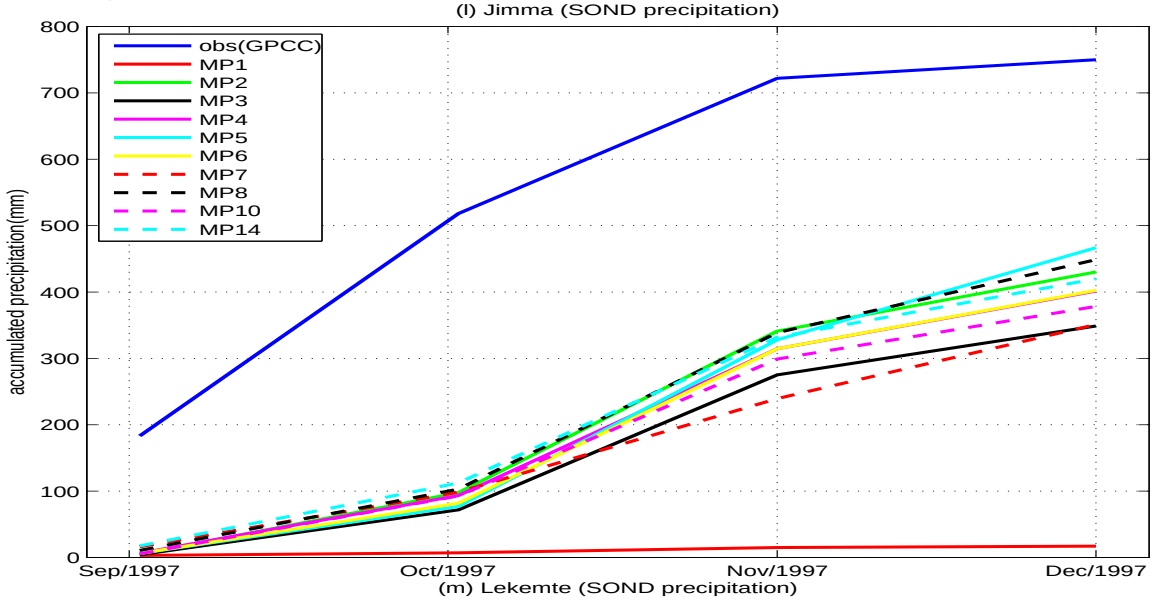
(l) Jimma (SOND precipitation)
accumulated precipitation(mm)
obs(GPCC)
MP1
MP2
MP3
MP4
MP5
MP6
MP7
MP8
MP10
MP14
0
100
200
300
400
500
600
700
800
Sep/1997
Oct/1997
Nov/1997
Dec/1997

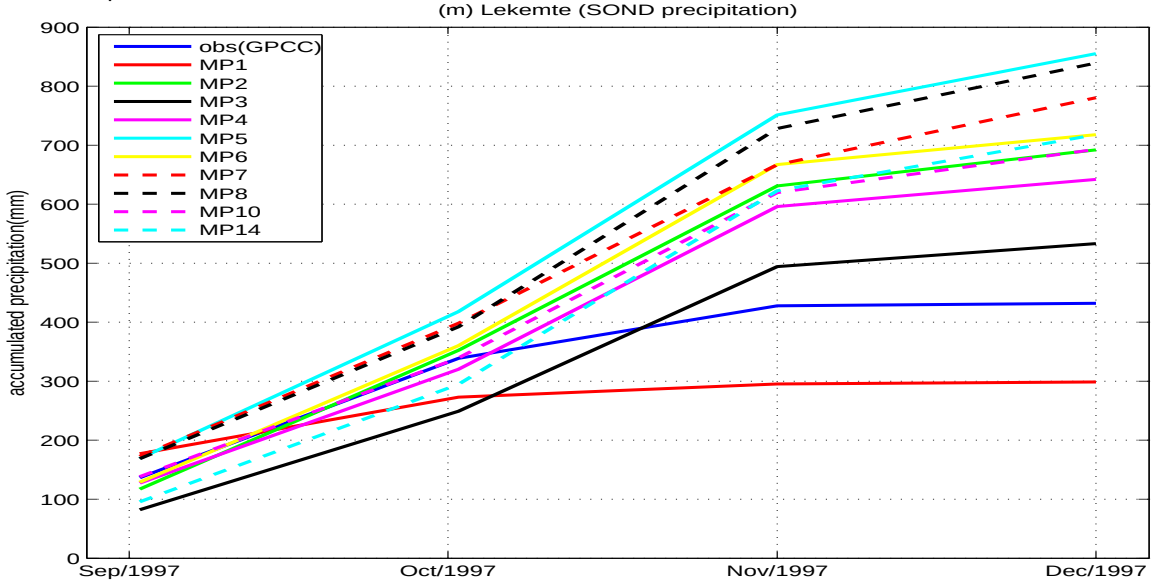
(m) Lekemte (SOND precipitation)
accumulated precipitation(mm)
obs(GPCC)
MP1
MP2
MP3
MP4
MP5
MP6
MP7
MP8
MP10
MP14
0
100
200
300
400
500
600
700
800
900
Sep/1997
Oct/1997
Nov/1997
Dec/1997

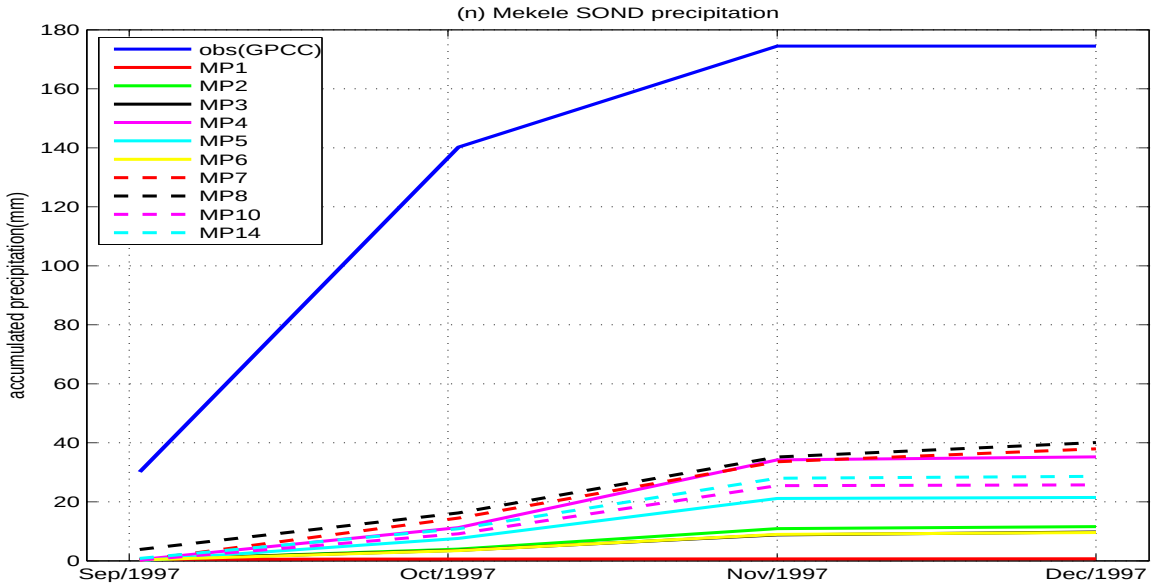
(n) Mekele SOND precipitation
accumulated precipitation(mm)
obs(GPCC)
MP1
MP2
MP3
MP4
MP5
MP6
MP7
MP8
MP10
MP14
0
20
40
60
80
100
120
140
160
180
Sep/1997
Oct/1997
Nov/1997
Dec/1997

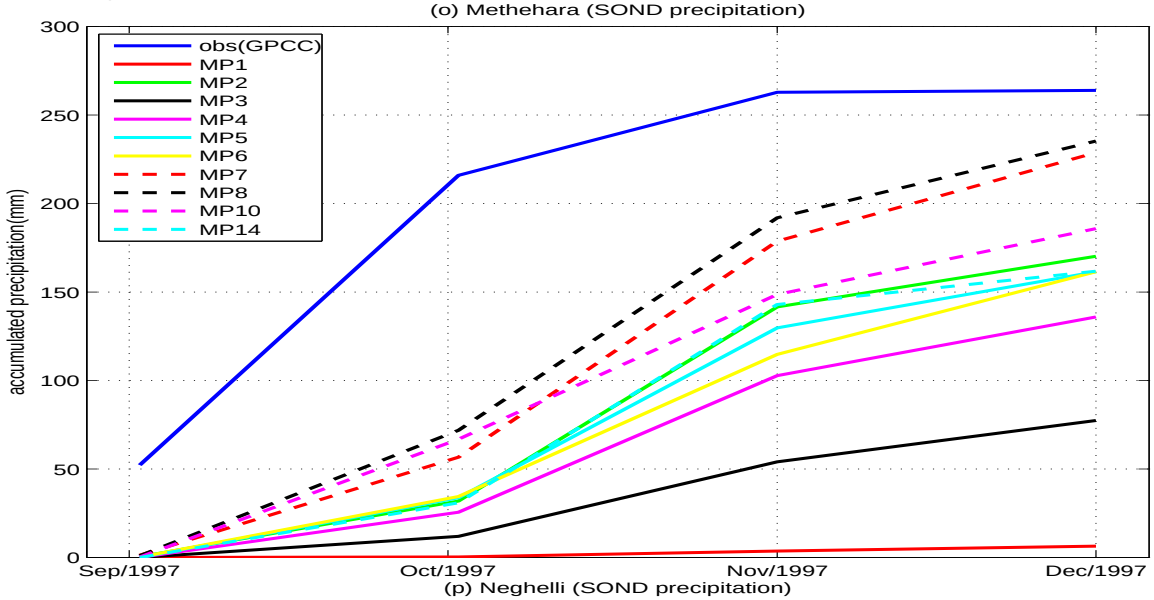
(o) Methehara (SOND precipitation)
accumulated precipitation(mm)
obs(GPCC)
MP1
MP2
MP3
MP4
MP5
MP6
MP7
MP8
MP10
MP14
0
50
100
150
200
250
300
Sep/1997
Oct/1997
Nov/1997
Dec/1997

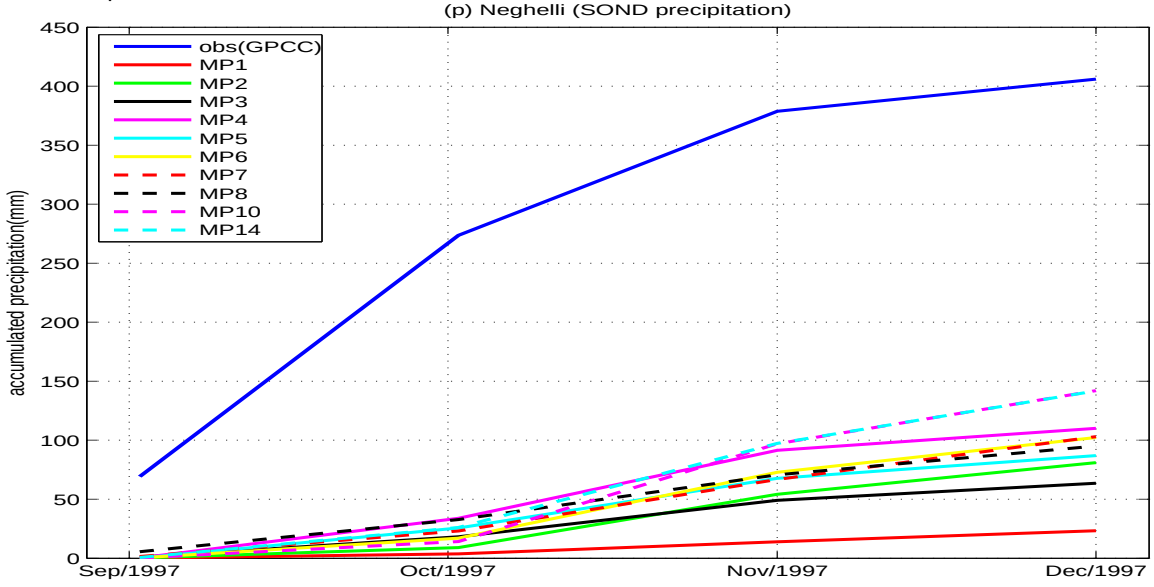
(p) Neghelli (SOND precipitation)
accumulated precipitation(mm)
obs(GPCC)
MP1
MP2
MP3
MP4
MP5
MP6
MP7
MP8
MP10
MP14
0
50
100
150
200
250
300
350
400
450
Sep/1997
Oct/1997
Nov/1997
Dec/1997

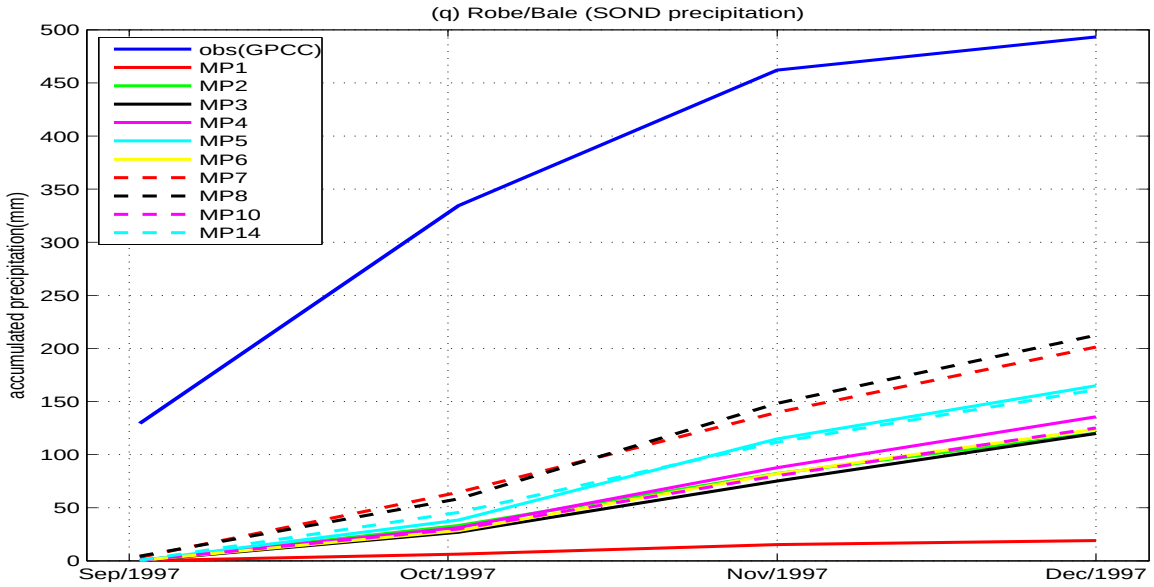

Figure 6.3: Accumulated total grid scale precipitation: WRF simulated precipitation using 10 microphysics and GPCC precipitation.

From Table 14 of the appendix, we categorized the MPs based on their proximity to the observation (GPCC) as in Table 6.1.

Rank	Eth	A.A	ARM	HWS	BRD	CCH	DMR	DRD	GD	GNR	GR	HMDA	JMM	LKMT	ML	MTHA	NGL	RB
first	mp8	mp1	mp8	mp8	mp10	mp8	mp8	mp10	mp8	mp8	mp8	mp2	mp5	mp3	mp8	mp8	mp10	mp8
second	mp7	mp3	mp7	mp4	mp8	mp5	mp10	mp8	mp7	mp10	mp7	mp6	mp8	mp1	mp7	mp7	mp14	mp7
thrid	mp5	mp14	mp4	mp10	mp6	mp7	mp5	mp4	mp10	mp14	mp6	mp8	mp2	mp4	mp14	mp10	mp4	mp7
fourth	mp10	mp6	mp2	mp5	mp7	mp14	mp7	mp7	mp6	mp7	mp10	mp5	mp14	mp10	mp10	mp14	mp7	mp14

Table 6.1: The first four MPs nearest to the observed GPCC precipitation for El Niño (1997). Where Eth=Ethiopia, A.A=Addis Ababa, ARM=Arbaminch, HWS=Hawasa, BRD=Baherdar, CCH=Combolcha, DMR=Debrmarkos, DRD=Diredawa, GD=Gode, GNR=Gondar, GR=Gore, HMDA=Harameda, JMM=Jimma, LKMT=Lekemte, ML=Mekele, MTHA=Methehara, NGL=Neghelli, RB=Robe.

The best MP for Ethiopia as a whole, Arbaminch, Hawasa, Combolcha, Debremarkos, Gode, Gondar, Gore, Mekele, Methehara, and Robe/Bale is MP8 (Table 6.1). MP10 is also best for Bahirdar, Diredawa, and Neghelli. For Addis Ababa, Jimma, Lekemte and Harameda, the preferable MP are MP1, MP5, MP3 and MP2 respectively. Based on this fact, among the 17 selected places the first rank of 10 places are occupied with MP8 and 3 places with MP10. The rest 4 places first rank is occupied by MP1, MP3, MP2 and MP5. Therefore the MP with a large number of hydrometer such as MP8, is the best MP in capturing precipitation. The minimum and maximum

precipitation captured by MP8 are 40.1 mm for Mekele and 606 mm for Gore respectively.

6.3 Statistical Analysis

1. Statistical analysis using spatial mean over Ethiopia

In this section the statistical tools such as Correlation Coefficient, root mean square error (RMSE), mean absolute error (MAE), bias, and are used to validate the precipitation capturing skill of each microphysics during El Niño year against GPCC precipitation. The correlation coefficient over the country is given in Fig. 6.4.

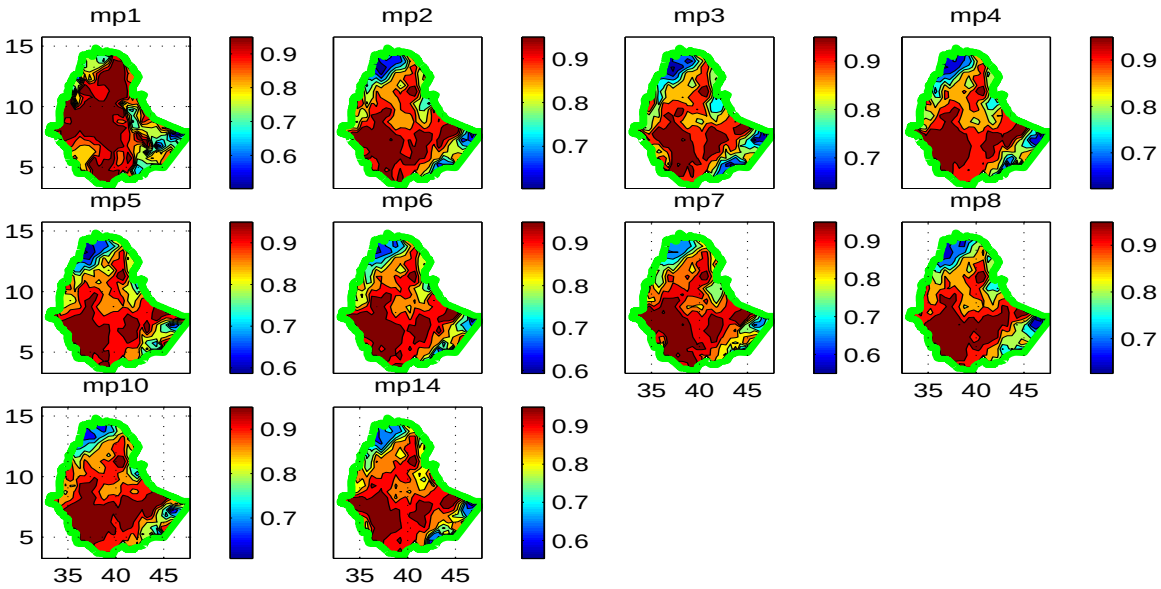

Figure 6.4: Correlation coefficient of accumulated total grid scale precipitation.

Spatial mean accumulated total grid scale correlation coefficient, bias, MAE and RMSE over Ethiopia are shown in Table 6.2.

Statistical tools	mp1	mp2	mp3	mp4	mp5	mp6	mp7	mp8	mp10	mp14
corrcoef	0.8925	0.8713	0.8672	0.8692	0.8691	0.8740	0.8699	0.8745	0.8829	0.8640
BIAS	-203.65	-153.40	-172.76	-156.10	-149.16	-153.76	-140.05	-125.97	-147.27	-161.04
MAE	206.45	169.00	181.35	169.95	168.40	169.13	159.75	151.85	162.36	172.18
RMSE	248.10	212.63	225.79	214.00	210.77	212.87	204.09	193.10	205.15	216.24

Table 6.2: Correlation coefficient, bias, MAE, and RMSE of accumulated total grid scale precipitation for El Niño (1997).

The accumulated total grid scale precipitation over Ethiopia show that the best three MP using correlation coefficient are MP1, MP10, and MP8 (see Table 6.2). Using bias the first three MP are MP8, MP6, and MP10. Making use of RMSE the first three MPs are MP8, MP7, and MP10. For MAE, MP8, MP7 and MP10 are also the first three best MP. MP1 is the best one using correlation coefficient which is 0.8925, and the correlation coefficient of MP10, MP8 and MP7 are 0.8829, 0.8745, and 0.8699 respectively. Therefore based on correlation coefficient, bias, MAE, and RMSE, the best three microphysics in capturing precipitation during El Niño year are MP8, MP7, and MP10.

2. Statistical analysis for the selected areas

From Table 4 of the appendix, the rank of accumulated total grid scale precipitation correlation coefficient for each selected places the first three best MP are displayed in Table 6.3.

rank	A.A	ARH	HWA	BAD	CCH	DBR	DRW	GD	GNR	GR	HMDA	JMA	LKT	ML	MER	NGL	RB
first	mp1	mp10	mp1	mp1	mp8	mp1	mp10	mp8	mp1	mp1	mp1	mp1	mp1	mp10	mp10	mp4	mp1
second	mp3	mp7	mp10	mp10	mp7	mp10	mp8	mp4	mp10	mp2	mp3	mp10	mp2	mp7	mp8	mp3	mp7
third	mp8	mp8	mp8	mp8	mp6	mp3	mp5	mp3	mp8	mp5	mp2	mp8	mp4	mp8	mp6	mp8	mp14

Table 6.3: The first three best MPs precipitation in capturing skill using correlation coefficient for El Niño (1997).

The correlation coefficient of Addis Ababa, Hawasa, Bahirdar, Debremarkos, Gondar, Gore, Harameda, Jimma, Lekemte, and Robe/Bale for the best microphysics (MP1) is

0.974, 0.993, 0.988, 0.995, 0.998, 0.957, 0.997, 0.959, 0.987, and 0.99 respectively. MP10 is the best MP for Arbaminch, Diredawa, Mekele, and Methehara with a correlation coefficient 0.984, 0.832, 0.9, and 0.918 restrictively. Similarly MP8 are the best MP for Combolcha and Gode with correlation coefficient value of 0.963 and 0.891 respectively. Finally MP4 is the first one for Neghelli with correlation coefficient 0.961. The rest of the statistical tools; bias, MAE, and RMSE are given, like the correlation coefficient, using tables from the appendix.

Using bias Table 5 from the appendix, the first three best MPs are summarized in Table 6.4.

rank	A.A	ARH	HWA	BAD	CCH	DBR	DRW	GD	GNR	GR	HMDA	JMA	LKT	ML	MER	NGL	RB
first	mp1	mp8	mp8	mp10	mp8	mp8	mp8	mp8	mp8	mp8	mp5	mp8	mp4	mp8	mp8	mp7	mp8
second	mp14	mp7	mp10	mp8	mp5	mp10	mp10	mp7	mp10	mp10	mp2	mp2	mp3	mp7	mp7	mp8	mp7
third	mp7	mp4	mp5	mp7	mp7	mp5	mp7	mp14	mp6	mp7	mp6	mp5	mp14	mp3	mp2	mp14	mp5

Table 6.4: The first three MPs based on bias for the selected areas for El Niño (1997).

The best MP for Arbaminch, Hawasa, Combolcha, Debremarkos, Diredawa, Gode, Gondar, Gore, Jimma, Mekele, Methehara, and Robe is MP8 in terms low bias. The first place for Addis Ababa, Bahirdar, Harameda, Lekemte, and Neghelli is occupied by MP1, MP10, MP5, MP4, and MP7 respectively. Therefor MP8 is best for 12 places with a maximum and a minimum value 257.26 mm for Jimma and 17.22 mm for Hawasa respectively.

Using Table 6 from the appendix, the first three best MP for MAE is given in Table 6.5.

rank	A.A	ARH	HWA	BAD	CCH	DBR	DRW	GD	GNR	GR	HMDA	JMA	LKT	ML	MER	NGL	RB
first	mp1	mp8	mp8	mp10	mp8	mp8	mp8	mp8	mp4	mp8	mp2	mp8	mp3	mp8	mp8	mp7	mp8
second	mp14	mp7	mp10	mp8	mp5	mp10	mp10	mp7	mp8	mp10	mp6	mp2	mp10	mp7	mp7	mp8	mp7
thrid	mp3	mp4	mp4	mp7	mp7	mp5	mp7	mp14	mp10	mp7	mp8	mp5	mp4	mp4	mp5	mp14	mp14

Table 6.5: The first three MPs based on MAE for the selected areas for El Niño (1997).

The best MP for Arbaminch, Hawasa, Combolcha, Debremarkos, Diredawa, Gode, Gore, Jimma, Mekele, Methehara, and Robe is MP8 in terms of MAE (Table 6.5). The first place for Addis Ababa, Bahirdar, Gondar, Harameda, Lekemte, and Neghelli is occupied by MP1, MP10, MP4, MP2, MP3, and MP7 respectively. Therefor MP8 is best for 11 places. The maximum and minimum MAE for MP8 is 257 mm for Jimma and 45 mm for Combolcha respectively.

Using RMSE Table 7 from the appendix the first three best MP is given in Table 6.6

rank	A.A	ARH	HWA	BAD	CCH	DBR	DRW	GD	GNR	GR	HMDA	JMA	LKT	ML	MER	NGL	RB
first	mp1	mp8	mp10	mp10	mp8	mp8	mp8	mp8	mp8	mp8	mp2	mp8	mp3	mp8	mp8	mp7	mp8
second	mp3	mp7	mp8	mp8	mp5	mp10	mp10	mp7	mp10	mp10	mp6	mp2	mp4	mp7	mp7	mp8	mp7
thrid	mp7	mp5	mp5	mp6	mp7	mp5	mp7	mp14	mp6	mp5	mp8	mp5	mp10	mp4	mp5	mp14	mp14

Table 6.6: The first three MPs based on RMSE for the selected areas for El Niño (1997).

The best MP for Arbaminch, Combolcha, Debremarkos, Diradawa, Gode, Gore, Jimma, Mekele, Methehara, and Robe is MP8 with respect its RMSE (see Table 6.6). The first place for Bahirdar, and Hawasa, is occupied by MP10. For Addis Ababa, Harameda, Lekemte, and Neghelli MP1, MP2, MP3, and MP7 respectively. Therefore MP8 is best for 11 places. The maximum and minimum RMSE for MP8 is 271 mm for Jimma and 57.7 mm for Combolcha, respectively.

In general for El Niño (1997) using correlation coefficient, bias, MAE, and RMSE the lion's share is taken by MP8 for both (using spatial mean) over the country and selected sample regions.

6.4 Grid Scale Precipitation Compared to Observed Precipitation for La Niña Year (1999)

6.4.1 Accumulated Total Grid Scale Precipitation over Ethiopia

Accumulated total grid scale precipitation captured by all the selected microphysics and total observation precipitation (GPCC) using contour plot is given in Fig. 6.5

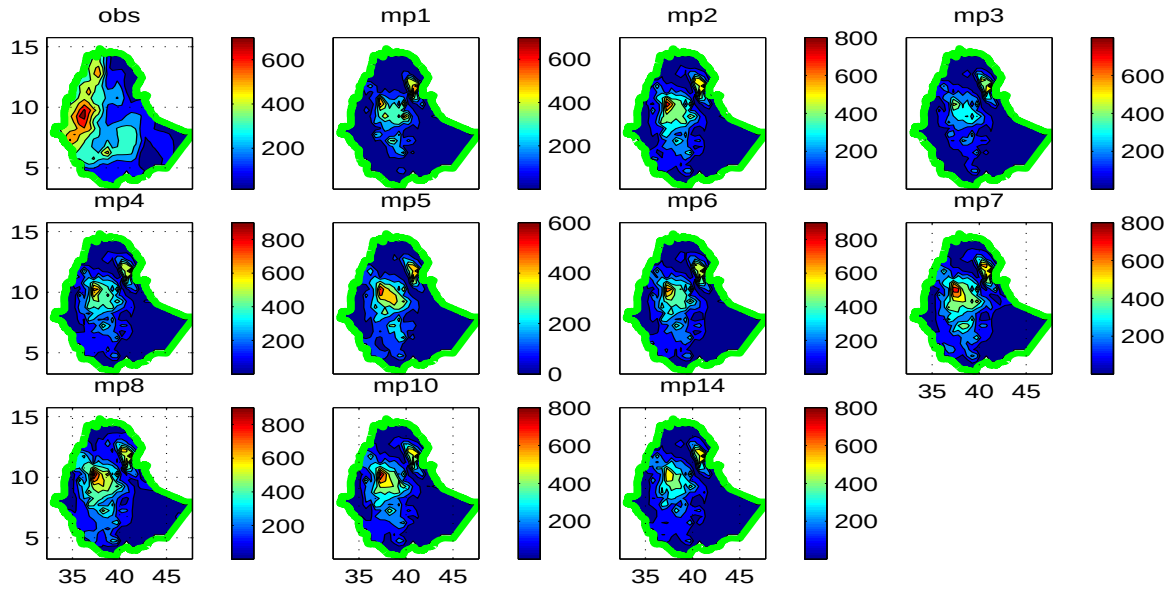

Figure 6.5: Precipitation over Ethiopia: accumulated total grid scale and accumulated GPCC precipitation.

Fig 6.5 roughly shows that the maximum GPCC precipitation is observed along the western and northern territory of the country whereas the model precipitation maximum value are shifted to the center. Concerning the maximum value the observed (GPCC) and MP1, MP3 and MP5 are similar with maximum value of 600 mm. The rest microphysics have a maximum value of 800 mm.

6.4.2 Grid Scale Accumulated Precipitation for Selected Places

To identify the best MP the line plot of accumulated total grid scale Precipitation for the selected regions and over the country (using spatial mean) is given in Fig. 6.6.

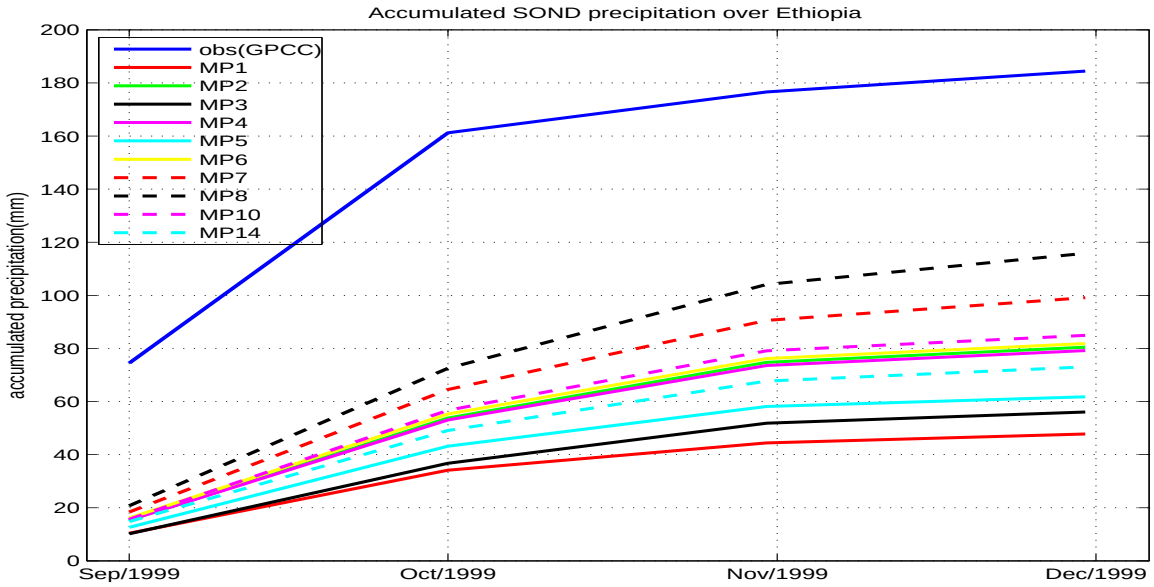

Figure 6.6: Accumulated total grid scale precipitation line plot for each MP for Ethiopia using spatial mean.

Fig 6.6 shows that eventhough all MP underestimate the GPCC precipitation, the order of precipitation capturing skill is MP8, MP7, MP10, MP6, MP4, MP2, MP14, MP5, MP3, and MP1.

The line plot of accumulated total grid scale La Niña year for the selected region against the accumulated GPCC precipitation is shown in Fig. 6.7

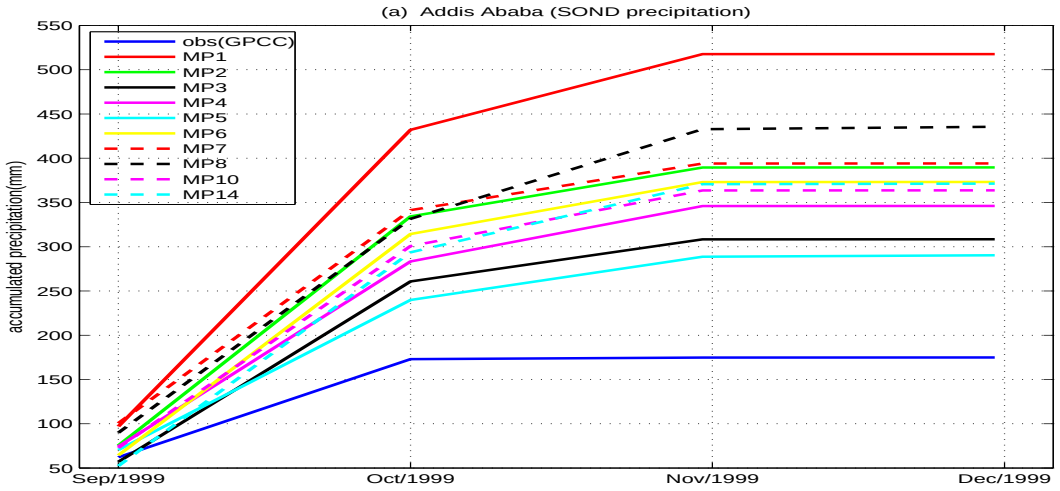

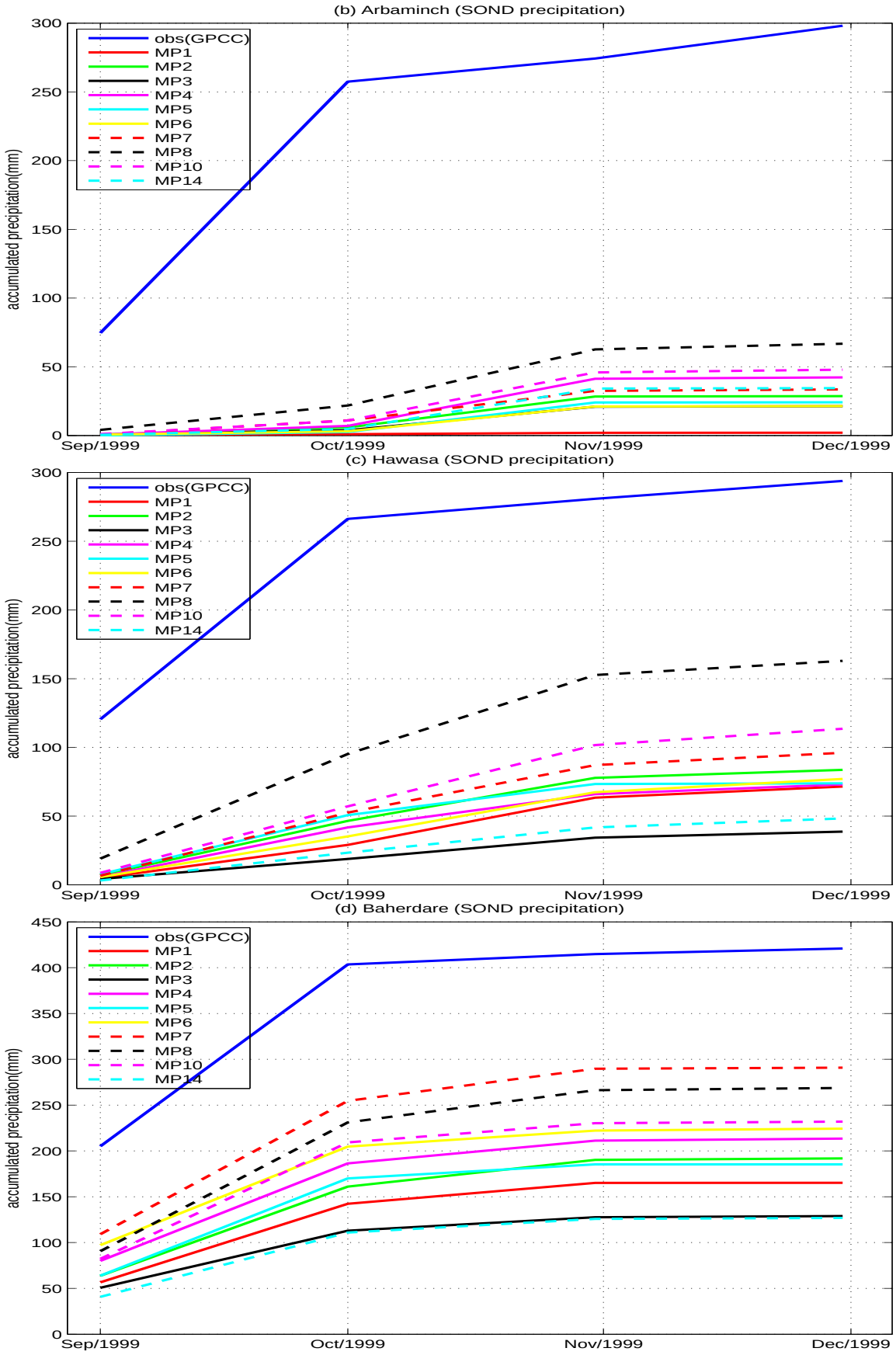
(b) Arbaminch (SOND precipitation)
accumulated precipitation(mm)
obs(GPCC)
MP1
MP2
MP3
MP4
MP5
MP6
MP7
MP8
MP10
MP14
Sep/1999
Oct/1999
Nov/1999
Dec/1999
(c) Hawasa (SOND precipitation)
accumulated precipitation(mm)
(d) Baherdare (SOND precipitation)
accumulated precipitation(mm)

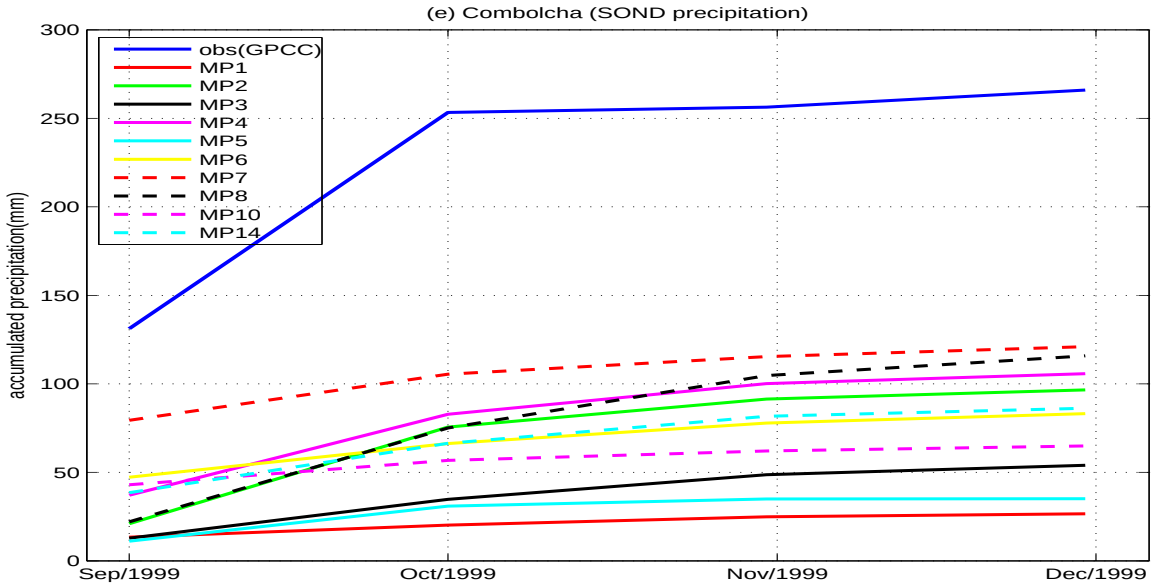
(e) Combolcha (SOND precipitation)
accumulated precipitation(mm)
obs(GPCC)
MP1
MP2
MP3
MP4
MP5
MP6
MP7
MP8
MP10
MP14
0
50
100
150
200
250
300
Sep/1999
Oct/1999
Nov/1999
Dec/1999

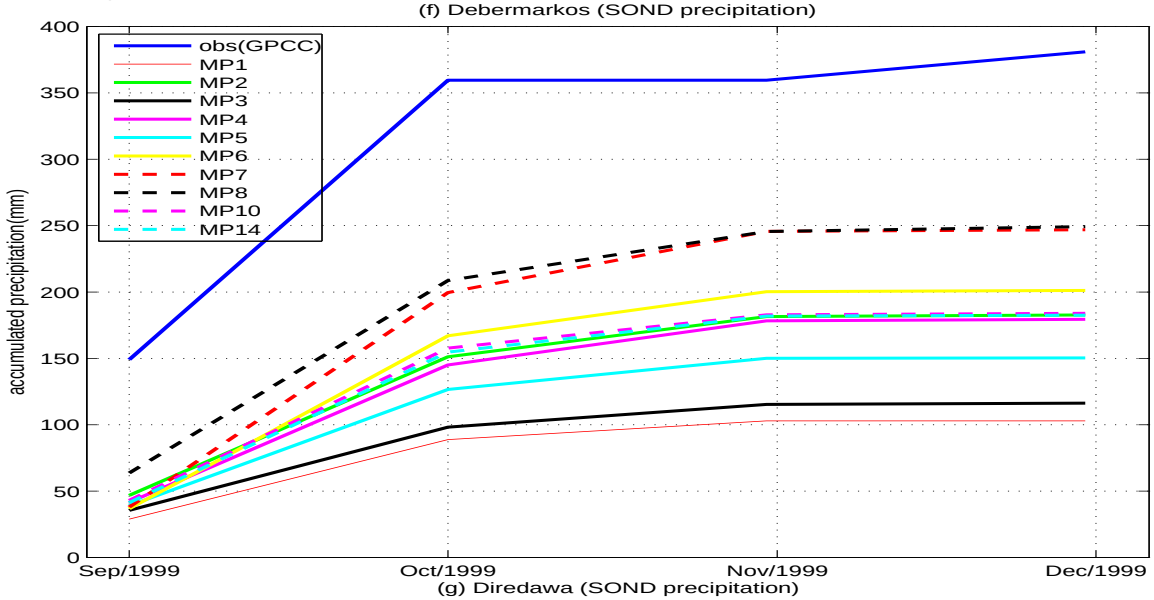
(f) Debermarkos (SOND precipitation)
accumulated precipitation(mm)
obs(GPCC)
MP1
MP2
MP3
MP4
MP5
MP6
MP7
MP8
MP10
MP14
0
50
100
150
200
250
300
350
400
Sep/1999
Oct/1999
Nov/1999
Dec/1999

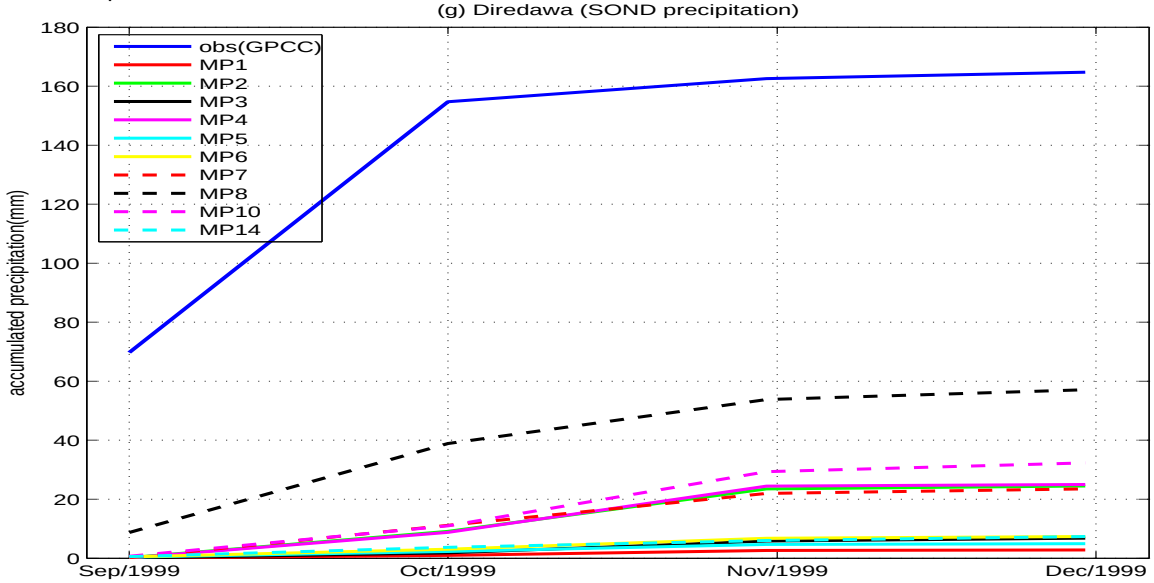
(g) Diredawa (SOND precipitation)
accumulated precipitation(mm)
obs(GPCC)
MP1
MP2
MP3
MP4
MP5
MP6
MP7
MP8
MP10
MP14
0
20
40
60
80
100
120
140
160
180
Sep/1999
Oct/1999
Nov/1999
Dec/1999

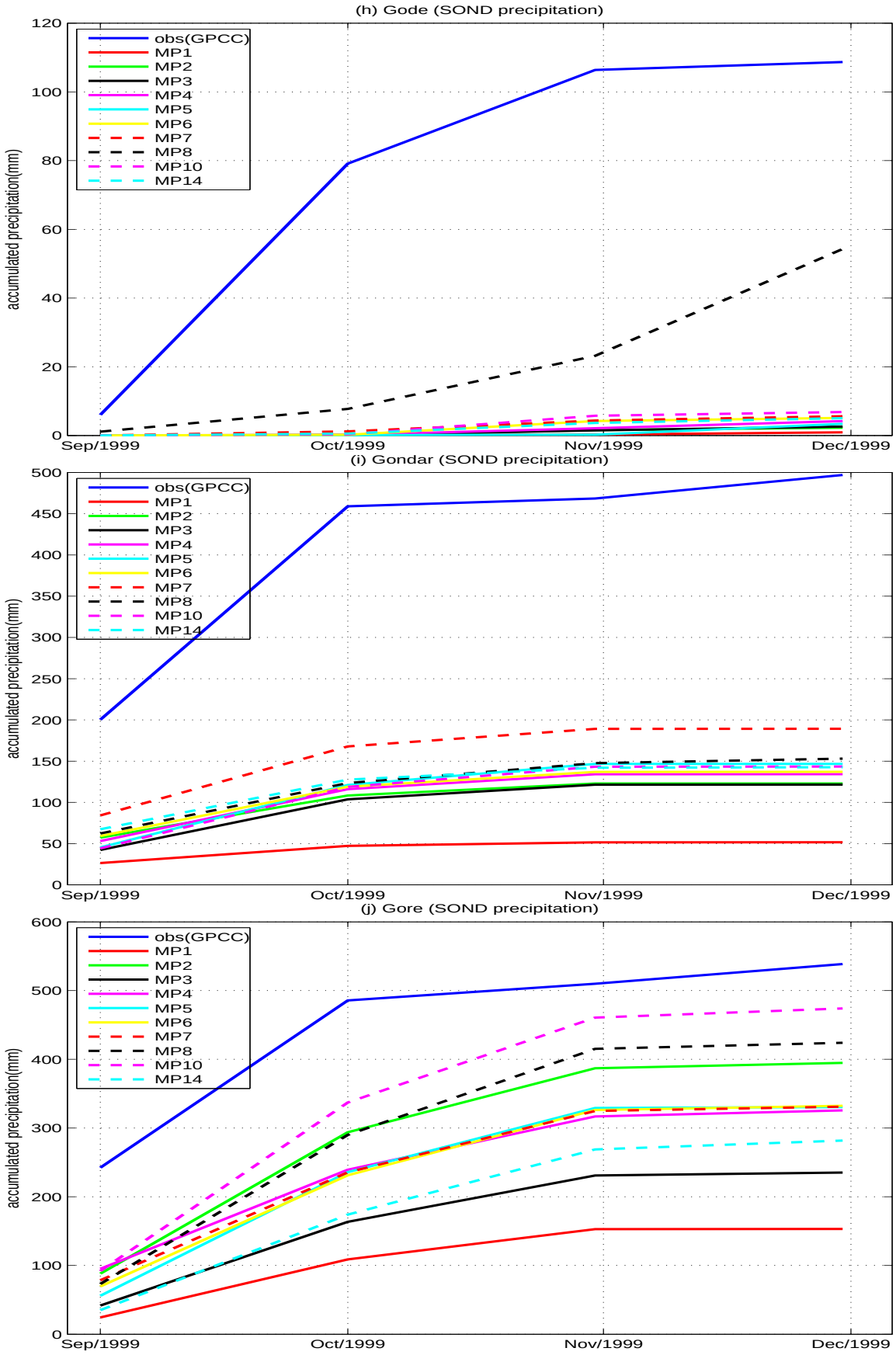
(h) Gode (SOND precipitation)
accumulated precipitation(mm)
obs(GPCC)
MP1
MP2
MP3
MP4
MP5
MP6
MP7
MP8
MP10
MP14
Sep/1999
Oct/1999
Nov/1999
Dec/1999
(i) Gondar (SOND precipitation)
(j) Gore (SOND precipitation)

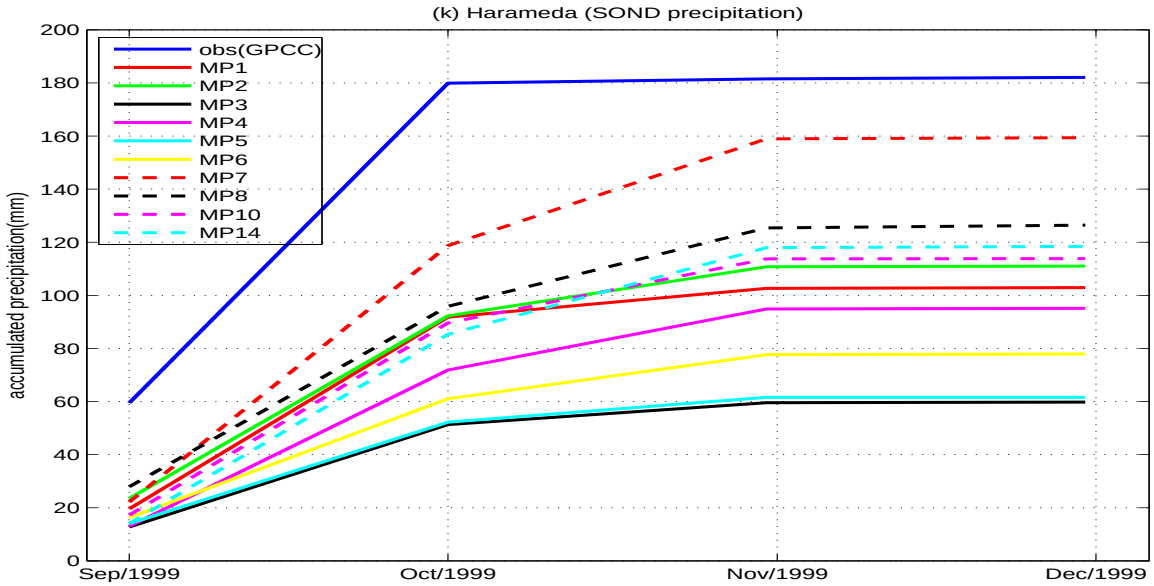
(k) Harameda (SOND precipitation)
accumulated precipitation(mm)
obs(GPCC)
MP1
MP2
MP3
MP4
MP5
MP6
MP7
MP8
MP10
MP14
0
20
40
60
80
100
120
140
160
180
200
Sep/1999
Oct/1999
Nov/1999
Dec/1999

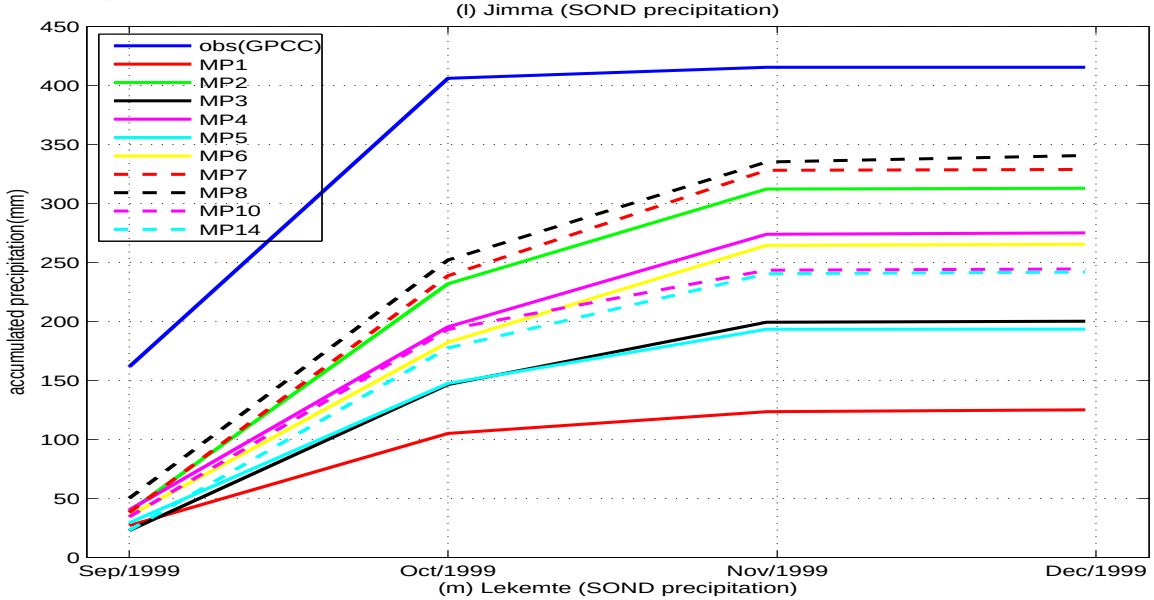
(l) Jimma (SOND precipitation)
accumulated precipitation(mm)
obs(GPCC)
MP1
MP2
MP3
MP4
MP5
MP6
MP7
MP8
MP10
MP14
0
50
100
150
200
250
300
350
400
450
Sep/1999
Oct/1999
Nov/1999
Dec/1999

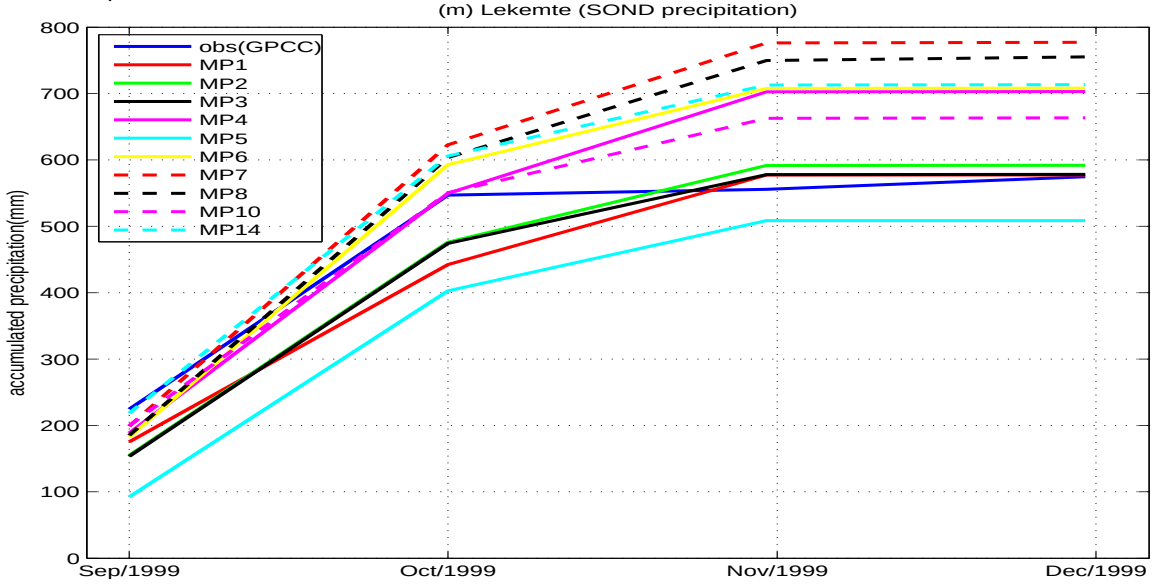
(m) Lekemte (SOND precipitation)
accumulated precipitation(mm)
obs(GPCC)
MP1
MP2
MP3
MP4
MP5
MP6
MP7
MP8
MP10
MP14
0
100
200
300
400
500
600
700
800
Sep/1999
Oct/1999
Nov/1999
Dec/1999

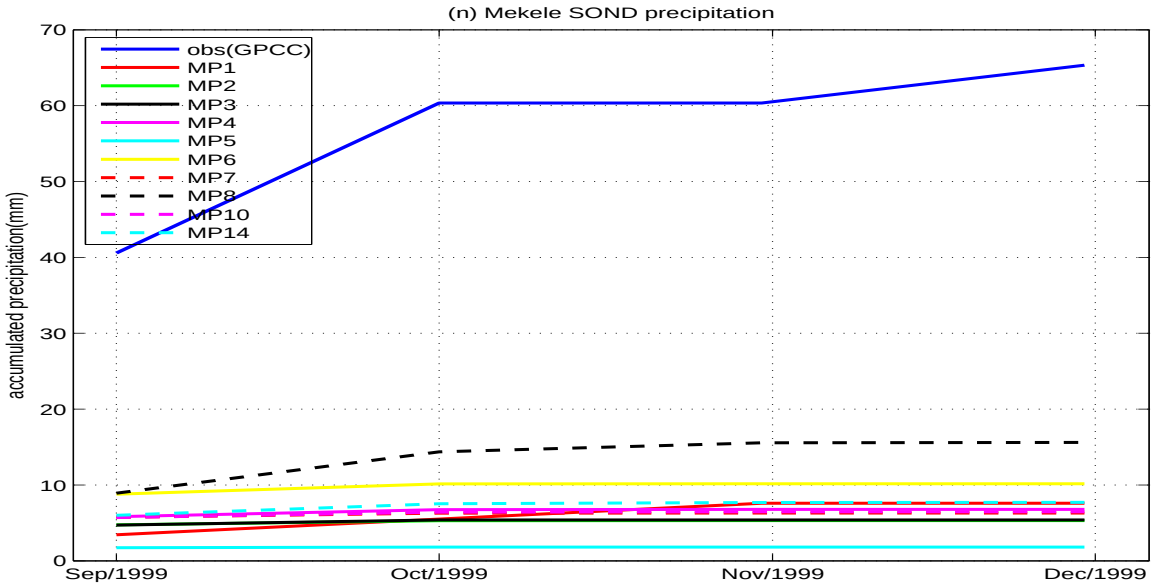
(n) Mekele SOND precipitation
accumulated precipitation(mm)
obs(GPCC)
MP1
MP2
MP3
MP4
MP5
MP6
MP7
MP8
MP10
MP14
0
10
20
30
40
50
60
70
Sep/1999
Oct/1999
Nov/1999
Dec/1999

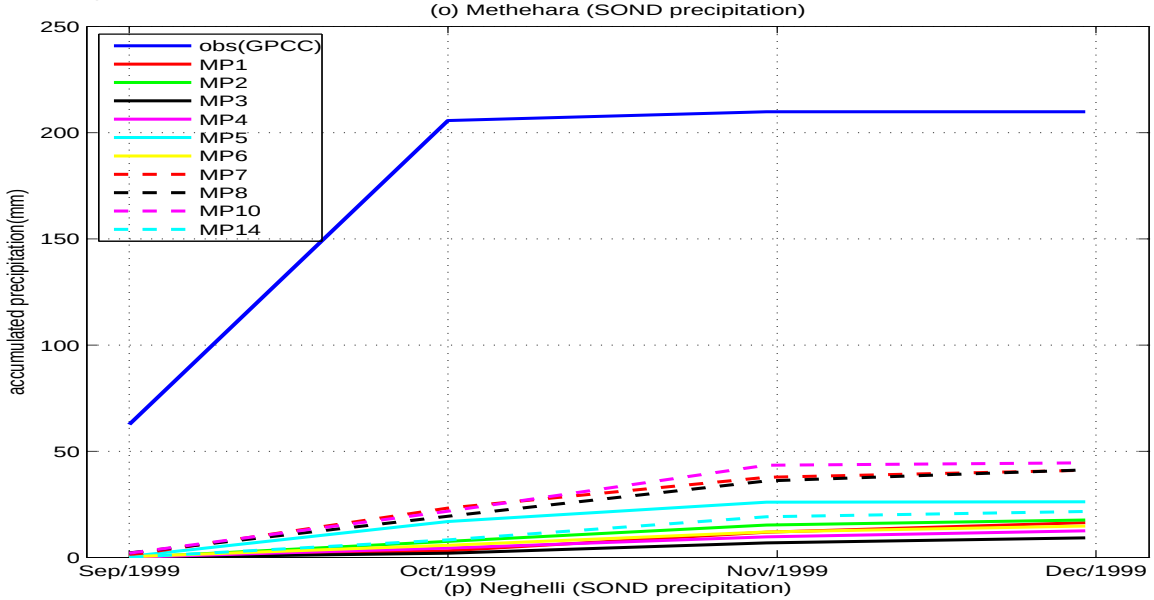
(o) Methehara (SOND precipitation)
accumulated precipitation(mm)
obs(GPCC)
MP1
MP2
MP3
MP4
MP5
MP6
MP7
MP8
MP10
MP14
0
50
100
150
200
250
Sep/1999
Oct/1999
Nov/1999
Dec/1999

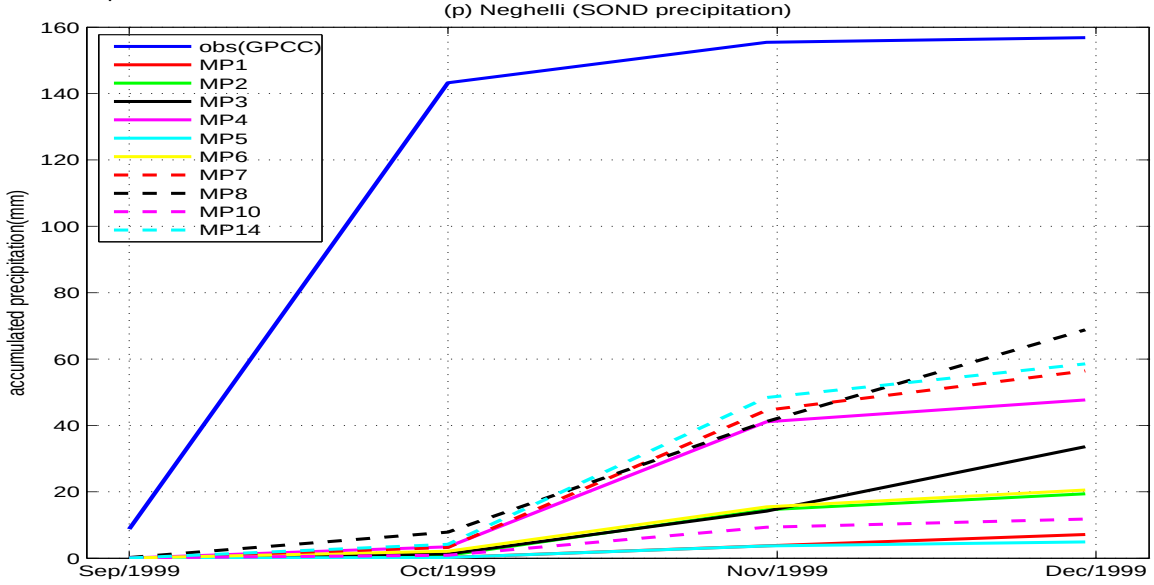
(p) Neghelli (SOND precipitation)
accumulated precipitation(mm)
obs(GPCC)
MP1
MP2
MP3
MP4
MP5
MP6
MP7
MP8
MP10
MP14
0
20
40
60
80
100
120
140
160
Sep/1999
Oct/1999
Nov/1999
Dec/1999

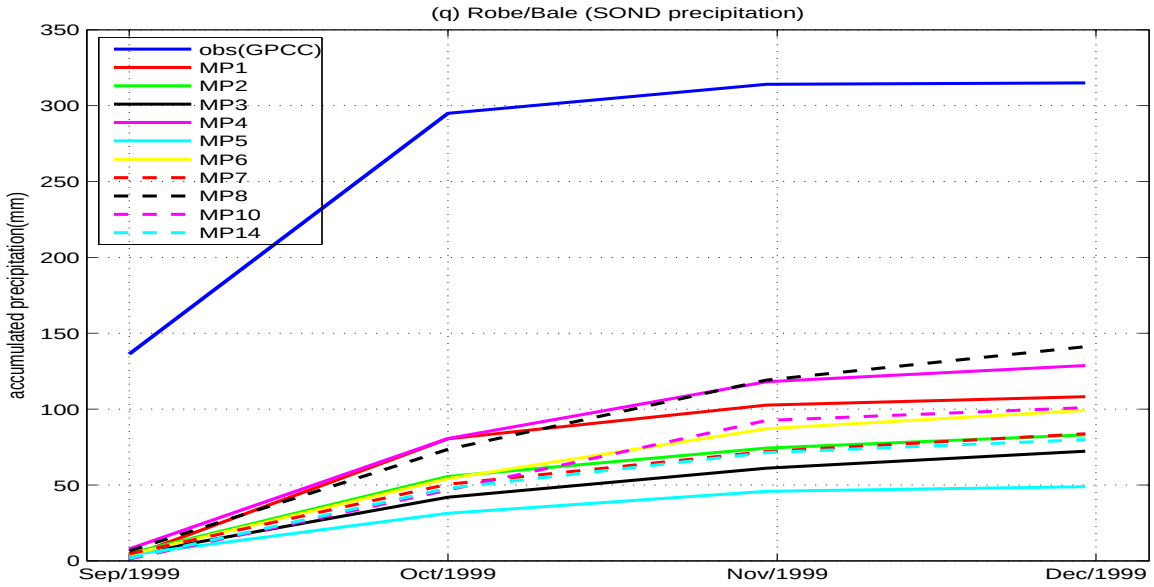

Figure 6.7: Accumulated total grid scale precipitation: for the 10 microphysics and accumulated GPCC precipitation.

From Table 2 of the appendix, we categorized the MPs based on their proximity to the observation(GPCC) as in Table 6.7.

Rank	Eth	A.A	ARM	HWS	BRD	CCH	DMR	DRD	GD	GNR	GR	HMDA	JMM	LKMT	ML	MTHA	NGL	RB
First	mp8	mp5	mp8	mp8	mp7	mp7	mp8	mp8	mp8	mp7	mp10	mp7	mp8	mp1	mp8	mp10	mp8	mp8
second	mp7	mp3	mp10	mp10	mp8	mp8	mp7	mp10	mp10	mp8	mp8	mp8	mp7	mp3	mp6	mp8	mp14	mp4
thrid	mp10	mp4	mp4	mp7	mp10	mp4	mp6	mp4	mp7	mp5	mp2	mp14	mp2	mp2	mp14	mp7	mp7	mp1
fourth	mp6	mp10	mp14	mp2	mp6	mp2	mp10	mp2	mp6	mp10	mp5	mp10	mp4	mp5	mp1	mp5	mp4	mp10

Table 6.7: The first four MPs nearest to the observed GPCC precipitation for La Niña (1999).

The best MP for Ethiopia as a whole, Debremarkos, Hawasa, Jimma, Arbamich, Diredawa, Gode, Mekele, Robe, and Negellie is mp8 (Table 6.7). MP7 is also best for Combolcha, Bahirdar, Gondar, and Harameda. MP10 is also best for Gore and Methehara. For Addis Ababa and Lekemite the preferable MP are MP5 and MP1 respectively. Based on this fact, among the 17 selected places 9 places are occupied with MP8 and 4 places with MP7 as a best MP. The first rank of the rest 4 places are occupied by MP5, MP10, and MP1. Therefore the MP with a large number of hydrometer such as MP8, MP7 and MP10 are the best MP in capturing precipitation. The accumulated

total grid scale precipitation captured by MP8 for the selected region, the minimum and maximum accumulated total grid scale precipitation is observed over Mekele (15.6 mm) and Jimma (341 mm).

6.5 Statistical Analysis

1. Statistical analysis for the country using spatial mean

In this section the statistical tools such as correlation coefficient, root mean square error (RMSE), mean absolute error (MAE), and bias are applied to validate the precipitation capturing skill each MP during La Niña year against GPCC precipitation.

The correlation coefficient over the country is given in Fig. 6.8.

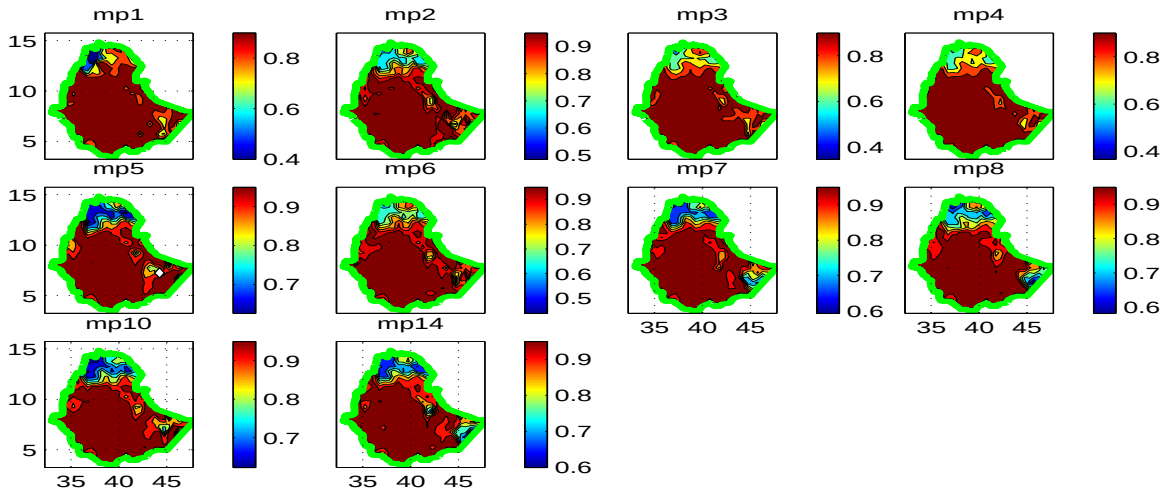

Figure 6.8: Accumulated total grid scale precipitation Correlation Coefficient over Ethiopia for the selected microphysics.

Spatial mean accumulated total grid scale Correlation Coefficient, bias, MAE and RMSE over Ethiopia is shown in Table 6.8.

Statistical tools	mp1	mp2	mp3	mp4	mp5	mp6	mp7	mp8	mp10	mp14
corrcoef	0.9012	0.9017	0.9018	0.9045	0.9117	0.9066	0.9068	0.9078	0.9071	0.9064
BIAS	-108.05	-85.74	-103.40	-86.41	-97.45	-84.40	-73.24	-63.76	-82.08	-90.38
MAE	121.28	106.92	115.44	106.67	110.90	106.22	100.93	98.38	102.69	106.51
RMSE	168.24	151.53	161.05	150.07	154.94	150.27	144.03	139.73	144.50	149.50

Table 6.8: Correlation Coefficient, Bias, MAE and RMSE of Accumulated total grid scale precipitation for La Niña (1999).

The accumulated total grid scale precipitation over Ethiopia shows that the best three MP using correlation coefficient are MP5, MP8, and MP10 (see Table 6.8). Using MAE the first three MP are MP8, MP7, and MP10. Similarly using bias MP8, MP7 and MP10 are the first three best MP. Finally using RMSE the first three MP are MP8, MP7 and MP10.

Therefore based on bias, MAE and RMSE the best three microphysics in capturing precipitation for La Niña year are MP8, MP7 and MP10. MP5 is the best one using correlation coefficient which is 0.912, and the correlation coefficient of MP8, MP7, and MP10 are 0.908, 0.907, and 0.907 respectively. For the correlation coefficients are almost equal, MP8 takes the priority based on all statistical tools.

2. Statistical analysis for the selected areas

From Table 8 of the appendix the rank of accumulated total grid scale precipitation correlation coefficient for each selected places the first three best MP are displayed in Table 6.9.

rank	A.A	ARH	HWA	BAD	CCH	DBR	DRW	GD	GNR	GR	HMDA	JMA	LKT	ML	MER	NGL	RB
first	mp1	mp1	mp5	mp5	mp5	mp1	mp8	mp8	mp4	mp1	mp3	mp1	mp3	mp10	mp5	mp1	mp1
second	mp7	mp3	mp4	mp10	mp2	mp10	mp14	mp10	mp6	mp2	mp1	mp10	mp5	mp14	mp7	mp10	mp5
thrid	mp3	mp14	mp14	mp6	mp1	mp3	mp1	mp7	mp7	mp7	mp2	mp5	mp2	mp6	mp8	mp4	mp2

Table 6.9: The first three best MPs precipitation in capturing skill using correlation coefficient for La Niña (1999).

The correlation coefficient MP1 for Addis Ababa, Arbaminch, Gore, Debremarkos, Jimma, Neghelli and Robe/Bale are 0.983, 0.913, 0.972, 0.987, 0.983, 0.738, and 0.976

respectively. MP5 is best for Hawasa, Bahirdar, Combolcha and Methehara with a value 0.958, 0.997, 0.981, and 0.887 respectively. Similarly MP8 is best for Gode and Diredawa with a value 0.814 and 0.933 respectively. MP3 is also best for Harameda and Lekemite with correlation coefficient 0.991 and 0.979 respectively. Finally MP4 and MP10 have a correlation coefficient 0.987 mm and 0.989 mm for Gondar and Mekele respectively. The rest of the statistical tools bias, MAE, and RMSE are given, like the correlation coefficient, using concerned tables from the appendix.

Using bias Table 9 from the appendix the first three best MPs are summarized in Table 6.10.

rank	A.A	ARH	HWA	BAD	CCH	DBR	DRW	GD	GNR	GR	HMDA	JMA	LKT	ML	MER	NGL	RB
first	mp5	mp8	mp8	mp7	mp7	mp8	mp8	mp8	mp8	mp8	mp7	mp8	mp6	mp8	mp7	mp8	mp8
second	mp3	mp10	mp10	mp8	mp8	mp7	mp7	mp7	mp7	mp10	mp8	mp7	mp10	mp6	mp8	mp14	mp4
third	mp14	mp7	mp6	mp10	mp6	mp	mp10	mp6	mp4	mp2	mp1	mp4	mp14	mp14	mp10	mp7	mp14

Table 6.10: The first three MPs based on bias for the selected areas for La Niña (1999).

The best MP for Arbaminch, Hawasa, Debremarkos, Direidiwa, Gode, Gondar, Gore, Jimma, Mekele, Neghelli, and Robe is MP8 in terms low bias. The first place for Bahirdar, Combolcha, Harameda, and Methehara is occupied by MP7. For Addis Ababa and Lekemte the best microphysics are MP5 and MP6 respectively. Therefore MP8 is best for 11 places, MP7 for 4 places, and MP5 and MP6 for the rest two places. The minimum and maximum bias for MP8 is 42.20 mm for Mekele and 197.25 mm for Gondar respectively. Here the lion's share is taken by MP8.

Using MAE Table 10 from the appendix, the first three best MP are given in Table 6.11.

rank	A.A	ARH	HWA	BAD	CCH	DBR	DRW	GD	GNR	GR	HMDA	JMA	LKT	ML	MER	NGL	RB
first	mp5	mp8	mp8	mp7	mp7	mp8	mp8	mp8	mp8	mp8	mp7	mp8	mp14	mp8	mp7	mp8	mp8
second	mp3	mp10	mp10	mp8	mp8	mp7	mp7	mp7	mp7	mp10	mp8	mp7	mp10	mp6	mp8	mp14	mp4
thrid	mp14	mp7	mp6	mp10	mp6	mp	mp10	mp6	mp4	mp2	mp1	mp4	mp6	mp14	mp10	mp7	mp14

Table 6.11: The first three MPs based on MAE for the selected areas for La Niña (1999).

The best MP for Arbaminch, Hawasa, Debremarkos, Direidiwa, Gode, Gondar, Gore, Jimma, Mekele, Neghelli, and Robe is MP8 in terms of MAE (Table 6.11). The first place for Bahirdar, Combolcha, Harameda, and Methehara is occupied by MP7. For Addis Ababa and Lekemte the best microphysics are MP5 and MP14 respectively. Therefor MP8 is best for 11 places, MP7 for 4 places, and MP5 and MP6 for the rest two places. The RMSE value are the same as value of MAE. The minimum and maximum MAE for MP8 is 42.20 mm for Mekele and 197.25 mm for Gondar respectively. Here the lion share is taken by MP8.

In general for La Niña (1999) using correlation coefficient, bias, MAE, and RMSE the lion's share is taken by MP8 for both (using spatial mean) over the country and selected sample regions.

6.6 Grid Scale Precipitation Compared to Observed Precipitation for Normal Year (2004)

6.6.1 Accumulated Total Grid Scale Precipitation over Ethiopia

Accumulated total grid scale precipitation captured by all the selected microphysics and total observation precipitation (GPCC) using contour plot is given in Fig. 6.9. The figure roughly shows that the maximum GPCC precipitation is observed along the western and southern territory of the country whereas the model precipitation maximum value are shifted to the northern part of the country. Concerning the maximum value, the observed (GPCC) and MP7 are similar with maximum value of 600 mm. For MP1, MP2, MP4, MP6, MP10 and MP14, we detected precipitation reaching a maximum of 400 mm. The rest microphysics have a maximum value of 300 mm and 500 mm.

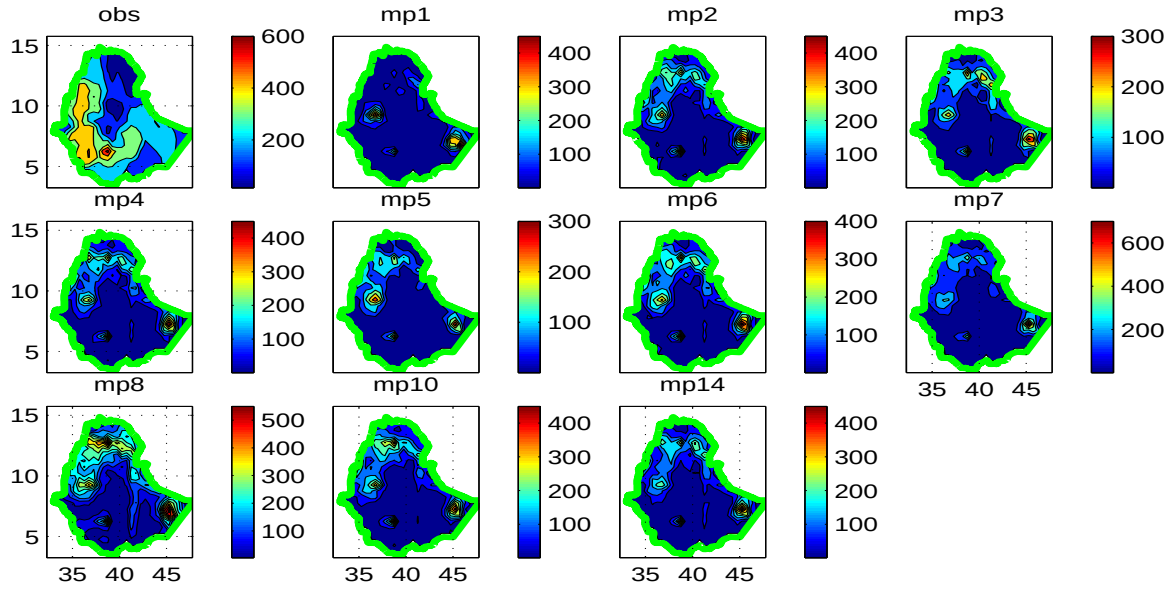

Figure 6.9: Accumulated total grid scale and accumulated GPCC precipitation data.

6.6.2 Grid Scale Accumulated Precipitation for Selected Places

To identify the best MP accumulated Precipitation, line plots are considered for the selected places. The plot for the country and each selected places are given here under.

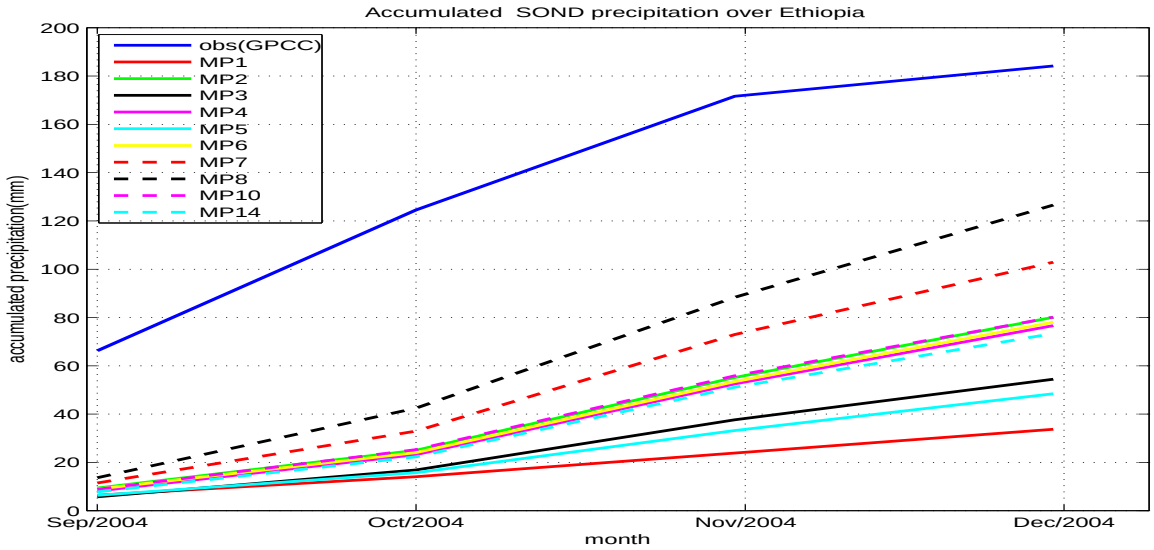

Figure 6.10: Accumulated total grid scale precipitation for each MP and GPCC accumulated precipitation line plot using spatial mean for Ethiopia.

Fig 6.10, Shows that all MP underestimates accumulated total grid scale precipitation, the order of precipitation capturing skill is MP8, MP7, MP10, MP2, MP6, MP4, MP14,

MP3, MP5 and MP1. The accumulated total grid scale precipitation of MP8 is 127 mm. The line plot and the selected sample region also given in Fig. 6.11

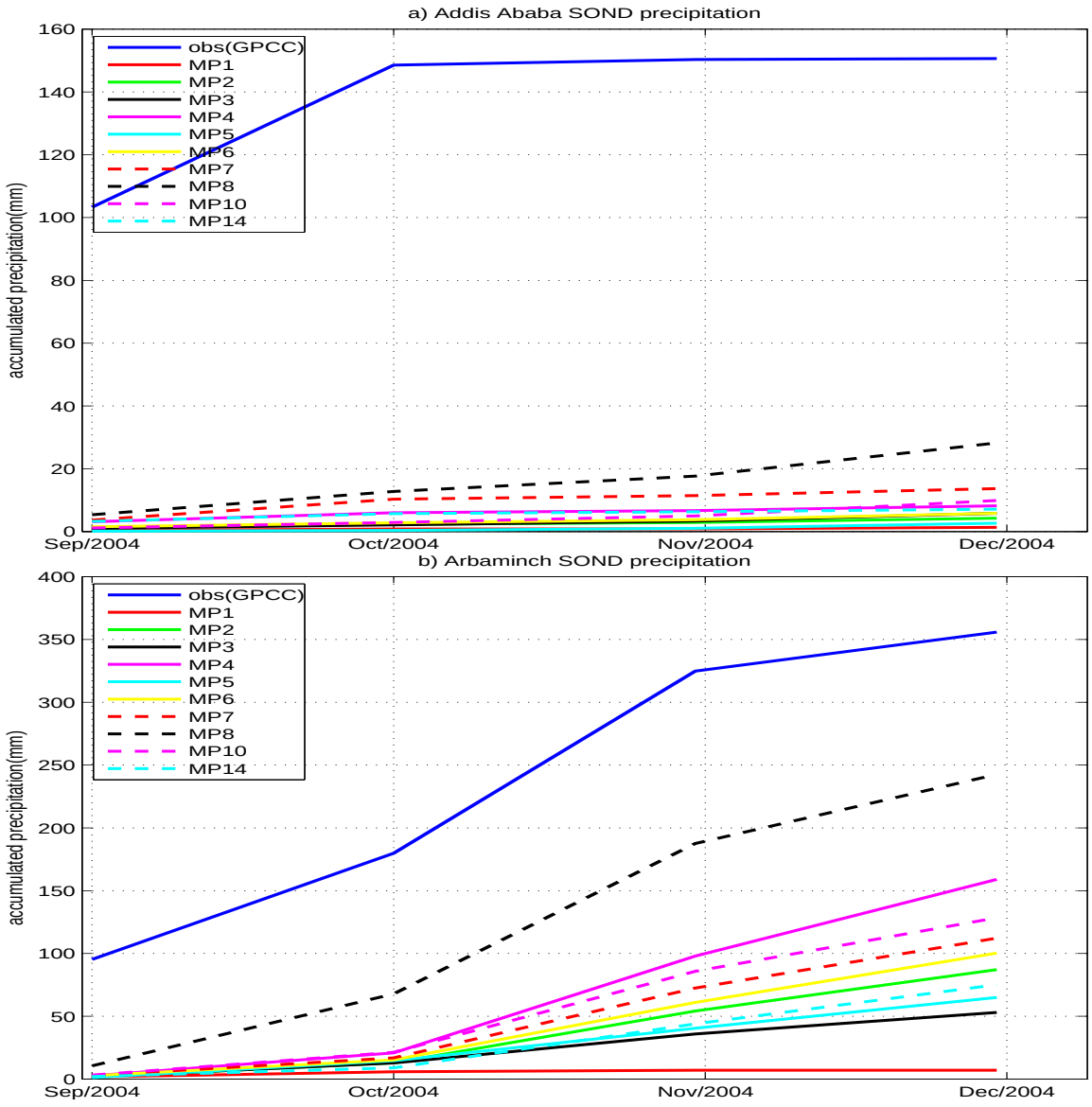

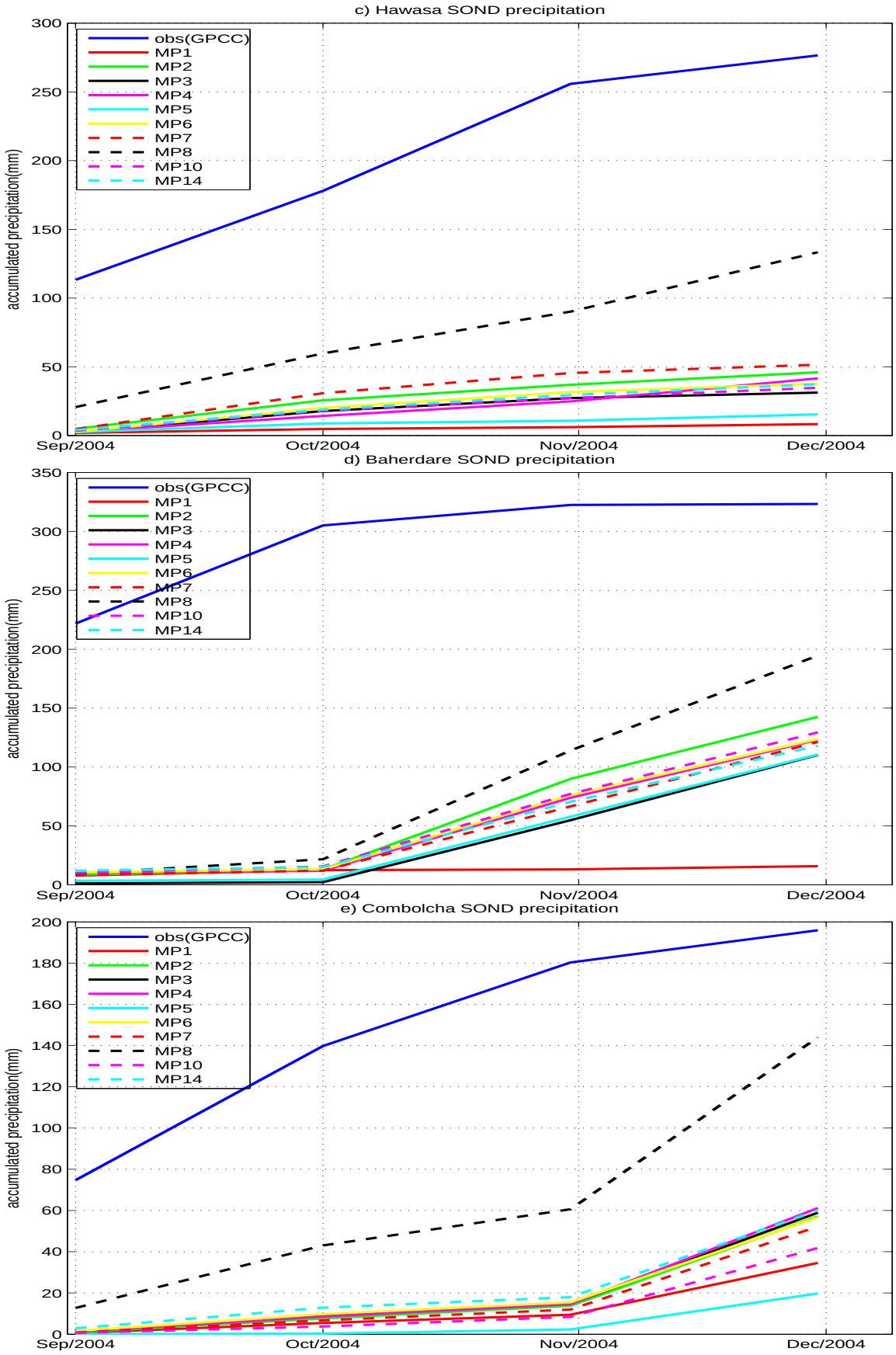
c) Hawasa SOND precipitation
accumulated precipitation(mm)
obs(GPCC)
MP1
MP2
MP3
MP4
MP5
MP6
MP7
MP8
MP10
MP14
Sep/2004
Oct/2004
Nov/2004
Dec/2004
d) Baherdare SOND precipitation
e) Combolcha SOND precipitation

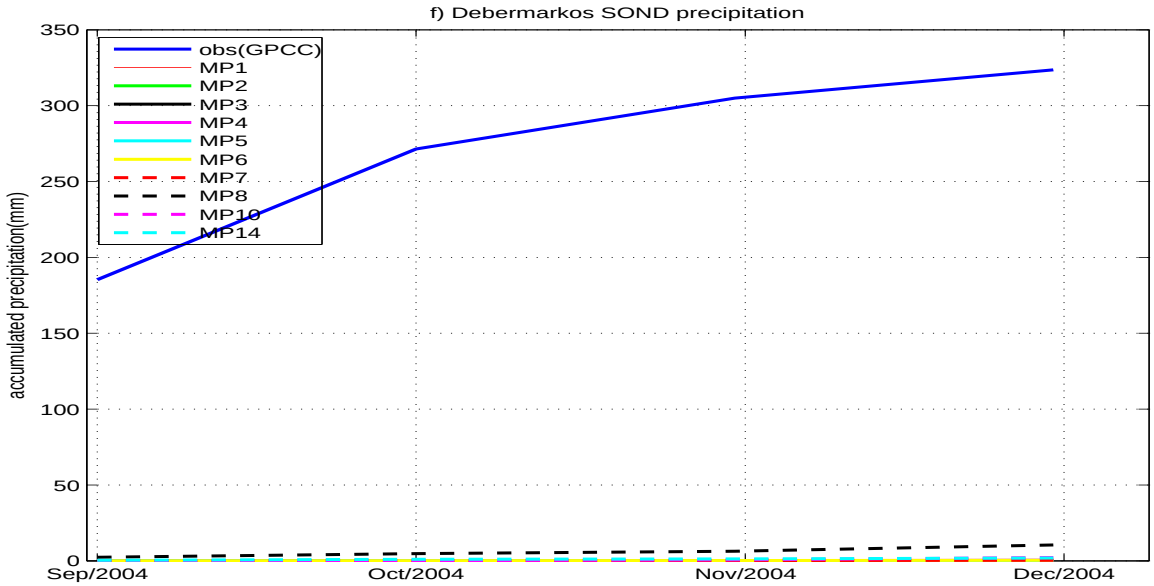
f) Debermarkos SOND precipitation
accumulated precipitation(mm)
obs(GPCC)
MP1
MP2
MP3
MP4
MP5
MP6
MP7
MP8
MP10
MP14
0
50
100
150
200
250
300
350
Sep/2004
Oct/2004
Nov/2004
Dec/2004

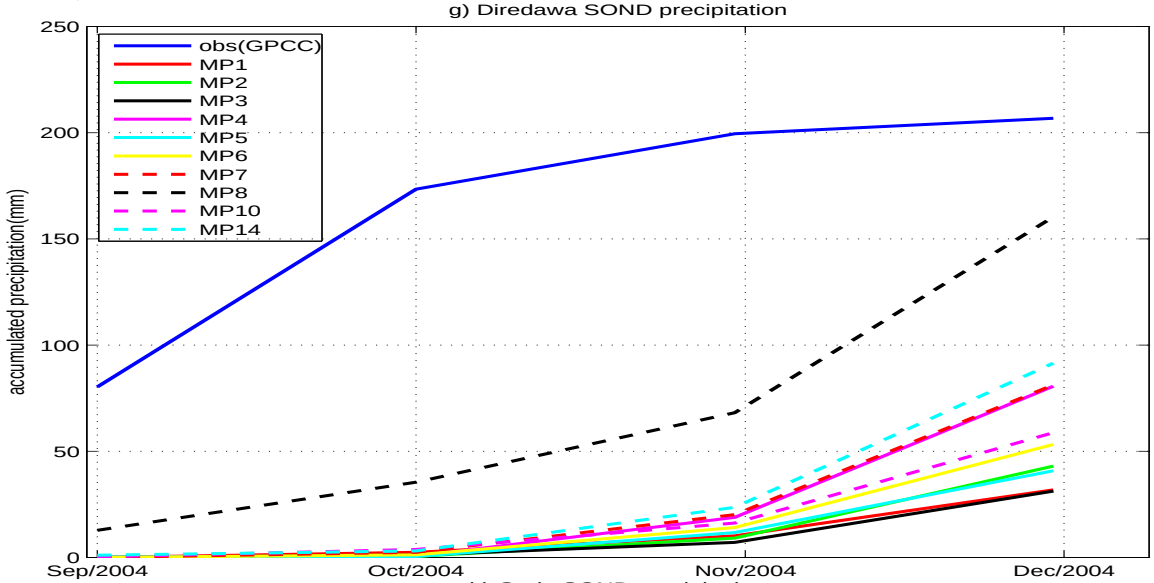
g) Diredawa SOND precipitation
accumulated precipitation(mm)
obs(GPCC)
MP1
MP2
MP3
MP4
MP5
MP6
MP7
MP8
MP10
MP14
0
50
100
150
200
250
Sep/2004
Oct/2004
Nov/2004
Dec/2004

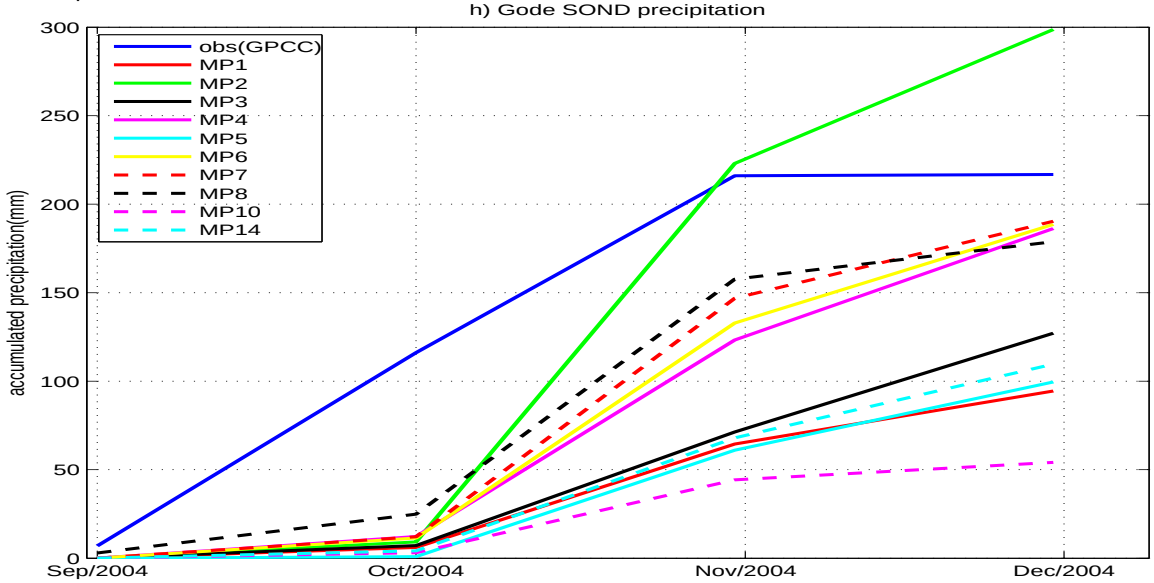
h) Gode SOND precipitation
accumulated precipitation(mm)
obs(GPCC)
MP1
MP2
MP3
MP4
MP5
MP6
MP7
MP8
MP10
MP14
0
50
100
150
200
250
300
Sep/2004
Oct/2004
Nov/2004
Dec/2004

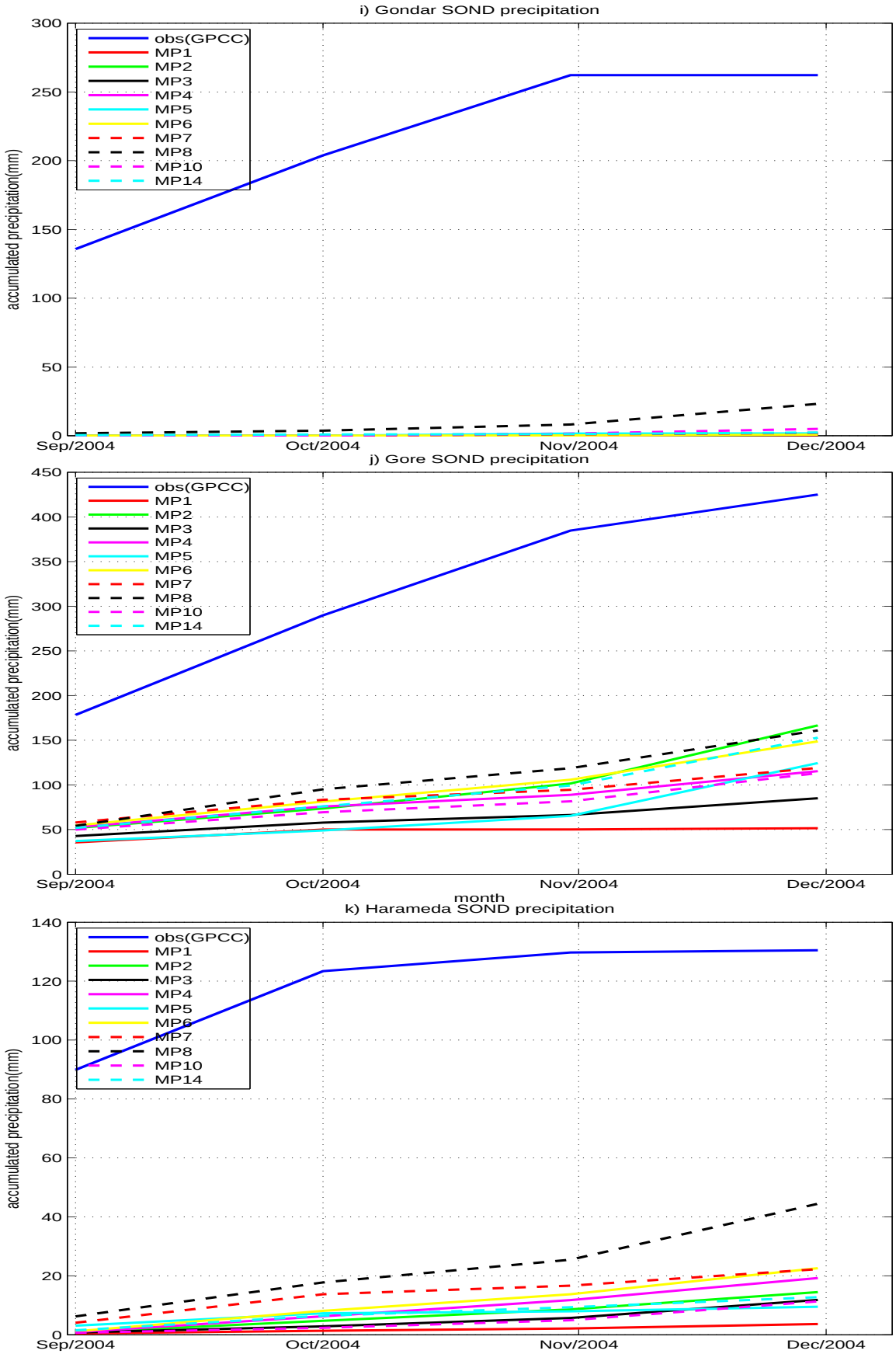
i) Gondar SOND precipitation
accumulated precipitation(mm)
obs(GPCC)
MP1
MP2
MP3
MP4
MP5
MP6
MP7
MP8
MP10
MP14
Sep/2004
Oct/2004
Nov/2004
Dec/2004
j) Gore SOND precipitation
accumulated precipitation(mm)
month
k) Harameda SOND precipitation
accumulated precipitation(mm)

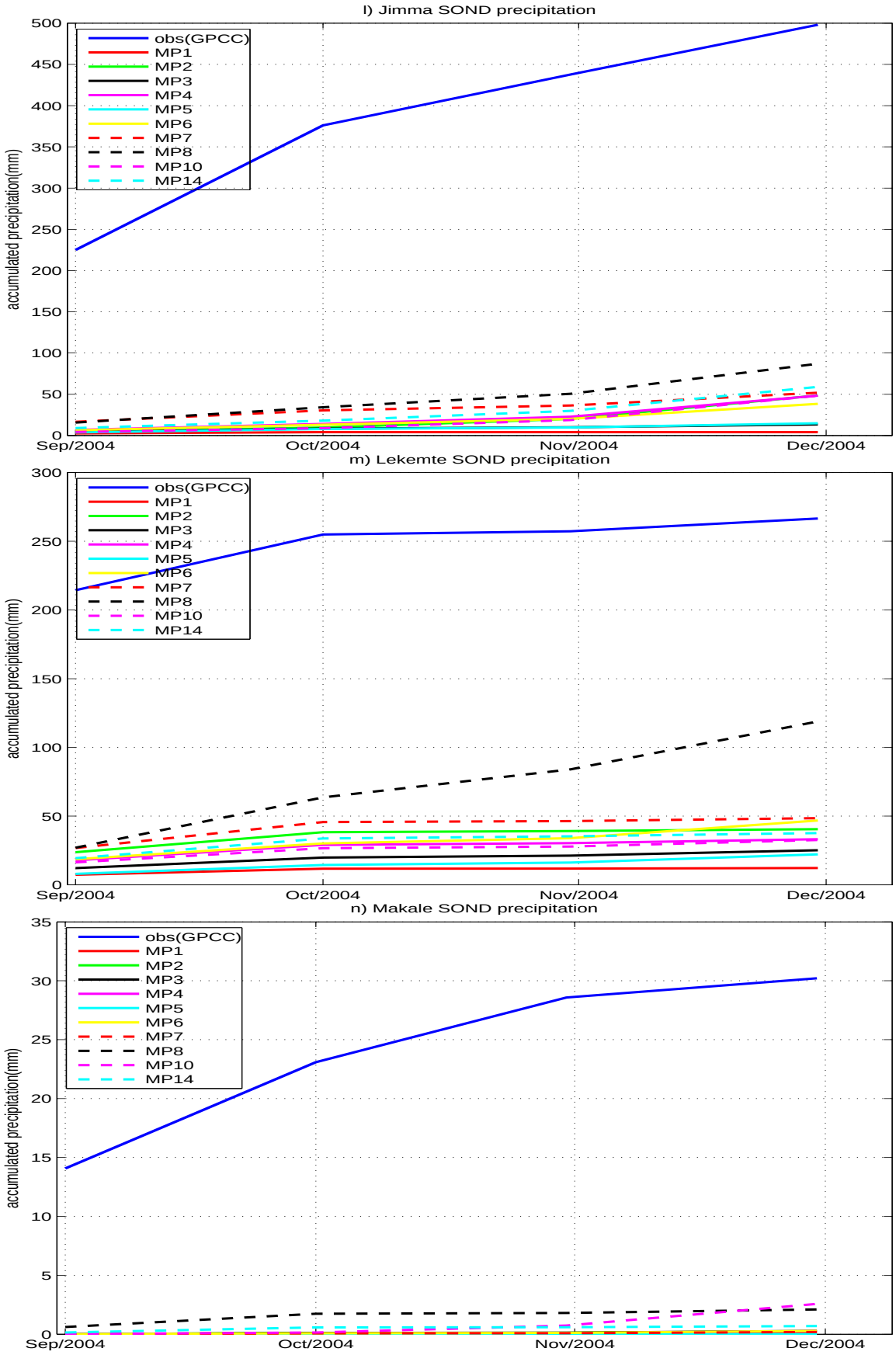
l) Jimma SOND precipitation
accumulated precipitation(mm)
obs(GPCC)
MP1
MP2
MP3
MP4
MP5
MP6
MP7
MP8
MP10
MP14
Sep/2004
Oct/2004
Nov/2004
Dec/2004
m) Lekemte SOND precipitation
n) Makale SOND precipitation

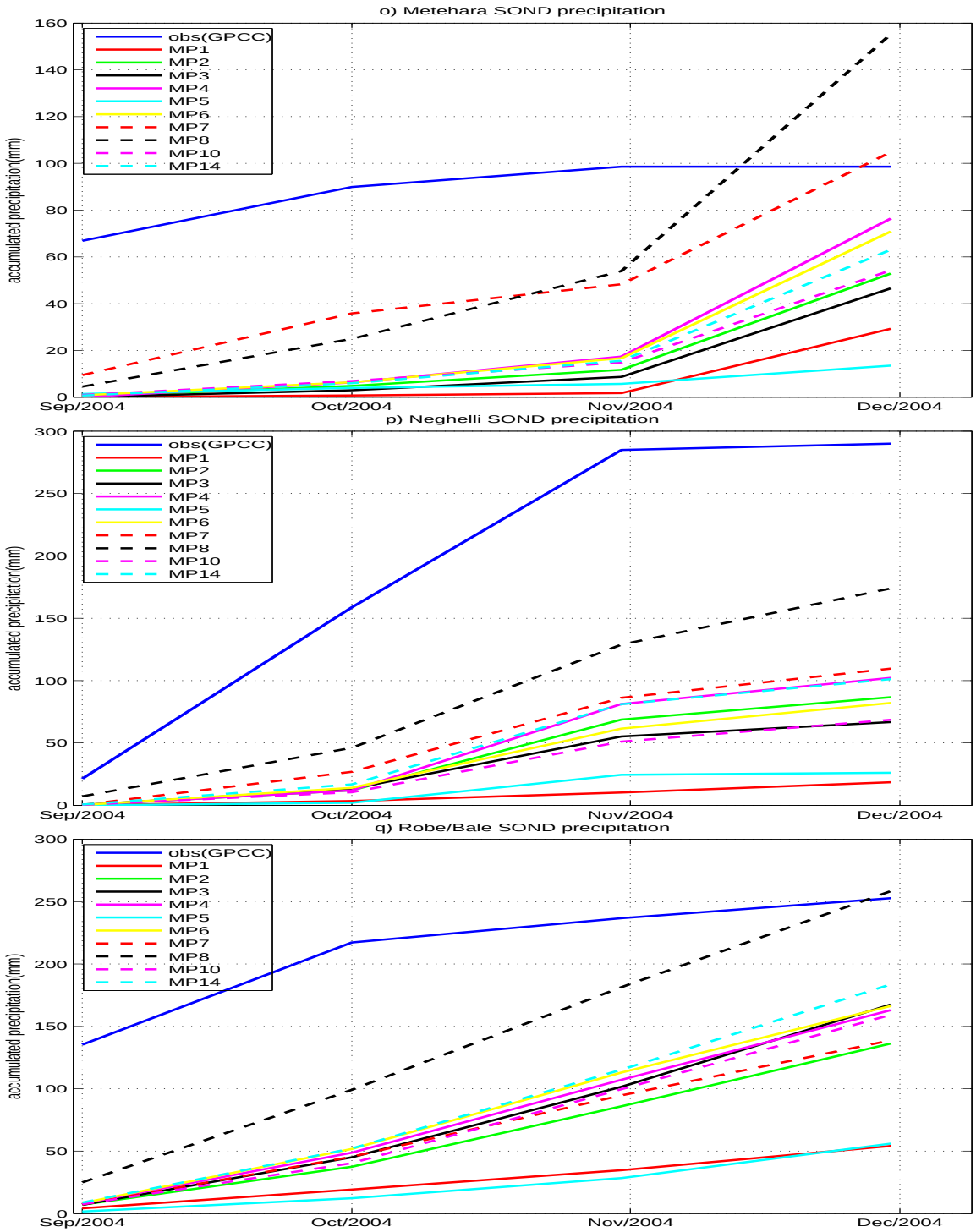

Figure 6.11: Accumulated total grid scale precipitation each selected place and GPCC data.

From Table 3 of the appendix, we categorized the MPs based on their proximity to the observation(GPCC) precipitation as in Table 6.12.

Rank	Eth	A.A	ARM	HWS	BRD	CCH	DMR	DRD	GD	GNR	GR	HMDA	JMM	LKMT	ML	MTHA	NGL	RB
first	mp8	mp8	mp8	mp8	mp8	mp8	mp8	mp8	mp7	mp8	mp2	mp8	mp8	mp8	mp8	mp10	mp8	mp8
second	mp7	mp7	mp4	mp7	mp2	mp14	mp10	mp14	mp6	mp10	mp8	mp6	mp14	mp7	mp8	mp7	mp7	mp14
third	mp10	mp10	mp10	mp2	mp10	mp3	mp14	mp4	mp4	mp14	mp14	mp7	mp7	mp6	mp14	mp4	mp4	mp3
fourth	mp2	mp4	mp7	mp4	mp6	mp2	mp6	mp7	mp8	mp7	mp6	mp4	mp10	mp2	mp3	mp6	mp14	mp6

Table 6.12: The first four MPs nearest to the observed GPCC precipitation for Normal year (2004).

The best MP for Ethiopia as a whole, Hawasa, Bahirdar, Addis Ababa, Debremarkos, Combolcha, Jimma, Harameda, Negellie, Arbamich, Diradiwa, Mekele, and Robe/Bale Gondar and Lekemte is MP8 (Table 6.12). For Gode, Gore and Methehara are the preferable MP are MP7, MP2, and MP10 respectively. Based on this fact among the 17 selected place 14 places are occupied with MP8. The rest 3 places of the first rank is occupied by MP7, MP2 and MP10. Therefore, the MP with a large number of hydrometer such as MP8 is the best MP in capturing precipitation.

The accumulated total grid scale precipitation captured by MP8 for the selected region, the minimum and maximum accumulated total grid scale precipitation is observed over Mekele (2.1 mm) and Robe/Bale (258 mm) respectively.

6.7 Statistical Analysis

1. Statistical analysis for Ethiopia using spatial mean

In this section the statistical tools such as correlation coefficient, root mean square error (RMSE), and mean absolute error (MAE) are applied to validate the precipitation capturing skill of each MP during Normal year against GPCC precipitation. The correlation coefficient over the Country is given in Fig. 6.12.

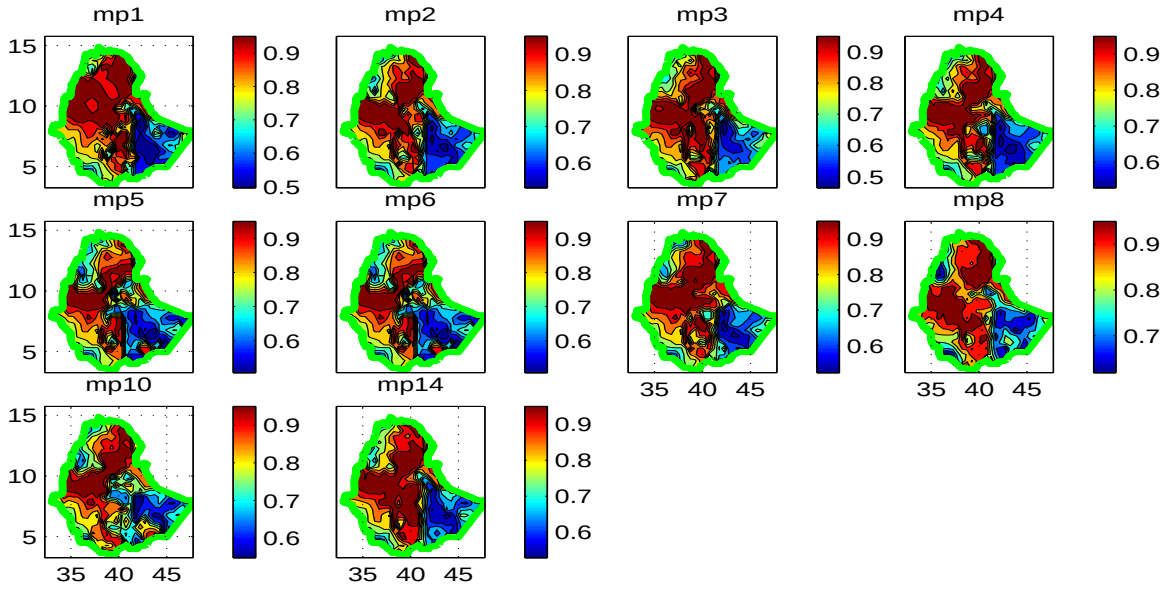

Figure 6.12: Accumulated total grid scale precipitation correlation coefficient over Ethiopia for 10 MP .

Spatial mean accumulated total grid scale Correlation Coefficient, bias, MAE and RMSE over Ethiopia is shown in Table 6.13.

Statistical tools	mp1	mp2	mp3	mp4	mp5	mp6	mp7	mp8	mp10	mp14
corrcoef	0.8366	0.8204	0.8195	0.8195	0.7935	0.7935	0.8282	0.8655	0.8334	0.8349
BIAS	-111.09	-89.02	-103.12	-91.52	-104.11	-90.48	-77.59	-64.34	-88.39	-93.01
MAE	118.57	109.76	114.75	111.54	114.55	109.89	108.09	102.14	108.65	111.69
RMSE	148.26	137.29	143.57	139.15	142.93	136.93	134.94	130.07	136.69	139.47

Table 6.13: Correlation coefficient, bias, MAE and RMSE of accumulated total grid scale precipitation for Normal year (2004).

The accumulated total grid scale precipitation over Ethiopia shows that the best three MP using correlation coefficient are MP8, MP1, and MP14 (see Table 6.13). Using bias the first three MP are MP8, MP7 and MP10. Similarly for both MAE and RMSE, the first three MP are MP8, MP7, and MP10. Therefore, based on bias, MAE, and RMSE the best three microphysics in capturing precipitation for normal year are MP8, MP7 and MP10. Therefore the best MP for the Country is MP8.

2. Statistical analysis for the selected areas

From, Table 12 of the appendix the rank of accumulated total grid scale correlation coefficient for each selected places the first three best MP are displayed in Table 6.14.

Rank	A.A	ARM	HWS	BRD	CCH	DMR	DRD	GD	GNR	GR	HMDA	JMM	LKMT	ML	MTHA	NGL	RB
first	mp7	mp8	mp10	mp1	mp8	mp1	mp8	mp8	mp5	mp8	mp7	mp7	mp3	mp8	mp7	mp7	mp1
second	mp14	mp7	mp6	mp8	mp14	mp14	mp14	mp7	mp14	mp7	mp5	mp3	mp4	mp7	mp5	mp3	mp7
thrid	mp4	mp14	mp14	mp2	mp10	mp2	mp1	mp10	mp6	mp3	mp14	mp5	mp1	mp3	mp8	mp14	mp8

Table 6.14: The first three best MPs in capturing precipitation skill using correlation coefficient for Normal year (2004).

The correlation coefficient of Addis Ababa, Harameda, Jimma, Metehara, and Neghelli are the best microphysics is MP7 with a value 0.965, 0.913, 0.973, 0.787 and 0.996 respectively. MP8 is the best MP for Arbamich, Combolcha, Direidiwa, Gode, Gore and Mekele are the best microphysics with a value 0.987, 0.881, 0.795, 0.924, 0.976 and 0.905 respectively. Similarly MP1 are best MP for Bahirdar, Debremarkos and Robe/Bale using correlation coefficient with a value 0.749, 0.986, and 0.961 respectively. Finally MP10 with a value 0.99, MP5 with a value 0.964, and MP3 with a value 1 for Hawasa, Gondar and Lekemte respectively. Here MP8 for 6 places, MP7 for 5 places, MP1 for 3 places and the other 3 MP for 3 places are the best MP. Therefore MP8 is the best one. The rest of the statistical tools bias, MAE, and RMSE are given, like the correlation coefficient, using concerned tables from the appendix.

Using bias Table 13 from the appendix the first three best MPs are summarized in Table 6.15.

rank	A.A	ARH	HWA	BAD	CCH	DBR	DRW	GD	GNR	GR	HMDA	JMA	LKT	ML	MER	NGL	RB
first	mp8	mp8	mp8	mp8	mp8	mp8	mp8	mp2	mp8	mp8	mp8	mp8	mp8	mp8	mp8	mp8	mp8
second	mp7	mp10	mp7	mp2	mp14	mp14	mp14	mp8	mp10	mp6	mp7	mp7	mp7	mp10	mp7	mp7	mp4
thrid	mp4	mp7	mp2	mp10	mp4	mp10	mp7	mp7	mp14	mp14	mp6	mp14	mp6	mp14	mp4	mp14	mp6

Table 6.15: The first three MPs based on bias for the selected areas for Normal year (2004).

The best microphysics except Gode for each selected area is MP8 in terms low bias.

The first place for Gode is occupied by MP2. Therefor MP8 is best for 16 places with a maximum and a minimum value of 337.30 mm for Jimma and 22.43 mm for Mekele respectively. Here the lion's share is taken by MP8.

Using Table 14 from the appendix, the first three best MP for MAE is given in Table 6.16.

rank	A.A	ARH	HWA	BAD	CCH	DBR	DRW	GD	GNR	GR	HMDA	JMA	LKT	ML	MER	NGL	RB
first	mp8	mp8	mp8	mp8	mp8	mp8	mp8	mp8	mp8	mp8	mp78	mp8	mp8	mp8	mp7	mp8	mp8
second	mp7	mp4	mp7	mp2	mp14	mp14	mp14	mp2	mp10	mp6	mp7	mp7	mp7	mp10	mp8	mp7	mp14
thrid	mp4	mp10	mp2	mp10	mp3	mp10	mp7	mp7	mp14	mp14	mp6	mp14	mp6	mp14	mp4	mp14	mp6

Table 6.16: The first three MPs based on MAE and RMSE for the selected areas for Normal year (2004).

The best MP for each selected area is MP8 in terms of MAE (Table 6.16). But the first place for Metehara is occupied by MP7. Therefor MP8 is best for 16 places with a maximum and a minimum value 337.30 mm for Jimma and 22.43 mm for Mekele respectively. The best MP for RMSE is same to MAE.

In general, for Normal (2004) using correlation coefficient, bias, MAE, and RMSE validation the lions share is taken by MP8 (Thompson scheme) for both (using spatial mean) over the country and selected sample regions.

Chapter 7

Summary and Conclusions

The weather research and forecasting (WRF) model is a numerical weather predication (NWP) and atmosphere simulation system designed for both research and operational application.

For the objective of this study is to identify the skill of microphysics scheme in WRF in capturing SOND precipitation during El Niño, La Niña , and normal years, the selected microphysics are Kessler, Lin et al (Purdue), WRF Single-Moment 3-class, WRF Single-Moment 5-class, Eta (Ferrer), WRF Single-Moment 6-class, Goddard microphysics, New Thompson et al., Morrison double-moment, and WRF Double-Moment 5-class schemes. The simulation is carried out using single domain employing 10 km by 10 km grid separation.

The precipitation data obtained for each events from the simulation are validated applying the statistical tools; bias, MAE, RMSE, and correlation coefficient.

The analysis has shown that precipitation capturing skill of most microphysics are almost same for all events. The result has pointed out that the best 3 microphysics for each event in order are;

- Morrison 2-moment, Thompson, and WSM6 for El Niño year,
- Thompson, Goddard, and Morrison 2-moment for La Niña year, and

- Thompson, Goddard, and Morrison 2-moment for Normal year.

In brief, the WRF microphysics is not robust enough to reproduce short rains over Ethiopia as revealed by large discrepancies between simulated and observed precipitation. Howvever, this study concludes that MP8 has relatively better performance than the remaining nine WRF microphysics. This indicates that as the number of hydrometer of microphysics increases, and also the precipitation capturing skill increases. Therfore, we recommend that the insight obtained in this studied be used to improve the WRF microphysics in the direction of working to include more hydrometer.

Appendix

country	obs(GPCC)	mp1	mp2	mp3	mp4	mp5	mp6	mp7	mp8	mp10	mp14
Ethiopia	325.0	25.1	125.0	89.0	121.0	134.0	123.0	153.0	178.0	133.0	111.0
Addis Ababa	169.0	124.0	346.0	263.0	355.0	419.0	313.0	308.0	502.0	371.0	277.0
Arbaminch	748.0	1.97	170.0	75.0	193.0	164.0	126.0	245.0	252.0	153.0	72.9
Hawasa	434.0	21.6	305.0	194.0	366.0	326.0	320.0	278.0	481.0	354.0	207.0
Baherdar	371.0	117.0	198.0	121.0	265.0	233.0	295.0	268.0	366.0	373.0	171.0
Combolcha	372.0	26.8	177.0	155.0	180.0	258.0	172.0	237.0	447.0	232.0	237.0
Debermarkos	460.0	56.4	180.0	151.0	189.0	246.0	211.0	222.0	324.0	251.0	163.0
Direḍiwa	328.0	6.3	84.6	63.5	144.0	122.0	72.8	125.0	165.0	187.0	46.1
Gode	410.0	3.95	7.44	7.14	9.64	0.418	12.4	28.1	43.8	12.5	27.3
Gondar	342.0	4.39	63.5	26.2	61.1	90.4	100.0	109.0	190.0	114.0	114.0
Gore	625.0	49.3	391.0	304.0	314.0	363.0	427.0	441.0	606.0	414.0	401.0
Harameda	190.0	14.3	190.0	101.0	148.0	200.0	199.0	137.0	180.0	152.0	162.0
Jimma	750.0	17.2	430.0	349.0	401.0	467.0	402.0	351.0	449.0	378.0	420.0
Lekemte	432.0	299.0	692.0	533.0	642.0	855.0	718.0	780.0	839.0	693.0	718.0
Mekele	174.0	0.694	11.6	9.78	35.2	21.5	9.6	38.0	40.1	25.7	28.6
Metehara	264.0	6.43	170.0	77.4	136.0	161.0	161.0	229.0	235.0	186.0	162.0
Neghelli	406.0	23.2	81.0	63.5	110.0	86.9	102.0	103.0	95.0	142.0	142.0
Robe	493.0	19.1	120.0	120.0	136.0	165.0	124.0	201.0	212.0	125.0	161.0

Table 1: All MPs of accumulated total grid scale precipitation, and observed precipitation (GPCC) of El Niño year (1997).

country	obs(GPCC)	mp1	mp2	mp3	mp4	mp5	mp6	mp7	mp8	mp10	mp14
Ethiopia	184.0	47.8	80.5	56.1	79.2	61.8	81.8	99.1	116.0	84.9	73.0
AddisAbaba	175.0	518.0	390.0	309.0	346.0	290.0	373.0	394.0	435.0	364.0	371.0
Arbaminch	298.0	2.0	28.6	21.3	42.3	24.2	21.4	33.5	66.8	47.9	34.5
Hawasa	294.0	71.5	83.7	38.7	73.1	73.9	77.1	96.1	163.0	114.0	48.3
Baherdar	421.0	165.0	192.0	129.0	213.0	185.0	224.0	291.0	269.0	232.0	127.0
Combolcha	266.0	26.6	96.6	54.0	106.0	35.1	83.1	121.0	116.0	64.9	86.2
Debermarkos	381.0	103.0	183.0	116.0	179.0	150.0	201.0	247.0	249.0	184.0	183.0
Direditwa	165.0	2.78	24.5	6.8	25.0	4.93	7.36	23.5	57.1	32.3	7.35
Gode	109.0	0.936	2.24	2.59	4.19	3.39	5.13	5.62	54.3	6.82	5.04
Gondar	497.0	51.6	123.0	122.0	134.0	147.0	137.0	189.0	153.0	143.0	143.0
Gore	539.0	153.0	395.0	235.0	326.0	330.0	332.0	331.0	424.0	474.0	282.0
Harameda	182.0	103.0	111.0	59.8	95.1	61.6	77.9	159.0	126.0	114.0	118.0
Jimma	415.0	125.0	313.0	200.0	275.0	194.0	265.0	329.0	341.0	244.0	242.0
Lekemte	575.0	577.0	592.0	578.0	703.0	509.0	708.0	777.0	755.0	663.0	713.0
Mekele	65.3	7.6	5.3	5.39	6.78	1.81	10.2	6.29	15.6	6.46	7.71
Metehara	210.0	16.4	17.7	9.27	12.6	26.2	14.8	41.1	41.3	44.5	21.7
Neghelli	157.0	7.15	19.4	33.6	47.7	4.91	20.5	56.4	68.8	11.8	58.6
Robe/Bale	315.0	108.0	83.0	72.3	129.0	48.9	99.1	83.8	141.0	101.0	79.9

Table 2: All MPs of accumulated total grid scale precipitation, and observed precipitation (GPCC) of La Niña year (1999).

country	obs(GPCC)	mp1	mp2	mp3	mp4	mp5	mp6	mp7	mp8	mp10	mp14
Ethiopia	184.0	33.7	80.1	54.4	76.6	48.4	78.0	103.0	127.0	80.1	73.4
AddisAbaba	151.0	1.35	4.25	5.82	8.19	2.68	5.8	13.7	28.2	9.88	7.15
Arbaminch	356.0	7.07	87.2	53.1	159.0	65.0	100.0	112.0	243.0	128.0	75.1
Hawasa	277.0	8.3	45.9	31.2	41.5	15.3	37.8	51.5	133.0	34.7	37.3
Baherdar	323.0	15.9	143.0	110.0	123.0	111.0	124.0	121.0	195.0	129.0	118.0
Combolcha	196.0	34.6	57.1	58.9	61.2	19.7	56.7	52.2	144.0	41.8	60.1
Debermarkos	324.0	0.0513	0.167	0.255	0.378	0.0321	0.398	0.379	10.5	2.21	1.89
Direditwa	207.0	31.9	43.0	31.3	80.7	40.9	53.2	81.2	160.0	58.8	91.5
Gode	217.0	94.5	299.0	127.0	186.0	99.6	189.0	190.0	179.0	54.1	110.0
Gondar	262.0	0.0815	0.807	0.522	1.26	1.67	0.733	1.99	23.2	4.91	2.34
Gore	425.0	51.5	167.0	85.0	115.0	124.0	149.0	119.0	161.0	113.0	153.0
Harameda	130.0	3.64	14.5	11.8	19.2	9.5	22.6	22.3	44.5	11.3	12.7
Jimma	498.0	4.13	48.5	13.5	48.3	14.9	38.4	51.9	87.0	48.3	59.0
Lekemte	267.0	12.2	40.5	25.2	33.2	22.2	46.8	48.5	119.0	32.6	37.7
Mekele	30.2	0.098	0.256	0.281	0.259	0	0.28	0.189	2.1	2.57	0.695
Methehara	98.6	29.3	52.9	46.5	76.4	13.5	70.9	105.0	155.0	54.3	63.1
Neghelli	290.0	18.5	86.7	66.7	102.0	26.1	82.1	110.0	174.0	68.6	101.0
Robe	253.0	54.1	136.0	167.0	163.0	55.9	166.0	139.0	258.0	159.0	184.0

Table 3: All MPs of accumulated total grid scale precipitation and observed precipitation (GPCC) of Normal year (2004).

- El Niño year(1997)

country	mp1	mp2	mp3	mp4	mp5	mp6	mp7	mp8	mp10	mp14
AddisAbaba	0.974	0.914	0.922	0.905	0.915	0.919	0.919	0.919	0.913	0.916
Arbaminch	0.978	0.978	0.981	0.979	0.963	0.981	0.98	0.978	0.984	0.978
Hawasa	0.993	0.936	0.938	0.935	0.929	0.926	0.938	0.948	0.951	0.937
Baherdar	0.988	0.895	0.926	0.925	0.893	0.933	0.914	0.89	0.927	0.903
Combolcha	0.851	0.958	0.954	0.948	0.948	0.956	0.958	0.963	0.95	0.95
Debermarkos	0.995	0.93	0.938	0.936	0.914	0.917	0.935	0.936	0.938	0.93
Direditwa	0.721	0.78	0.778	0.802	0.816	0.813	0.791	0.829	0.832	0.721
Gode	0.841	0.877	0.885	0.887	0.77	0.856	0.828	0.891	0.842	0.853
Gondar	0.998	0.852	0.856	0.849	0.852	0.849	0.853	0.865	0.868	0.837
Gore	0.957	0.917	0.9	0.904	0.911	0.897	0.891	0.908	0.905	0.881
Harameda	0.997	0.913	0.917	0.885	0.892	0.9	0.889	0.902	0.896	0.879
Jimma	0.959	0.929	0.923	0.928	0.908	0.923	0.927	0.929	0.932	0.93
Lekemte	0.987	0.957	0.949	0.951	0.944	0.933	0.915	0.912	0.917	0.903
Mekele	0.781	0.872	0.846	0.874	0.89	0.872	0.895	0.89	0.9	0.879
Metehara	0.705	0.841	0.841	0.843	0.858	0.864	0.845	0.896	0.918	0.842
Neghelli	0.897	0.939	0.948	0.961	0.947	0.946	0.907	0.945	0.94	0.921
Robe	0.99	0.937	0.937	0.932	0.943	0.942	0.959	0.946	0.94	0.952

Table 4: Correlation coefficient of accumulated total grid scale precipitation of each selected area for El Niño year (1997).

country	mp1	mp2	mp3	mp4	mp5	mp6	mp7	mp8	mp10	mp14
AddisAbaba	-18.21	79.05	38.69	70.41	127.20	65.95	56.74	144.61	78.88	36.47
Arbaminch	-398.12	-282.14	-323.96	-273.83	-276.00	-289.56	-242.84	-229.45	-288.25	-307.74
Hawasa	-256.56	-95.00	-155.44	-85.03	-78.16	-97.08	-110.77	-17.22	-74.24	-158.90
Baherdar	-196.78	-137.29	-214.95	-121.58	-134.46	-95.94	-94.74	-66.80	-38.99	-165.70
Combolcha	-243.54	-152.88	-172.57	-153.91	-113.64	-156.77	-115.69	-31.42	-133.57	-125.15
Debermarkos	-316.49	-235.06	-259.90	-233.59	-207.87	-228.44	-217.07	-160.33	-204.06	-248.49
Direditwa	-235.41	-174.75	-179.27	-166.77	-158.73	-175.87	-156.50	-113.15	-137.48	-184.36
Gode	-270.24	-266.78	-266.46	-267.00	-271.34	-264.39	-252.25	-243.46	-265.19	-263.02
Gondar	-254.35	-173.08	-208.17	-164.48	-170.14	-149.78	-162.32	-138.76	-148.94	-174.37
Gore	-470.82	-276.38	-342.09	-303.54	-251.47	-262.55	-251.39	-172.94	-230.71	-312.52
Harameda	-113.91	-27.22	-77.71	-42.45	-11.80	-27.76	-52.13	-30.22	-48.45	-48.50
Jimma	-521.56	-269.13	-339.91	-282.47	-270.27	-288.38	-275.83	-257.26	-287.11	-283.16
Lekemte	-144.6093	71.28	-41.88	34.90	134.61	80.60	114.84	160.91	62.18	47.32
Mekele	-128.54	-118.28	-119.36	-108.20	-112.31	-116.37	-104.72	-97.96	-112.59	-115.11
Metehara	-195.3084	-108.5610	-145.9421	-115.4307	-112.3121	-118.71	-84.72	-76.11	-113.3995	-116.6695
Neghelli	-265.63	-249.81	-251.11	-231.58	-234.77	-236.60	-212.97	-215.32	-235.30	-231.30
Robe/Bale	-323.63	-247.53	-437.41	-233.85	-228.61	-232.87	-209.96	-199.84	-250.68	-220.15

Table 5: Bias of accumulated total grid scale precipitation using 10 microphysics for El Niño year (1997).

country	mp1	mp2	mp3	mp4	mp5	mp6	mp7	mp8	mp10	mp14
AddisAbaba	23.9	79.5	51.4	72.0	127.0	73.4	60.8	145.0	84.3	50.9
Arbaminch	398.0	282.0	324.0	274.0	276.0	290.0	243.0	229.0	288.0	308.0
Hawasa	257.0	95.0	155.0	95.6	98.5	100.0	111.0	84.3	86.4	159.0
Baherdar	197.0	137.0	215.0	122.0	134.0	95.9	94.7	66.8	39.0	166.0
Combolcha	244.0	153.0	173.0	154.0	114.0	157.0	116.0	45.0	134.0	125.0
Debermarkos	316.0	235.0	260.0	234.0	208.0	228.0	217.0	160.0	204.0	248.0
Direidiwa	235.0	175.0	179.0	167.0	159.0	176.0	157.0	113.0	137.0	184.0
Gode	270.0	267.0	266.0	267.0	271.0	264.0	252.0	243.0	265.0	263.0
Gondar	254.0	173.0	208.0	72.0	170.0	150.0	162.0	139.0	149.0	174.0
Gore	471.0	276.0	342.0	304.0	251.0	263.0	251.0	173.0	231.0	313.0
Harameda	114.0	28.3	77.7	42.4	47.5	30.0	52.1	33.5	48.4	48.5
Jimma	522.0	269.0	340.0	282.0	270.0	288.0	276.0	257.0	287.0	283.0
Lekemte	145.0	100.0	53.9	81.5	135.0	97.7	115.0	161.0	88.1	105.0
Mekele	129.0	118.0	119.0	108.0	112.0	116.0	105.0	98.0	113.0	115.0
Metehara	195.0	109.0	146.0	115.0	101.0	119.0	84.7	76.1	113.0	117.0
Neghelli	266.0	250.0	251.0	232.0	235.0	237.0	213.0	215.0	235.0	231.0
Robe	324.0	248.0	249.0	234.0	229.0	233.0	210.0	200.0	251.0	220.0

Table 6: Mean absolute error of accumulated total grid scale precipitation using 10 microphysics for El Niño year (1997).

country	mp1	mp2	mp3	mp4	mp5	mp6	mp7	mp8	mp10	mp14
AddisAbaba	25.2	106.0	64.8	98.2	160.0	96.4	81.5	185.0	111.0	62.8
Arbaminch	467.0	317.0	370.0	307.0	307.0	327.0	270.0	254.0	325.0	348.0
Hawasa	274.0	113.0	162.0	110.0	109.0	119.0	122.0	98.4	97.0	165.0
Baherdar	209.0	143.0	223.0	126.0	139.0	100.0	101.0	80.0	51.5	171.0
Combolcha	272.0	164.0	187.0	165.0	121.0	169.0	123.0	57.7	142.0	134.0
Debermarkos	335.0	241.0	268.0	240.0	214.0	234.0	224.0	166.0	208.0	256.0
Direidiwa	262.0	194.0	199.0	186.0	177.0	195.0	175.0	132.0	155.0	205.0
Gode	314.0	310.0	309.0	310.0	315.0	307.0	292.0	282.0	308.0	305.0
Gondar	275.0	184.0	222.0	175.0	181.0	160.0	174.0	149.0	159.0	185.0
Gore	495.0	284.0	351.0	312.0	260.0	272.0	262.0	193.0	241.0	322.0
Harameda	122.0	40.1	80.8	53.4	49.8	42.8	59.3	43.9	56.5	57.1
Jimma	564.0	282.0	354.0	295.0	287.0	301.0	289.0	271.0	299.0	296.0
Lekemte	169.0	124.0	70.1	90.0	188.0	127.0	157.0	210.0	111.0	119.0
Mekele	141.0	129.0	130.0	117.0	122.0	127.0	113.0	106.0	122.0	125.0
Metehara	213.0	118.0	156.0	125.0	111.0	127.0	98.4	86.1	120.0	126.0
Neghelli	292.0	273.0	275.0	252.0	255.0	257.0	229.0	233.0	256.0	251.0
Robe	346.0	258.0	259.0	243.0	236.0	241.0	217.0	206.0	261.0	227.0

Table 7: Root mean square error accumulated total grid scale precipitation using 10 microphysics for El Niño year (1997).

- La Niña Year(1999)

country	mp1	mp2	mp3	mp4	mp5	mp6	mp7	mp8	mp10	mp14
AddisAbaba	0.983	0.976	0.981	0.975	0.975	0.974	0.982	0.961	0.971	0.968
Arbaminch	0.913	0.814	0.864	0.833	0.803	0.823	0.839	0.84	0.824	0.845
Hawasa	0.939	0.940	0.95	0.957	0.958	0.94	0.955	0.945	0.934	0.956
Baherdar	0.992	0.988	0.992	0.991	0.997	0.996	0.992	0.99	0.996	0.99
Combolcha	0.975	0.98	0.963	0.974	0.981	0.972	0.972	0.955	0.965	0.965
Debermarkos	0.987	0.984	0.984	0.979	0.983	0.983	0.982	0.983	0.986	0.982
Direḍiwa	0.91	0.883	0.874	0.871	0.9	0.875	0.901	0.933	0.885	0.91
Gode	0.759	0.78	0.704	0.75	0.616	0.777	0.787	0.814	0.798	0.782
Gondar	0.979	0.984	0.983	0.987	0.983	0.987	0.986	0.978	0.985	0.986
Gore	0.972	0.972	0.968	0.968	0.965	0.962	0.972	0.963	0.965	0.962
Harameda	0.986	0.981	0.991	0.969	0.98	0.971	0.971	0.966	0.976	0.952
Jimma	0.983	0.962	0.966	0.958	0.97	0.954	0.965	0.959	0.973	0.966
Lekemte	0.955	0.976	0.979	0.97	0.978	0.977	0.972	0.973	0.974	0.975
Mekele	0.965	0.98	0.982	0.982	0.983	0.984	0.969	0.982	0.989	0.987
Metehara	0.766	0.859	0.757	0.846	0.887	0.848	0.885	0.877	0.873	0.824
Neghelli	0.738	0.678	0.663	0.711	0.698	0.702	0.674	0.691	0.731	0.685
Robe/Bale	0.976	0.938	0.918	0.921	0.943	0.92	0.94	0.9	0.906	0.923

Table 8: Correlation coefficient of accumulated total grid scale: WRF Simulate precipitation using 10 microphysics for La Niña year (1999).

country	mp1	mp2	mp3	mp4	mp5	mp6	mp7	mp8	mp10	mp14
AddisAbaba	175.63	130.97	56.03	90.21	45.23	100.85	132.57	125.17	78.46	68.69
Arbaminch	-190.64	-163.65	-164.26	-157.70	-174.39	-164.80	-157.82	-132.75	-156.02	-169.82
Hawasa	-154.67	-136.75	-158.93	-134.21	-157.61	-128.91	-129.78	-91.10	-126.20	-155.05
Baherdar	-203.65	-192.70	-251.29	-185.76	-201.41	-169.30	-123.49	-128.0	-163.26	-231.85
Combolcha	-187.60	-166.06	-182.19	-159.56	-196.45	-155.04	-131.40	-154.58	-173.67	-162.02
Debermarkos	-213.45	-135.23	-188.84	-154.69	-168.29	-135.89	-113.06	-97.52	-143.12	-157.41
Direḍiwa	-121.30	-104.68	-113.19	-109.39	-124.90	-110.578	-99.04	-78.72	-103.76	-114.08
Gode	-74.39	-72.09	-72.62	-72.74	-74.62	-70.23	-67.87	-50.83	-70.90	-70.50
Gondar	-330.36	-226.01	-257.89	-207.72	-264.50	-210.26	-200.51	-197.25	-227.48	-224.72
Gore	-317.40	-166.01	-269.23	-193.24	-217.22	-193.99	-177.48	-121.36	-131.34	-255.89
Harameda	-52.65	-56.77	-83.99	-72.35	-90.52	-68.95	-20.46	-42.11	-62.72	-68.38
Jimma	-223.69	-121.50	-191.20	-111.88	-192.86	-128.98	-94.68	-93.97	-137.88	-136.23
Lekemte	-64.40	-72.51	-116.45	-29.18	-134.18	-5.07	32.45	39.40	-8.98	-20.59
Mekele	-51.93	-52.61	-52.77	-49.51	-54.61	-47.93	-51.29	-42.20	-49.25	-48.77
Metehara	-164.37	-159.28	-165.25	-160.65	-152.97	-158.61	-116.38	-144.88	-148.23	-158.55
Neghelli	-111.90	-102.86	-104.53	-97.56	-111.76	-103.41	-93.78	-73.34	-108.94	-89.91
Robe/Bale	-172.79	-170.92	-262.26	-154.53	-208.54	-160.45	-169.70	-141.12	-171.52	-157.45

Table 9: Bias of accumulated total grid scale: WRF Simulate precipitation using 10 microphysics for La Niña year (1999).

country	mp1	mp2	mp3	mp4	mp5	mp6	mp7	mp8	mp10	mp14
AddisAbaba	176.0	131.0	58.9	90.2	49.4	102.0	133.0	125.0	80.5	77.1
Arbaminch	191.0	164.0	164.0	158.0	174.0	165.0	158.0	133.0	156.0	170.0
Hawasa	155.0	137.0	159.0	134.0	158.0	129.0	130.0	91.1	126.0	155.0
Baherdar	204.0	193.0	251.0	186.0	201.0	169.0	123.0	128.0	163.0	232.0
Combolcha	188.0	166.0	182.0	160.0	196.0	155.0	131.0	155.0	174.0	162.0
Debermarkos	213.0	135.0	189.0	155.0	168.0	136.0	113.0	97.5	143.0	157.0
Direditwa	121.0	105.0	113.0	109.0	125.0	111.0	99.0	78.7	104.0	114.0
Gode	74.4	72.1	72.6	72.7	74.6	70.2	67.9	50.8	70.9	70.5
Gondar	330.0	226.0	258.0	208.0	265.0	210.0	201.0	197.0	227.0	225.0
Gore	317.0	166.0	269.0	193.0	217.0	194.0	177.0	121.0	131.0	256.0
Harameda	52.6	56.8	84.0	72.3	90.5	69.0	20.5	42.1	62.7	68.4
Jimma	224.0	122.0	191.0	112.0	193.0	129.0	94.7	94.0	138.0	136.0
Lekemte	64.4	72.5	116.0	48.5	134.0	45.8	62.7	67.1	43.3	37.7
Mekele	51.9	52.6	52.8	49.5	54.6	47.9	51.3	42.2	49.2	48.8
Metehara	164.0	159.0	165.0	161.0	153.0	159.0	142.0	145.0	148.0	159.0
Neghelli	112.0	103.0	105.0	97.6	112.0	103.0	93.8	73.3	109.0	89.9
Robe/Bale	173.0	171.0	178.0	155.0	209.0	160.0	170.0	141.0	172.0	157.0

Table 10: Mean absolute error of accumulated tota grid scale: WRF Simulated precipitation using 10 microphysics for La Niña year (1999).

country	mp1	mp2	mp3	mp4	mp5	mp6	mp7	mp8	mp10	mp14
AddisAbaba	199.0	153.0	68.6	106.0	57.8	120.0	148.0	145.0	95.0	88.5
Arbaminch	203.0	174.0	174.0	167.0	185.0	175.0	167.0	142.0	165.0	180.0
Hawasa	158.0	139.0	162.0	136.0	161.0	131.0	132.0	95.0	129.0	158.0
Baherdar	208.0	196.0	258.0	189.0	205.0	173.0	125.0	129.0	165.0	236.0
Combolcha	188.0	166.0	182.0	160.0	196.0	155.0	131.0	155.0	174.0	162.0
Debermarkos	221.0	139.0	195.0	158.0	173.0	139.0	115.0	99.3	146.0	161.0
Direditwa	125.0	107.0	116.0	112.0	129.0	113.0	101.0	80.2	106.0	117.0
Gode	84.9	82.1	82.8	82.9	85.2	79.8	77.0	57.8	80.7	80.2
Gondar	346.0	235.0	266.0	215.0	274.0	219.0	209.0	204.0	236.0	234.0
Gore	324.0	169.0	273.0	196.0	219.0	197.0	180.0	129.0	137.0	259.0
Harameda	54.1	59.1	87.9	75.1	95.0	72.0	25.7	44.6	65.1	71.1
Jimma	230.0	126.0	195.0	117.0	197.0	133.0	102.0	101.0	140.0	139.0
Lekemte	79.9	81.8	120.0	57.4	138.0	47.4	72.3	79.9	44.7	43.5
Mekele	52.7	53.4	53.5	50.3	55.4	48.7	52.1	42.7	50.0	49.5
Metehara	175.0	169.0	176.0	170.0	162.0	168.0	150.0	153.0	157.0	168.0
Neghelli	127.0	117.0	119.0	111.0	127.0	117.0	107.0	86.2	124.0	102.0
Robe/Bale	175.0	174.0	181.0	157.0	213.0	163.0	172.0	145.0	175.0	160.0

Table 11: Root mean square error of accumulated total grid scale precipitation using 10 microphysics for La Niña year (1999).

- Normal Year(2004)

country	mp1	mp2	mp3	mp4	mp5	mp6	mp7	mp8	mp10	mp14
AddisAbaba	0.805	0.858	0.792	0.882	0.79	0.767	0.965	0.848	0.712	0.946
Arbaminch	0.893	0.972	0.975	0.973	0.972	0.975	0.986	0.987	0.976	0.978
Hawasa	0.969	0.988	0.988	0.977	0.969	0.99	0.984	0.976	0.99	0.989
Baherdar	0.749	0.684	0.654	0.664	0.654	0.673	0.659	0.689	0.673	0.677
Combolcha	0.834	0.816	0.816	0.813	0.683	0.822	0.805	0.881	0.836	0.836
Debermarkos	0.986	0.976	0.973	0.868	0.936	0.887	0.857	0.948	0.749	0.984
Direḍiwa	0.761	0.705	0.754	0.685	0.675	0.721	0.724	0.795	0.689	0.761
Gode	0.884	0.885	0.849	0.877	0.859	0.882	0.893	0.924	0.888	0.875
Gondar	0.733	0.782	0.88	0.697	0.964	0.88	0.879	0.809	0.798	0.896
Gore	0.879	0.913	0.951	0.94	0.847	0.932	0.952	0.976	0.919	0.925
Harameda	0.723	0.804	0.721	0.807	0.883	0.813	0.913	0.766	0.719	0.817
Jimma	0.911	0.865	0.951	0.881	0.95	0.898	0.973	0.947	0.859	0.883
Lekemte	0.985	0.991	1.0	1.0	0.974	0.949	0.932	0.956	0.967	0.961
Mekele	0.729	0.832	0.842	0.842	0.57	0.836	0.853	0.905	0.781	0.837
Metehara	0.535	0.665	0.593	0.657	0.712	0.661	0.787	0.693	0.679	0.626
Neghelli	0.929	0.937	0.95	0.939	0.927	0.936	0.966	0.932	0.941	0.942
Robe/Bale	0.961	0.907	0.914	0.908	0.842	0.915	0.925	0.925	0.882	0.896

Table 12: Correlation coefficient of accumulated total grid scale precipitation using 10 microphysics for Normal year (2004).

country	mp1	mp2	mp3	mp4	mp5	mp6	mp7	mp8	mp10	mp14
Addis Ababa	-137.34	-135.49	-135.12	-132.19	-137.14	-134.72	-128.42	-122.18	-133.46	-132.60
Arbaminch	-233.53	-199.90	-212.97	-215.92	-208.63	-194.08	-187.81	-111.80	-179.22	-206.41
Hawasa	-200.65	-177.59	-186.28	-185.13	-196.61	-182.86	-172.83	-129.93	-185.07	-183.49
Baherdar	-280.83	-229.64	-251.01	-238.31	-249.06	-237.22	-241.04	-208.19	-235.13	-239.22
Combolcha	-135.15	-127.81	-126.66	-126.28	-142.08	-126.81	-129.73	-82.58	-134.03	-124.23
Debermarkos	-271.31	-271.24	-271.20	-271.16	-271.32	-271.15	-271.16	-265.34	-270.58	-270.18
Direḍiwa	-153.87	-151.83	-155.11	-139.94	-151.68	-147.85	-139.03	-95.82	-145.23	-135.16
Gode	-97.71	-6.24	-87.59	-58.53	-98.60	-55.76	-51.64	-47.91	-113.61	-93.52
Gondar	-215.96	-215.77	-215.83	-215.66	-215.21	-215.77	-215.26	-206.85	-214.37	-214.82
Gore	-272.63	-221.08	-256.47	-236.25	-250.46	-221.82	-230.76	-212.23	-240.93	-224.47
Harameda	-116.50	-111.23	-113.10	-108.84	-111.42	-106.98	-104.21	-94.90	-113.57	-110.88
Jimma	-380.45	-363.47	-375.12	-361.18	-375.14	-364.71	-350.37	-337.30	-364.08	-355.21
Lekemte	-237.46	-212.84	-228.65	-220.63	-233.05	-215.87	-206.41	-174.87	-222.39	-216.73
Mekele	-23.95	-23.87	-23.86	-23.87	-23.99	-23.87	-23.90	-22.43	-23.12	-23.48
metehara	-80.54	-71.04	-73.92	-63.46	-82.35	-64.80	-38.89	-28.82	-69.25	-67.16
Neghelli	-180.69	-146.82	-154.86	-139.85	-175.59	-149.26	-133.00	-99.70	-156.12	-138.84
Robe	-182.50	-143.84	-130.29	-128.81	-185.99	-125.68	-138.99	-69.54	-133.87	-120.59

Table 13: Bias of accumulated total grid scale precipitation using 10 microphysics for Normal year (2004).

country	mp1	mp2	mp3	mp4	mp5	mp6	mp7	mp8	mp10	mp14
AddisAbaba	137.0	135.0	135.0	132.0	137.0	135.0	128.0	122.0	133.0	133.0
Arbaminch	234.0	200.0	213.0	169.0	209.0	194.0	188.0	112.0	179.0	206.0
Hawasa	201.0	178.0	186.0	185.0	197.0	183.0	173.0	130.0	185.0	183.0
Baherdar	281.0	230.0	251.0	238.0	249.0	237.0	241.0	208.0	235.0	239.0
Combolcha	135.0	128.0	127.0	126.0	142.0	127.0	130.0	82.6	134.0	124.0
Debermarkos	271.0	271.0	271.0	271.0	271.0	271.0	271.0	265.0	271.0	270.0
Direidiwa	154.0	152.0	155.0	140.0	152.0	148.0	139.0	95.8	145.0	135.0
Gode	97.7	50.7	87.6	58.5	98.6	55.8	51.6	47.9	114.0	93.5
Gondar	216.0	216.0	216.0	132.0	215.0	216.0	215.0	207.0	214.0	215.0
Gore	273.0	221.0	256.0	236.0	250.0	222.0	231.0	212.0	241.0	224.0
Harameda	117.0	111.0	113.0	109.0	111.0	107.0	104.0	94.9	114.0	111.0
Jimma	380.0	363.0	375.0	361.0	375.0	365.0	350.0	337.0	364.0	355.0
Lekemte	237.0	213.0	229.0	221.0	233.0	216.0	206.0	175.0	222.0	217.0
Mekele	24.0	23.9	23.9	23.9	24.0	23.9	23.9	22.4	23.1	23.5
Metehara	80.5	71.0	73.9	63.5	82.4	64.8	42.0	57.2	69.2	67.2
Neghelli	181.0	147.0	155.0	140.0	176.0	149.0	133.0	99.7	156.0	139.0
Robe	182.0	144.0	130.0	129.0	186.0	126.0	139.0	72.4	134.0	121.0

Table 14: MAE of accumulated total grid scale precipitation using 10 microphysics for Normal year (2004).

country	mp1	mp2	mp3	mp4	mp5	mp6	mp7	mp8	mp10	mp14
AddisAbaba	139.0	137.0	136.0	133.0	139.0	136.0	129.0	123.0	135.0	134.0
Arbaminch	256.0	213.0	230.0	176.0	224.0	206.0	199.0	113.0	189.0	221.0
Hawasa	210.0	184.0	194.0	192.0	206.0	190.0	179.0	133.0	193.0	191.0
Baherdar	284.0	233.0	254.0	241.0	252.0	240.0	244.0	215.0	238.0	242.0
Combolcha	140.0	132.0	131.0	131.0	148.0	131.0	134.0	86.9	139.0	129.0
Debermarkos	276.0	276.0	276.0	276.0	276.0	276.0	276.0	270.0	276.0	275.0
Direidiwa	160.0	158.0	161.0	146.0	157.0	153.0	145.0	104.0	151.0	141.0
Gode	112.0	67.5	101.0	71.4	113.0	68.4	63.9	57.4	131.0	107.0
Gondar	222.0	222.0	222.0	222.0	221.0	222.0	221.0	212.0	220.0	221.0
Gore	287.0	229.0	269.0	247.0	260.0	231.0	242.0	220.0	252.0	233.0
Harameda	118.0	112.0	114.0	109.0	112.0	108.0	105.0	95.4	114.0	112.0
Jimma	394.0	374.0	388.0	372.0	388.0	376.0	362.0	346.0	375.0	365.0
Lekemte	238.0	213.0	229.0	221.0	234.0	216.0	207.0	176.0	223.0	217.0
Mekele	24.8	24.7	24.7	24.7	24.8	24.7	24.7	23.2	23.8	24.3
Metehara	81.5	73.0	75.5	68.1	83.0	68.6	46.9	57.7	71.1	70.0
Neghelli	208.0	166.0	176.0	157.0	202.0	169.0	150.0	113.0	178.0	156.0
Robe	185.0	146.0	134.0	132.0	188.0	129.0	141.0	85.5	137.0	125.0

Table 15: RMSE of accumulated total grid scale precipitation using 10 microphysics for Normal year (2004).

Bibliography

[1] Holton, J.R. (1992). An Introduction to Dynamic Meteorology. Academic Press.

[2] Steinfeld, J. I. (1998). Atmospheric chemistry and physics: from air pollution to climate change. Environment: Science and Policy for Sustainable Development, 40(7), 26-26.

[3] Jacobson, M. Z. (2005). Fundamentals of atmospheric modeling. Cambridge university press.

[4] Academic American Encyclopedia. (1994). El Niño. PRODIGY interactive personal service. Groiler Electronic Publishing Inc.

[5] Claire, S. (2016). El Niño in Ethiopia: Programme observations on the impact of the Ethiopia drought and recommendations for action, Retrieved from Oxfam: http://www.oxfam.ca/emergencies/drought-in-ethiopia

[6] Schlesinger, W. H. (1991). Biogeochemical Analysis of Global Change. Academic Press Inc.

[7] Middleton, W. E. (1966). History of the Theories of Rain and other forms of precipitation. Watts.

[8] PRUPPACHER, H. R., & KLETT, J. D. (1997). Microphysics of clouds and precipitation. Kluwer Academic.

[9] Pouncy, F. J. (2003). A history of cloud codes and symbols. Weather, 58(2), 69-80.

[10] Blanchard, D. C. (2004). From raindrops to volcanoes: adventures with sea surface meteorology. Courier Corporation.

[11] KESSLER, E. (1969). On the Distribution and Continuity of Water Substance in Atmospheric Circulations. Meteor. Monogr.

[12] Ghosh, S., & Jonas, P. R. (1998). On the application of the classic Kessler and Berry schemes in Large Eddy Simulation models with a particular emphasis on cloud autoconversion, the onset time of precipitation and droplet evaporation. In Annales Geophysicae (Vol. 16, No. 5, pp. 628-637). Springer-Verlag.

[13] Lin, Y. L., Farley, R. D., & Orville, H. D. (1983). Bulk parameterization of the snow field in a cloud model. Journal of Climate and Applied Meteorology, 22(6), 1065-1092.

[14] Rutledge, S. A., & Hobbs, P. V. (1984). The mesoscale and microscale structure and organization of clouds and precipitation in midlatitude cyclones. XII: A diagnostic modeling study of precipitation development in narrow cold-frontal rainbands. Journal of the Atmospheric Sciences, 41(20), 2949-2972.

[15] Tao, W. K., Simpson, J., & McCumber, M. (1989). An ice-water saturation adjustment. Monthly Weather Review, 117(1), 231-235.

[16] Hong, S. Y., Dudhia, J., & Chen, S. H. (2004). A revised approach to ice microphysical processes for the bulk parameterization of clouds and precipitation. Monthly Weather Review, 132(1), 103-120.

[17] Skamarock, W. C., Klemp, J. B., Dudhia, J., Gill, D. O., Barker, D. M., Duda, M. G., ... & Powers, J. G. (2008). A Description of the Advanced Research WRF Version3.

[18] Hong, S. Y., & Lim, J. O. J. (2006). The WRF single-moment 6-class microphysics scheme (WSM6). J. Korean Meteor. Soc, 42(2), 129-151.

[19] Ryan, B. F. (1996). On the global variation of precipitating layer clouds. Bulletin of the American Meteorological Society, 77(1), 53-70.

[20] Thompson, G., Rasmussen, R. M., & Manning, K. (2004). Explicit forecasts of winter precipitation using an improved bulk microphysics scheme. Part I: Description and sensitivity analysis. Monthly Weather Review, 132(2), 519-542.

[21] Tao, W. K., & Simpson, J. (1993). The Goddard cumulus ensemble model. Part I: Model description. Terr. Atmos. Oceanic Sci, 4(1), 35-72.

[22] Morrison, H., & Pinto, J. O. (2006). Intercomparison of bulk cloud microphysics schemes in mesoscale simulations of springtime Arctic mixed-phase stratiform clouds. Monthly weather review, 134(7), 1880-1900.

[23] Kain, J. S. (2004). The KainFritsch Convective Parameterization: An Update. Journal of Applied Meteorology, 43(1).

[24] Noh, Y., Cheon, W. G., Hong, S. Y., & Raasch, S. (2003). Improvement of the K-profile model for the planetary boundary layer based on large eddy simulation data. Boundary-layer meteorology, 107(2), 401-427.

[25] Chen, F., & Dudhia, J. (2001). Coupling an advanced land surface-hydrology model with the Penn State-NCAR MM5 modeling system. Part I: Model implementation and sensitivity. Monthly Weather Review, 129(4), 569-585.

[26] Dyer, A. J., & Hicks, B. B. (1970). Fluxgradient relationships in the constant flux layer. Quarterly Journal of the Royal Meteorological Society, 96(410), 715-721.

[27] Bahaga, T. K., Kucharski, F., Tsidu, G. M., & Yang, H. (2016). Assessment of prediction and predictability of short rains over equatorial East Africa using a multi-model ensemble. Theoretical and Applied Climatology, 123(3-4), 637-649.

[28] Griffiths, J. F. (1972). Ethiopian highlands. World survey of climatology, 10, 369-388.

[29] Dinku, T., S. Chidzambwa, et al. (2008). Validation of high-resolution satellite rainfall products over complex terrain. International Journal of Remote Sensing 29(14): 40974110.

[30] Dinku, T., Connor, S. J., Ceccato, P., & Ropelewski, C. F. (2008). Comparison of global gridded precipitation products over a mountainous region of Africa. International Journal of Climatology, 28(12), 1627-1638.

[31] Viste, E. M. (2012). Moisture Transport and Precipitation in Ethiopia.

[32] Dawit, A. (2010). Future climate of Ethiopia from PRECIS Regional Climate Model Experimental Design. Ethiopia http://www.metoffice.gov.uk/media/pdf/o/9/PRECIS-Experimental-Design-Dawit.pdf.

[33] Schneider, U., Becker, A., Finger, P., Meyer-Christoffer, A., Ziese, M., & Rudolf, B. (2013). GPCC's new land surface precipitation climatology based on quality-controlled in situ data and its role in quantifying the global water cycle.

[34] Dasari, H. P., Salgado, R., Perdigao, J., & Challa, V. S. (2014). A Regional Climate Simulation Study Using WRF-ARW Model over Europe and Evaluation for Extreme Temperature Weather Events. International Journal of Atmospheric Sciences.

Declaration

This thesis is my original work, has not been presented for a degree in any other University and that all the sources of material used for the thesis have been dully acknowledged.

Name: Amarech Alebie

Signature:– – – – – – – – – – –

Place and time of submission: Addis Ababa University, June 2016

This thesis has been submitted for examination with my approval as University advisor.

Name: Prof. Gizaw Mengistu Tsidu

(Bostwana International University of Science and Technology/Addis Ababa University)

Signature:– – – – – – – – ––